A STUDY OF THE ELECTRICAL DOUBLE LAYER IN NON-AQUEOUS SOLVENTS

by

David S. Reid, B.Sc.

SUMMARY

A study has been made of the electrical double layer at the interface between mercury and solutions of alkali chlorides in formamide. The differential capacitance of the double layer has been measured by the impedance bridge technique in the following solutions: 0.05m, 0.071m, 0.100m, and 0.500m potassium chloride at 25°C, 0.100m lithium, sodium, rubidium and caesium chlorides at 25°C, 0.100m potassium and caesium chlorides at 5°C and 45°C. The potential of the electrocapillary maximum has been measured in these same solutions by the streaming mercury technique, and the electrode charges calculated by integration of the capacitance data. The appearance of the capacitance-charge curves is discussed in terms of general double layer theory.

The interfacial tensions in 0.050m and 0.100m potassium chlorides and 0.050m, 0.0889m, 0.100m and 0.179m caesium chlorides have been measured using a capillary electrometer.

Capacitance and interfacial tension results have been employed in the calculation of the relative ionic surface excesses in 0.071m potassium chloride and

0.100m caesium chloride at 25°C. The resulting values suggest strongly that simultaneous specific adsorption of anions and cations is taking place over part of the potential range investigated. Accordingly, a tentative analysis has been developed to yield values for the components of charge in the double layer under conditions of simultaneous adsorption. A solvation model of specific adsorption is proposed to explain the constancy of cationic specific adsorption found to occur, and it is shown that this model is consistent with data for specific adsorption obtained in aqueous solution systems. The capacitance-charge curves are reconsidered in the light of the data for specific adsorption.

A STUDY OF THE ELECTRICAL DOUBLE LAYER IN NON-AQUEOUS SOLVENTS

A THESIS

Submitted to the University of Glasgow

for the degree of

DOCTOR OF PHILOSOPHY

by

David S. Reid, B.Sc.

Supervisor

Professor G.H. Nancollas

September, 1966

PREFACE.

A portion of the work described in this thesis was carried out in the Chemistry Department of the University of Glasgow under the direction of Professor J. Monteath Robertson C.B.E., F.R.S. The final year of the work was carried out furth of Glasgow in the Chemistry Department of the State University of New York at Buffalo.

I wish to express my sincere gratitude to Professor G.H. Nancollas for his guidance and encouragement throughout the period of research. Thanks are also due to Dr. H.S. Dunsmore and Mr. D. McGregor for their help in the programming of the KDF 9 computer, and to Dr. C.A. Vincent for helpful discussion of the results.

I also thank the Carnegie Trust for the Universities of Scotland, and the State University of New York for maintainance grants which made this research possible.

David S. Reid.....

CONTENTS

Summary

INTRODUCTION 1

THEORY 11

Gouy-Chapman theory 13

Double layer in absence of s.a. 15

The Watts-Tobin Theory 17

The Macdonald and Barlow Theory 21

Double layer in the presence of s.a. 24

Components of charge analysis, (one ion s.a.) ... 28

The Esin and Markov effect 30

Grahame's model of the double layer 33

Devanathan's model of the double layer ... 36

APPARATUS AND EXPERIMENTAL PROCEDURE 41

General introduction 42

Transformer ratio-arm bridge 47

Use of an a.c. bridge for the measurement of the impedance of a d.m.e. 53

Self-timing bridge method for measuring the impedance of a d.m.e. 55

Balance detection 57

Bridge standardisation 66

Drop birth detector 69

D.C. polarisation unit 73

Audio frequency standardisation 76
Pulse counter 77
Monitoring 80
Differential capacitance cell 81
Electrocapillary apparatus 86
Capillary electrometer cell 89
Electrocapillary maximum apparatus 91
Preparation of materials 94
Preparation of solutions 95
Reference electrodes 97
General run procedures 100
RESULTS 106
Method of calculation 107
Tables of experimental results 114
Plots of experimental results 137
DISCUSSION 142
Capacitance-charge curves 143
Electrocapillary curves 150
Esin and Markov Plot 152
Relative surface excesses 154
Components of charge analysis for simultaneous s.a. 162
S.a. on the "solvation model" 174
Modified Watts-Tobin theory 180
APPENDICES 184
BIBLIOGRAPHY 196

SUMMARY.

A study has been made of the electrical double layer at the interface between mercury and solutions of alkali chlorides in formamide. The differential capacitance of the double layer has been measured by the impedance bridge technique in the following solutions: 0.050m, 0.071m, 0.100m, and 0.500m potassium chloride at 25°C, 0.100m lithium, sodium, rubidium and caesium chlorides at 25°C, 0.100m potassium and caesium chlorides at 5°C and 45°C. The potential of the electrocapillary maximum has been measured in these same solutions by the streaming mercury technique, and the electrode charges calculated by integration of the capacitance data. The appearance of the capacitance-charge curves is discussed in terms of general double layer theory.

The interfacial tensions in 0.050m and 0.100m potassium chlorides and 0.050m, 0.0889m, 0.100m and 0.179m caesium chlorides have been measured using a capillary electrometer.

Capacitance and interfacial tension results have been employed in the calculation of the relative ionic surface excesses in 0.071m potassium chloride and 0.100m caesium chloride at 25°C. The resulting values suggest strongly that simultaneous specific adsorption of anions and cations is taking place over part of the potential

range investigated . Accordingly, a tentative analysis has been developed to yield values for the components of charge in the double layer under conditions of simultaneous adsorption. A solvation model of specific adsorption is proposed to explain the constancy of cationic specific adsorption found to occur, and it is shown that this model is consistent with data for specific adsorption obtained in aqueous solution systems. The capacitance-charge curves are reconsidered in the light of the data for specific adsorption.

INTRODUCTION

Across any boundary between two phases there normally exists a difference in electrical potential due to the redistribution of the electrical charges of particles from the bulk of the phase to form an interfacial layer. This array of oppositely charged particles and oriented dipoles in juxtaposition at a phase boundary is normally referred to as the electrical double layer. Such an effect is caused by the tendency of all systems to assume a position of minimum free energy, and it has been shown (1) that there are four main mechanisms responsible for its formation:

(I) charge transfer across the interface,

(II) unequal adsorption of oppositely charged ions,

(III) adsorption and orientation of dipoles,

(IV) deformation of polarisable ions, atoms or molecules at the interface.

Familiar examples of double layers are those formed when a metal dips into a solution of its ions, at liquid junctions, or when a metal is heated in a vacuum. An exact study of the double layer is most easily carried out using metal - solution interfaces because it is possible to vary the potential difference between the phases without changing their composition. If, on applying a potential, no current flows across the interface in such a system, then the double layer is electrically similar to a capacitor of large specific capacitance. The magnitude of this

specific capacitance is a measure of the electronic charge on the metal surface. Knowledge of the capacitance, therefore, leads directly to the electronic surface charge, which in turn yields further information about the structure of the double layer.

Another property of the interface which may readily be studied in some systems is the interfacial tension. As is to be expected, this too varies with the potential difference across the interface, and a knowledge of this variation can yield still more information about the structue of the double layer.

A detailed knowledge of the double layer is of fundamental importance, since on it depend the explanations of many natural phenomena. Thus, since the electrokinetic ζ- potential is largely determined by double layer properties, electro-osmosis, electrophoresis, streaming potentials and similar effects are dependent on double layer formation. Many heterogeneous processes, such as electrode reactions require a thorough knowledge of double layer phenomena for their complete understanding. Another phenomenon which depends largely upon the establishment of a double layer at an interface is the conduction of an electrical impulse along a nerve.

The main methods of investigation of the double layer are concerned with the direct or indirect determination of capacitance or interfacial tension at a metal-solution

interface. Early work on this problem was carried out by Lippmann (2) and Gouy (3) but not until Proskurnin and Frumkin (4) were reproducible capacitance data obtained. These authors showed that earlier irreproducibility was due to insufficient purification of the materials. Grahame (5) was the first to advocate the use of mercury as the metal, in the form of a dropping electrode. Mercury is pre-eminently suitable as the metal, since a pure, reproducible surface is easily obtained, and since its low chemical activity and high hydrogen overvoltage enable it to be used over a wide potential range in many solution systems. Mercury has the additional advantage that interfacial tensions between it and a solution phase may be readily measured. Early work on interfacial tensions was carried out by Gouy (3). It is important to realise that interfacial tension data on mercury are not nearly as susceptible to the presence of impurities as are capacitance data. This explains why early measurements of interfacial tension were of high precision even though no special precautions were taken to purify the solutions.

An ideal polarised electrode may be described as a metal-solution system for which no finite amount of charge may cross the interface during re-establishment of equilibrium after a small change in the potential difference between the phases. Such an electrode behaves like an

electrical capacitor without leakage. Unlike a simple capacitor, however, the capacitance of an ideal polarised electrode varies with applied potential, since it depends on the relative position of charges which may be different under altered conditions of electrical field. Because of this variation of capacitance with electrical field strength, it is usual to consider the differential capacitance of such systems, rather than the integral capacitance.

The differential capacitance C is defined as

$$C = dq / dE,$$

where q is the electrode charge, and E is the potential with respect to some reference electrode.

The integral capacitance K is defined as,

$$K = q / (E - E^{ecm}),$$

where E^{ecm} is the potential of the electrocapillary maximum. The difference between these two quantities is apparent from the diagram.

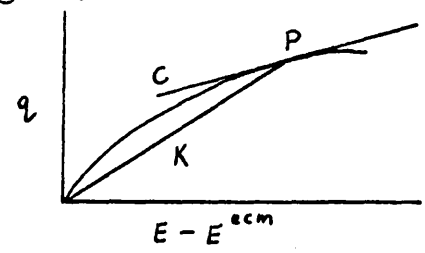

C is the gradient of the q vs. $(E-E^{ecm})$ curve at point P, whereas K is the gradient of the chord from the origin to P. It is clear from the diagram that C will be a much more

sensitive indicator of any changes in the charge as the potential is varied.

The first quantitive approach to double layer structure was given by Helmholtz (6) in 1879. He regarded the interface as a simple parallel plate capacitor. Thus

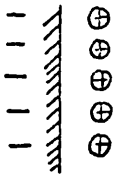

$$K = \frac{q}{(E-E^{ecm})} \cdot \frac{DD_o A}{4\pi d}$$

where as before K is the integral capacitance, q is the charge on the 'plates', and $E-E^{ecm}$ is the potential with respect to the electrocapillary maximum. D is the dielectric constant of the solvent, d is the distance of separation of the ' plates', A is the area of the electrode and D_o is a constant. For a simple parallel plate capacitor, K=C. This simple theory completely fails to explain the experimentally demonstrated variation of capacitance with potential.

In a treatment similar to that of Debye and Hückel in their ionic atmosphere theory, Gouy (7) and Chapman (8) independently considered the solution side of the double layer, postulating that thermal motion would result in this having a diffuse character. The solution side of the double layer was regarded as being the ionic atmosphere of the electrode. This theory gave values of capacitance which

were much higher than the corresponding measured values, and resulted in an exponential fall in potential with distance from the electrode.

Stern (9) then developed the theory further by making allowance for the finite size of ions, and also by considering the possibility of a specific interaction between ions and electrode. This theory may be regarded as a combination of the preceding two theories. Thus, the potential difference between the interface and the bulk solution is assumed to be made up of a linear fall across the "inner layer" and a exponential decay across the "diffuse layer". Stern considered that both cations and anions would be adsorbed simultaneously at the electrode surface, though in a footnote he pointed out that this need not be the case.

Grahame and Whitney (10) observed disagreement between experimental results, and values calculated on the basis of Stern's theory, and in his classic review (11) Grahame suggested that only anions could be specifically adsorbed. In recent years this assumption has been questioned especially by Frumkin, Damaskin and co-workers (12).

Grahame's concept of the double layer structure, upon which all modern ideas are based, postulates the existence of two "Helmholtz planes", an inner marking the distance of closest approach of anionic centres and

an outer marking the closest approach of cationic centres. Thus the double layer at a perfectly polarised electrode is considered to consist of:

(1) a metallic phase on the surface of which there is generally a surplus or deficit of electrons,

(11) a region of solution phase immediately adjacent to the metal into which no electrical centres can enter because of the physical size of the ions,

(111) a region accessible to the electrical centres of anions, but not of cations,

(1V) an outer diffuse layer region of the Gouy-Chapman type.

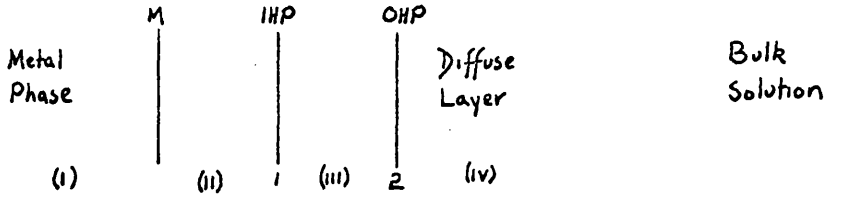

When anions are present at the inner Helmholtz plane (IHP) they are held to the metallic phase by short range forces, considered by Grahame to be of the covalent type (11). In this phenomenon, known as " specific adsorption " the distance between the metal and the IHP is considered to be approximately equal to the radius of the unhydrated ion. Thus, specific adsorption would require at least partial desolvation of the ion in question, and to make this process energetically favourable, the extent of metal-ion interaction must be considerable. Thus in general, anion

specific adsorption will be much easier than cation specific adsorption, and adsorption will be more likely for:

(1) ions which are easily polarised,

(11) ions which have weakly bound hydration sheaths.

The following situations commonly occur:

(a) Negative polarisation.

(1) No specific adsorption of cations.

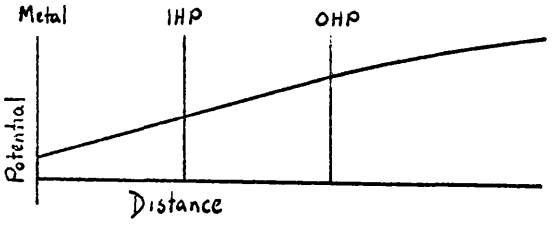

No ions at IHP. Cations form diffuse layer starting at the outer Helmholtz plane (OHP).

(11) Specific adsorption of cations. This is least common.

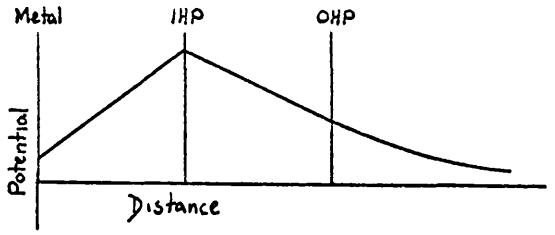

Cations present at IHP. Diffuse layer of anions.

(b) Positive polarisation.

(1) No specific adsorption of anions.

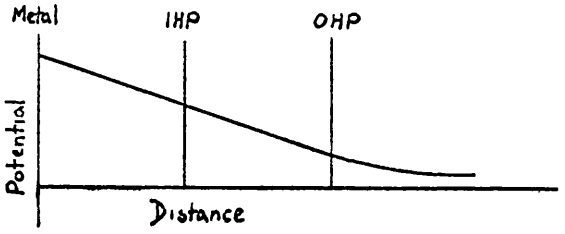

No ions at IHP. Anions form diffuse layer similar to that

in (a) (11).

(11) Specific adsorption of anions.

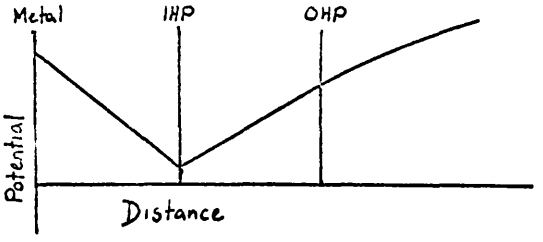

Anions present at IHP. Diffuse layer of cations similar to that in (a) (1).

If specific adsorption of anions is very strong it may occur at the potential of the electrocapillary maximum, where the metal is uncharged, or even at slightly cathodic potentials.

THEORY

THEORY

It is the purpose of modern theories of the double layer to describe the behaviour of the various regions at the interface between the metal and the solution, and hence to explain the experimental capacitance-potential curves. In the following section, some of the theories which have been developed will be presented. It is generally agreed that at the present stage of development of the double layer theory, the best characterised region is the diffuse layer, for which the Gouy-Chapman theory has proved satisfactory to a good first approximation. Minor discrepancies do exist between theory and experiment, but these are unimportant for present purposes. Theoretical treatments of the properties of the inner layer are much less satisfactory at present, and have met with only limited success in the quantitative treatment of the subject.

In addition to discussing, in a somewhat general fashion, the various theories put forward to explain capacitance-charge curves obtained in double layer studies, this section will be concerned to some extent with the information which one can derive from experimental results, assuming the commonly held ideas on double layer structure to be correct.

The Gouy-Chapman Theory.

If we assume equilibrium between any point in the double layer and the bulk of the solution for an ideal polarised electrode, we have for the ionic species i

$$\bar{\mu}_i = \bar{\mu}_i^s$$

where $\bar{\mu}_i$ and $\bar{\mu}_i^s$ are the electrochemical potentials of species i in the double layer and in the bulk solution respectively. This can be written in the approximate form

$$c_i = c_i^s e^{-z_i f \varphi} \qquad \ldots\ldots(1)$$

where $f = F/RT$, c_i and c_i^s are the concentrations of ion i at a distance x from the electrode and in the bulk solution respectively, z_i is the signed ionic valence of i and φ is is the potential at x with respect to the potential φ_6 in the bulk solution, which we set at zero. The Poisson equation gives us a relationship between c_i and φ in the following manner

$$\frac{\partial^2 \varphi^i}{\partial x^2} = \frac{-4\pi \rho}{\epsilon} \qquad \ldots\ldots(2)$$

where ρ is the charge density per unit volume and ϵ is the dielectric constant. Also

$$\rho = \sum z_i F c_i \qquad \ldots\ldots(3)$$

Combining (1), (2) and (3) we have

$$\frac{d^2\varphi}{dx^2} = -\frac{4\pi}{\epsilon} \sum z_i F c_i^s e^{-z_i f \varphi} \qquad \ldots\ldots(4)$$

If we assume that ϵ is independent of x, this equation can be solved. The fact that this assumption is a drastic over-

simplification does not significantly affect the end result. Multiplication of (4) by $2d\varphi/dx$, followed by integration, yields

$$\left(\frac{d\varphi}{dx}\right)^2 = \frac{8\pi RT}{\epsilon} \sum c_i^s (e^{-z_i f\varphi} - 1) \qquad \ldots\ldots\ldots(5)$$

The charge on the electrode per unit area is related to $d\varphi/dx$ by Gauss' Theorem

$$4\pi q = -\epsilon \left(\frac{d\varphi}{dx}\right)_{x_2} \qquad \ldots\ldots\ldots(6)$$

where x_2 is the distance of the OHP. from the electrode. Combining (5) and (6) gives us

$$q = \pm \left[\frac{RT\epsilon}{2\pi} \sum c_i^s (e^{-z_i f\varphi} - 1)\right]^{1/2} \qquad \ldots\ldots\ldots(7)$$

This allows us to calculate q as a function of φ or vice versa. It should be remembered that in this treatment no account has been taken of specific adsorption , and that the theory in this form is not valid in the presence of specific adsorption. For a z-z electrolyte of concentration c^s, equation (7) takes the form

$$q = 2A \operatorname{Sinh}\left(\frac{|z| f \varphi_2}{2}\right) \qquad \ldots\ldots\ldots(8)$$

where $$A = + \left(\frac{RT\epsilon c^s}{2\pi}\right)^{1/2} \qquad \ldots\ldots\ldots(9)$$

In the original Gouy-Chapman theory ions were treated as point charges which could approach to within any distance of the electrode. As has been discussed in the introduction, this was a considerable oversimplification, and Stern (9), by postulating a plane of closest approach, brought the theoretical picture much closer to reality. Modern theories go one step further and postulate two

planes of closest approach. One, the IHP, is involved only with specific adsorption, and need not concern us at present. In the absence of specific adsorption, then, the double layer can be divided into two regions: the compact double layer between the electrode and the plane of closest approach, and the diffuse double layer extending from the plane of closest approach to the bulk of the solution. The derivation of the Gouy-Chapman theory given above evaluates the capacitance of the diffuse layer between just those regions, the outer Helmholtz plane and the bulk solution. The capacitance of the double layer may be regarded as made up of two separate capacitances in series with one another, that of the compact (or inner) layer, C_{M2} and that of the diffuse layer, $C_{2\text{-}S}$.

$$1/C_o = 1/C_{M2} + 1/C_{2\text{-}S} \qquad \text{.....(10)}$$

The subscripts M, 1, 2 and S in equation (10) refer to the metal, the IHP, the OHP and the bulk solution respectively, and C_o is the experimentally measured capacitance per unit area. The Gouy-Chapman theory gives for the capacitance of the diffuse double layer

$$C_{2\text{-}S} = |z| f A \cosh\left(\frac{|z| f \phi_2}{2}\right) \qquad \text{.....(11)}$$

Of all the systems for which it is generally agreed that specific adsorption is absent, the mercury surface in contact with an aqueous solution of sodium fluoride has been the most thoroughly studied. Grahame (13) tested the

validity of the modified Gouy-Chapman theory, assuming that at any given temperature C_{M-L} was a function only of the electrode charge, and not of the electrolyte concentration. At high concentrations the calculation of C_{M-L} from C_o involved only a small correction for C_{L-S}, since this was very large, and the resulting values of C_{M-L} could then be employed to calculate C_{L-S} under different conditions. Except at extreme anodic potentials, where fluoride ion may be specifically adsorbed, good agreement was obtained between the values of C_{L-S} determined by this method, and those expected on the Gouy-Chapman theory. As pointed out by Joshi and Parsons (14) this agreement does not conclusively prove the Gouy-Chapman theory to be satisfactory under all conditions, as the contribution of the diffuse double layer to the capacitance is small under conditions of high electrode charge.

Grahame (13) calculated values for C_{M-L} in aqueous solutions over the temperature range 0° C-85° C and the concentration range 0.001-0.9 M sodium fluoride (figure 1). These data have been employed for testing theories of the double layer which seek to explain the variations of C_{M-L} with electrode charge and with temperature in systems in which there is no specific adsorption. The most interesting treatments are those by Watts-Tobin (15) and Macdonald and Barlow (16,17).

Watts-Tobin considered the problem in sections. Firstly, since the capacity curves for sodium fluoride are very similar to those obtained for systems in which the anion is specifically adsorbed, he considered adsorption of positive ions from the metal or negative ions from the solution. Mercury atoms could be pulled out from the surface to form ad-atoms, and only the product of the dipole moment of the ad-atom and the charge induced on the metal by it would affect the potential drop from the metal to the OHP. This would also be true of anions adsorbed from the solution. Since there is no reason for both species to be at an equal distance from the metal surface, if both

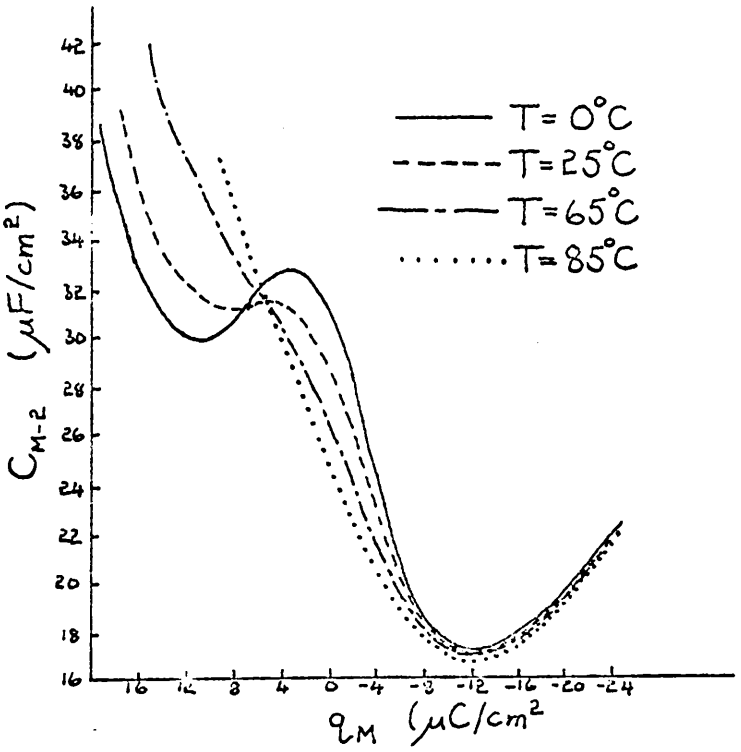

FIG. 1 C_{M-2} FOR NaF.

are formed then they will cluster together to form complexes.

are formed then they will cluster together to form complexes.

If the dipole moment of a complex is μ_1, positive in the direction from the metal to the solution, the potential drop from the metal to the OHP is φ_{M-2}, x_2 is the distance from the metal to the OHP, and the distance between complexes is large compared to x_2 then the number of complexes per unit area of surface is given by

$$n_1 = N_c \left(\frac{c_1}{c_o}\right)^m \exp\left\{\frac{\mu_1 \varphi_{M-2}/x_2 - W_o}{kT}\right\} \qquad \ldots\ldots\ldots(12)$$

In this equation N_c is the number of adsorption sites per unit area of metal surface and W_o the heat of adsorption of a complex in the absence of an electric field, but including image force attraction. W_o is measured at concentration c_o, the experimental concentration being c_1 and there being m ions in a complex. The contribution of the complexes to φ_{M-2} is $-4\pi n_1 \mu_1 / \epsilon_1$ where ϵ_1 is the dielectric constant of the first layer.

The hump in the capacitance curve is explained in terms of solvent orientation polarisation. At the hump it is proposed that there is an increase in the effective dielectric constant of the layer, marking the point at which the average dipole moment of the water in the layer changes sign. Water molecules are assumed to have two possible orientations at the mercury surface, with their dipole moments making angles $\mathrm{Cos}^{-1}(1/\sqrt{3})$ with the normal to the surface. If there are N free water molecules per unit area

of interface, of which L have a component of their dipole moment from the metal to the solution and M the other way, the energies of the dipole chains are given by

$$A = C' - \mu \varphi_{M-2}/\sqrt{3}\, x_2 \qquad \ldots\ldots\ldots(13)$$

$$B = D' + \mu \varphi_{M-2}/\sqrt{3}\, x_2 \qquad \ldots\ldots\ldots(14)$$

where μ is the dipole moment of the water molecule, and C' and D' are the adsorption energies of the water molecule in contact with the metal. Provided the layer across which the dipole chains run is not thick, the chains may be considered to be independent of one another, so that

$$L/M = \exp\left\{-(A-B)/kT\right\} \qquad \ldots\ldots\ldots(15)$$

The contribution of the water molecules to φ_{M-2} is

$$-4\pi(L-M)\mu/\sqrt{3}\epsilon_1 = -(4\pi N\mu/\sqrt{3}\epsilon_1)\tanh\left\{\frac{\mu(\varphi_{M-2}-V)}{\sqrt{3}\, x_2 kT}\right\} \qquad \ldots\ldots(16)$$

where $V = \sqrt{3}\, x_2 (C'-D')/2\mu$ $\qquad \ldots\ldots(17)$

If there is a surface charge q_{2M} on the metal balancing a charge q_2 on the OHP. ($q_{2M} = -q_2$) it contributes $4\pi q_{2M} x_2/\epsilon_1$ to φ_{M-2}. Since there is no specific adsorption considered, this is equivalent to assuming all the diffuse layer to be at the OHP. Adding the contributions we have

$$\varphi_{M-2} = \frac{4\pi q_{2M} x_2}{\epsilon_1} - \frac{4\pi N\mu_1}{\epsilon_1}\left(\frac{c_1}{c_0}\right)^m \exp\left\{\mu_1(\varphi_{M-2}-V_0)/x_2 kT\right\} - \frac{4\pi N\mu}{\sqrt{3}\,\epsilon_1}\tanh\left\{\mu(\varphi_{M-2}-V)/\sqrt{3}\, x_2 kT\right\} \qquad \ldots\ldots(18)$$

where we have put $V_0 = W_0 x_2/\mu_1$, and we have assumed $N_c = N$. Now

$$q_{2M} = \frac{\epsilon_1 \varphi_{M-2}}{4\pi x_2} + \frac{N\mu_1}{x_2}\left(\frac{c_1}{c_0}\right)^m \exp\left\{\frac{\mu_1(\varphi_{M-2}-V_0)}{x_2 kT}\right\} \frac{N\mu}{\sqrt{3}\, x_2}\tanh\left\{\frac{\mu(\varphi_{M-2}-V)}{\sqrt{3}\, x_2 kT}\right\} \qquad \ldots\ldots(19)$$

and $$C_{M\text{-}2} = \frac{\epsilon_1}{4\pi x_2} + \frac{N\mu_1^2}{x_2^2 kT}\left(\frac{c_i}{c_o}\right)^m \exp\left\{\frac{\mu_1(\varphi_{M\text{-}2} - V_o)}{x_2 kT}\right\} + \frac{N\mu^2}{3x_2^2 kT}\operatorname{sech}^2\left\{\frac{\mu(\varphi_{M\text{-}2} - V)}{\sqrt{3}\, x_2 kT}\right\} \quad \ldots\ldots(20)$$

This treatment depends on two simplifying assumptions,

(1) that there is a linear drop of potential across the inner region,

(11) ϵ_1 is a constant

It is also assumed that the OHP is a plane. As we shall see later, it is probably reasonable to make these assumptions under conditions of no specific adsorption, but in the case of specific adsorption of ions, serious objections can be raised on the grounds that the assumptions are no longer valid. Nevertheless, treatments of the double layer in the presence of specifically adsorbed ions which have made these simplifying assumptions have been remarkably successful. Two such treatments, those by Grahame (11) and Devanathan (18) are discussed in the section on specific adsorption.

The theory put forward by Watts-Tobin gives good agreement with Grahames experimental results, though it is insufficient to explain the experimental temperature dependence on the anodic side. In a later paper, Mott and Watts-Tobin (19) extended the theory to take into consideration specific adsorption. Electrostriction of the solvent was also considered in a qualitative fashion by Watts-Tobin (15), and he concluded that it should be sufficient to explain

the cathodic rise of capacitance curves in aqueous solutions.

Macdonald (16) and Macdonald and Barlow (17) proposed a model of the double layer in the absence of specific adsorption in which electrostriction was explicitly introduced. The earlier theory resulted in symmetrical capacitance curves about the electrocapillary maximum (e.c.m.) and was strongly criticised on this point. In the later paper, improvements to the early theory were proposed. The total mean potential difference across the double layer was written

$$\varphi_{M\text{-}S} = \frac{4\pi q_M x_2}{\epsilon_1} + \left(\frac{2kT}{e}\right) \sinh^{-1}\left(\frac{q_M}{2A}\right) \qquad \ldots\ldots(21)$$

$A = kT\epsilon_S/4\pi e L_D$ where ϵ_S is the dielectric constant of the solution, and $L_D = (kT\epsilon_S/8\pi c_0 e^2)^{1/2}$, where c_0 is the concentration of positive or negative ions in the bulk solution. Both x_2 and ϵ_1 are assumed to be dependent on E_1, the constant field in the compact double layer. The following relationships were put forward,

$$x_2/x_2^0 = (1+\beta P)^{-1} \qquad \ldots\ldots(22)$$

where $P = \epsilon_1 E_1^2/8\pi$ $\qquad \ldots\ldots(23)$

and x_2^0 is the value of x_2 at zero electrical pressure.

$$\epsilon_1 = \epsilon_\infty + (\epsilon_1^0 - \epsilon_\infty)\left[\sinh^{-1}(\sqrt{2b}\,E_1)\right]/(\sqrt{2b}\,E_1) \qquad \ldots\ldots(24)$$

where ϵ_1^0 is the value of ϵ_1 when there is no dielectric saturation, and ϵ_∞ is its value when the dipole contribution is fully saturated out. b and β are adjustable

parameters. The above equations were used to fit Grahame's data, by adjustment of β, b and ϵ_1°, and as already mentioned, the resulting capacitance curves were symmetrical about the e.c.m. Accordingly, in their second paper, Macdonald and Barlow introduced the concept of an effective field $\mathcal{E}_n$ which gave a small amount of dielectric saturation (dipole orientation) even at the e.c.m. and allowed the maximum ϵ_1 to occur at small positive (or negative) values of q_M. This is equivalent to Watts-Tobin's treatment of solvent orientation. Another difficulty in the earlier treatment was that equation (24) did not exhibit the correct high field behaviour. To improve the treatment, therefore, it was replaced in the second paper by

$$\epsilon_1 = 1 + \lambda^n(\epsilon_\infty - 1) + \lambda^r a\, h(E) \qquad \ldots\ldots(25)$$

where $$h(E) = [\tan^{-1}(\sqrt{b}\,.E)]/(\sqrt{b}\,.E) \qquad \ldots\ldots(26)$$

$$a = \epsilon_1^\circ - \epsilon_\infty \qquad \ldots\ldots(27)$$

and $$E = E_1 + \mathcal{E}_n \qquad \ldots\ldots(28)$$

$$\lambda = x_2^\circ/x_2 = (1 + m\alpha P)^{1/m} \qquad \ldots\ldots(29)$$

where α is a compressibility constant. The constants n, r, and m were taken as 1, 0, and 1 respectively. It was concluded that P would have electrostrictive as well as compressive contributions. The final expression for P was

$$P = \frac{(E_1^2/8\pi)[2\epsilon_\infty - 1 + a\,h(E)]}{1 - 2a(\epsilon_\infty - 1)(E_1^2/8\pi)} \qquad \ldots\ldots(30)$$

The final theory gave very good agreement with Grahame's data at all temperatures, the only significant disagreement being on the anodic side, possibly caused by specific adsorption, which was not included in the theory. In a later paper, Macdonald and Barlow (20) consider all presently available theories of the double layer in the absence of specific adsorption.

Since specific adsorption almost certainly occurs in the systems investigated in the present work, it is of interest to consider the present state of knowledge on systems in which specific adsorption occurs. Most investigations have been on aqueous systems, and accordingly theories of the double layer in the presence of specific adsorption have been developed mainly for aqueous systems. This work is considered in the next section.

The Electrical Double Layer in the Presence of Specific Adsorption.

Several methods are available for measuring the relative surface excesses $\Gamma_{\pm}$ of ions in the electrical double layer. These are described below.

1. Electrocapillary Method.

The relative ionic surface excess can be determined from the variation of interfacial tension, γ, with the chemical potential of the salt, μ_a, at constant $E_{\pm}$, where $E_{\pm}$ is the potential measured against a reference electrode reversible to the cation (anion) of the solution. The required relationship is

$$\left(\frac{\partial \gamma}{\partial \mu_a}\right)_{E_{\pm},T,P} = - \frac{\Gamma_{\mp}}{\nu_{\mp}} \qquad \ldots\ldots(31)$$

where $\nu_{\mp}$ is the number of anions (cations) produced from one molecule of salt. This relationship is of extreme importance as it allows the calculation of $\Gamma_{\pm}$ by rigourous thermodynamic means. Usually we need only determine one quantity, either Γ_+ or Γ_-, the other being obtained from the relationship $-q_M = z_+ F \Gamma_+ + z_- F \Gamma_-$. For greatest accuracy q_M should be evaluated by integration of capacitance data, as this is inherently more accurate than the equivalent differentiation of interfacial tension data.

2. Capacitance Method.

Grahame and Soderberg (21) considered the thermodynamics of the ideal polarised electrode and showed that

$$-\frac{dC_{\pm}}{dE} = z_{\pm}\nu_{\pm}F\left(\frac{\partial C}{\partial \mu_a}\right)_{E_{\mp}} \qquad \ldots\ldots(32)$$

where $C_{\pm}$ is the capacitance contribution from cations (anions) and is defined by the relation

$$z_{\pm}F\left(\frac{\partial \Gamma_{\pm}}{\partial E_{\mp}}\right)_{\mu_a} = -C_{\pm} \qquad \ldots\ldots(33)$$

Hence
$$C_{\pm} = \int\left(\frac{dC_{+}}{dE}\right) + K \qquad \ldots\ldots(34)$$

$$z_{\pm}F\Gamma_{\pm} = -\int C_{\pm}\,dE + K' \qquad \ldots\ldots(35)$$

Actual values of the integration constants K and K' (or $C_{\pm}$ or $\Gamma_{\pm}$ at any value of $E_{\mp}$) are required for the integration. Two methods are available for evaluating these, employing either (a) electrocapillary data or (b) diffuse double layer theory.

(a) The first integration constant is evaluated using the relationship at the e.c.m.

$$C_{\pm} = z_{\pm}\nu_{\pm}FC_{e.c.m.}\left(\frac{\partial E_{\mp}^{ecm}}{\partial \mu_a}\right) \qquad \ldots\ldots(36)$$

and the second integration constant is found from

$$\left(\frac{\partial \gamma}{\partial \mu_a}\right)_{e.c.m.} = -\Gamma_{salt_{e.c.m.}} = -\frac{\Gamma_{+}}{\nu_{+}} = -\frac{\Gamma_{-}}{\nu_{-}} \qquad \ldots\ldots(37)$$

(b) If it can be assumed that diffuse double layer theory holds, the integration constants may be readily evaluated. E.g. for specific adsorption of anions only, there will be no specific adsorption at sufficiently negative potentials, and C_{+} can be calculated from diffuse layer theory. The relationships used are equations (59), (61) and (63)

of reference (22).

$$\eta_+^d = A\left[v^+ + (1+v^2)^{1/2} - 1\right] \qquad \ldots\ldots(38)$$

$$C_+^{de} = \frac{C}{2}^{de}\left[1 + \frac{v}{(1+v^2)^{1/2}}\right] \qquad \ldots\ldots(39)$$

$$\frac{dC_+}{dE}^{de} = \frac{C_+}{2(1+v^2)^{1/2}}^{de} \cdot \left[\frac{\left\{(1+v^2)^{1/2}+v\right\}}{C^{de}} \cdot \frac{dC}{dE}^{de} - \frac{C^{de}}{2A(1+v^2)}\right] \qquad \ldots\ldots(40)$$

3. Devanathan's Model Method. (18)

This method, which has so far only been applied to aqueous solutions, is based on a postulated structure of the electrical double layer, and can be used to evaluate the surface excesses from the differential capacitance data at single concentrations. The calculated Γ_+ values have been shown to be in good agreement with the results obtained for halide ions and m-benzene disulphonate ions using the electrocapillary method. The model is discussed later in the thesis.

4. Parson's Method.

This, which involves a change of variable from E to q_M, was developed by Parsons (23). The basic relation, obtained from equation (37) when $q_M \neq 0$, is

$$\Gamma_+ = -\left(\frac{\partial \gamma}{\partial \mu_a}\right)_{q_M} - q_M\left(\frac{\partial E_-}{\partial \mu_a}\right)_{q_M} \qquad \ldots\ldots(41)$$

and, since

$$\left(\frac{\partial E_-}{\partial \mu_a}\right)_{q_M} = -\left(\frac{\partial \Gamma_+}{\partial q_M}\right)_{\mu_a} \qquad \ldots\ldots(42)$$

then

$$\Gamma_+ = -\left(\frac{\partial \gamma}{\partial \mu_a}\right)_{q_M} + q_M\left(\frac{\partial \Gamma_+}{\partial q_M}\right)_{\mu_a} \qquad \ldots\ldots(43)$$

This differential equation can be solved by point-wise progression, using values of $(\partial\gamma/\partial\mu_a)_{q_M}$ obtained for each value of q_M. The initial gradients are

$$\left(\frac{\partial\Gamma_+^{ecm}}{\partial q_M}\right)_{\mu_a} = -\left(\frac{\partial E_-^{ecm}}{\partial\mu_a}\right)_{q_M=0} \qquad \ldots\ldots(44)$$

5. Other Methods.

Various direct methods exist in which one of the ions is labelled with a radioactive isotope. Such studies have been carried out on platinum (24,25), but as yet the technique has not been applied to a mercury electrode. Other methods exist for evaluating relative surface excesses but these are based on the methods described here, and so will not be considered further.

Bockris, Müller, Wroblowa and Kovac (26) compared the results obtained from methods 1, 2 and 4, and put forward a theory to explain the discrepancies which arise in the results under what might be termed the extremes of conditions (concentration and polarisation).

When the experimental values for the surface excesses differ significantly from those calculated on the basis of diffuse layer theory, it is clear that superequivalent (or specific) adsorption must be taking place. If such is the case, it is possible to calculate the amount of specifically adsorbed ion, provided only that the other ions present in the solution are not specifically adsorbed. The basic calculation is given for the case where only anionic specific adsorption occurs. If we can assume that cations are not specifically adsorbed in the range of potentials being considered, then the charge in the diffuse layer due to cations, q_+^{2-s}, is given by

$$q_+^{2-s} = z_+ F \Gamma_+ \qquad \ldots\ldots(45)$$

where Γ_+ is an experimentally determined quantity. q_+^{2-s} can be related to φ_2 using diffuse double layer theory

$$q_+^{2-s} = A\left(e^{-z_+ f \varphi_2/2} - 1\right) \qquad \ldots\ldots(46)$$

where $z_\pm$ is the valence of the ion with the sign of its charge. This enables us to calculate φ_2, and thus q_-^{2-s}, the charge in the diffuse layer due to anions,

$$q_-^{2-s} = -A\left(e^{-z_- f \varphi_2/2} - 1\right) \qquad \ldots\ldots(47)$$

and finally we obtain the charge due to specifically adsorbed anions, $q_-^{'}$ from

$$q_- = z_- F \Gamma_- = q_-^{'} + q_-^{2-s} \qquad \ldots\ldots(48)$$

where q_- is the charge in the solution due to anions.

Thus, under suitable conditions, the amount of

specifically adsorbed ion can be evaluated. It must be borne in mind that the preceding analysis is not valid if specific adsorption of cations occurs.

The Esin and Markov Effect.

The variation of the potential of the e.c.m. with concentration, as measured against a constant reference electrode (i.e. in a cell with liquid junction) provides another indication of specific adsorption. From the equation

$$\left(\frac{\partial E_{\pm}}{\partial \mu_a}\right)_{q_m} = -\left(\frac{\partial \Gamma_{\mp}}{\partial q_m}\right)_{\mu_a} \qquad \ldots\ldots(49)$$

it follows that (27)

$$\left(\frac{\partial E_{\pm}}{\partial \ln a}\right)_{q_m} = -\frac{RT}{z_{\pm}F}\left(\frac{\partial q_{\mp}}{\partial q_m}\right)_a \qquad \ldots\ldots(50)$$

where a is the activity of the electrolyte. If a reference electrode of constant electrolyte activity is used, we have for a z-z electrolyte on variation of the activity of the electrolyte in contact with the ideal polarised electrode

$$E_{ref} = E_{\pm} \pm \frac{RT}{|z|F} \ln a_{\pm} + \text{constant} \qquad \ldots\ldots(51)$$

provided that the liquid junction between the constant reference electrode and the solution is constant. Here E_{ref} is the potential measured against the reference electrode in a cell with a liquid junction. $a_{\pm}$, the mean activity, is given by

$$a = (a_{\pm})^2 \qquad \text{for a } z\text{-}z \text{ electrolyte } \ldots\ldots(52)$$

Equation (50) then becomes

$$\left(\frac{\partial E_{ref}}{\partial \ln (a_{\pm}^2)}\right)_{q_m} = \pm\frac{RT}{|z|F}\left[\left(\frac{\partial q_{\mp}}{\partial q_m}\right)_a + \tfrac{1}{2}\right] \qquad \ldots\ldots(53)$$

Thus the shift in E_{ref} with $\ln a$ at constant q_m depends on $(\partial q_{\mp}/\partial q_m)_a$.

In the absence of specific adsorption, $q_{\mp}$ is accessible from Gouy-Chapman theory, leading to the following results:

$$\left(\frac{\partial q_-}{\partial q_m}\right)_a \longrightarrow 0 \qquad \text{for } q_m \rightarrow -\infty$$

$$\left(\frac{\partial q_-}{\partial q_m}\right)_a \longrightarrow -1 \qquad \text{for } q_m \rightarrow +\infty$$

and $$\left(\frac{\partial q_-}{\partial q_m}\right)_a \longrightarrow -\tfrac{1}{2} \qquad \text{for } q_m \rightarrow 0$$

Consequently the e.c.m. is independent of electrolyte activity when it is measured against a constant reference electrode under conditions of no specific adsorption. Plots of E_+ against $(2RT/F)\ln a_\pm$ at constant q_m for aqueous sodium fluoride (27) have the limiting gradients predicted above.

The variation of the value of E_{ref} at the e.c.m. on changing the electrolyte concentration, symptomatic of specific adsorption, was named the "Esin and Markov Effect" by Grahame (28). Esin and Markov (29) had observed a linear variation of the e.c.m. with the logarithm of electrolyte concentration. From Parsons' work it is now known that this was just a particular case of the linear variation of E_{ref} (or $E_\pm$) with $\ln a$ at constant charge on the electrode. Plots of $E_\pm$ against $(2RT/F)\ln a_\pm$ at constant q_m for three potassium halides show the gradient to be independent of q_m (actual values -1.36, -1.35 and -1.22 for KI, KBr and KCl respectively) (27). This would not be the case in the absence of specific adsorption. The Esin and Markov plot, then, provides us with a means of testing for the

presence (or absence) of specific adsorption.

Grahame's Model of the Double Layer.

Grahame (11) was led to modify Stern's model (9) of the double layer by the strong specific adsorption of most anions. He introduced the inner plane of closest approach, located at a distance x_1 from the electrode. This was the plane at which he considered anions to be specifically adsorbed. Non-specifically adsorbed ions were considered to approach to the OHP. at a distance x_2 from the electrode ($x_2 > x_1$). Grahame assumed some covalent bonding to exist between specifically adsorbed anions and the mercury electrode. His evidence for this (30) was the essentially linear relationship between the differential capacitance for various anions at the maximum positive polarisation attained and the logarithm of the saturation concentration of mercurous ion in the solutions of the salts tested. Levine, Bell and Calvert (31) rejected this postulate in favour of image energy as the origin of specific adsorption, and Bockris, Devanathan and Müller (32,32a) suggested that the degree and type of ion hydration was the principal factor affecting specific adsorption. It is considered at present that the explanation given by Bockris et al is the most plausible.

Potential Distributions.

(a) Diffuse double layer.

φ_2, the potential of the OHP. is considered as a function of E. The method of calculation of φ_2 has already been given for the case where only one ion is specifically adsorbed. In aqueous solution, φ_2 is identical for all electrolytes with univalent cations in the far cathodic region, a region where there is no anion specific adsorption. For $E>E_{\varphi}^{ecm}$, φ_2 becomes markedly positive only for potassium fluoride, as the fluoride ion is not specifically adsorbed, except perhaps at a large positive electrode charge. Other electrolytes have negative φ_2's at $E>E^{ecm}$. This is in agreement with independent data which suggest that the positive electrode charge is more than compensated for by the large negative charge of the specifically adsorbed ions.

(b) Compact double layer.

Two methods were put forward by Grahame (33) for calculating φ_1. One, based on a linear adsorption isotherm is tentative and will not be discussed. The second takes into account discreteness of charge effects in the inner plane. Ershler (34) showed that the difference of potential $\varphi_m - \varphi_2$, solely due to the charge q_1 of specifically adsorbed ions was given by

$$(\varphi_m - \varphi_2)_{q_1} = \frac{4\pi q_1 (x_2 - x_1)}{\epsilon_1} \qquad \ldots\ldots(54)$$

where ϵ_1 is the dielectric constant of the compact double layer, assumed independent of x. The difference in potential $(\varphi_1 - \varphi_2)_{q_1}$ may be expressed, as a first approximation, by assuming a linear drop of potential for $(\varphi_m - \varphi_2)_{q_1}$.

Thus $$(\varphi_1 - \varphi_2)_{q_1} = (\varphi_m - \varphi_2)_{q_1} \frac{x_2 - x_1}{x_2} \qquad \ldots\ldots(55)$$

which becomes

$$(\varphi_1 - \varphi_2)_{q_1} = \frac{4\pi q_1}{\epsilon_1} \frac{(x_2 - x_1)^2}{x_2} \qquad \ldots\ldots(56)$$

Since $x_1 < x_2$, $\quad |(\varphi_1 - \varphi_2)_{q_1}| < |(\varphi_m - \varphi_2)_{q_1}|$

Hence the shift in the e.c.m., which is related to the change of $(\varphi_m - \varphi_2)_{q_1}$ on variation of anion concentration is greater than the change of potential $(\varphi_1 - \varphi_2)_{q_1}$ affecting the adsorbed ions. This accounts for a discrepancy noted by Esin and Markov between the experimental shifts of the e.c.m. and the predictions of Stern's theory.

Since, on the parallel plate condenser approach,

$$(\varphi_m - \varphi_2)_{q_m} = \frac{4\pi q_m x_2}{\epsilon_1} \qquad \ldots\ldots(57)$$

we get for constant ϵ_1

$$\frac{x_2 - x_1}{x_1} = \frac{(\varphi_m - \varphi_2)_{q_1}}{(\varphi_m - \varphi_2)_{q_m}} \cdot \frac{q_m}{q_1} \qquad \ldots\ldots(58)$$

This expression can then be used in an analysis of the inner layer parameters.

Devanathan's Model.

This model is based on four postulates:

(1) specifically adsorbed ions occupy the IHP.,

(11) solvated ions remain at the OHP.,

(111) ions may not populate the region between the IHP. and the OHP.,

(1V) χ potentials due to water dipoles and electron overlap are negligible, or constant.

In the original paper (18) the signs of all potentials are wrong (c.f. Macdonald and Barlow (20)).

The total electrode charge/unit area is

$$q_M = -(q' + q^{2-s}) \qquad \ldots\ldots(59)$$

Since there is no charge between the metal and the IHP., the potential at the IHP. is

$$(\varphi_M - \varphi_1) = q_M \,|\, K_{M-1} \qquad \ldots\ldots(60)$$

where $K_{M-1} = \epsilon_1 / 4\pi x_1 \qquad \ldots\ldots(61)$

Similarly, the potential of the OHP. is given by

$$(\varphi_1 - \varphi_2) = -q_0^{2-s} / K_{1-2} \qquad \ldots\ldots(62)$$

where $K_{1-2} = \epsilon_1 / 4\pi (x_2 - x_1) \qquad \ldots\ldots(63)$

It should be noted that combination of equations (60) and (62) gives $\varphi_M - \varphi_2$ as the function of q' and q_M derived in Grahame's approach. Differentiation of equation (60) gives

$$\frac{d\varphi_M}{dq_M} = \frac{1}{C} = \frac{1}{K_{M-1}} + \frac{d\varphi_1}{dq_M} \qquad \ldots\ldots(64)$$

$d\varphi_1 / dq_M$ can be evaluated by differentiation of equation (62)

and introducing the relationship of equation (59). This yields the final expression

$$\frac{1}{C} = \frac{1}{K_{M-1}} + \left(\frac{1}{C_{2-S}} + \frac{1}{K_{1-2}}\right)\left(1 + \frac{dq'}{dq_M}\right) \qquad \ldots\ldots(65)$$

which on rearrangement gives

$$\left(1 + \frac{dq'}{dq_M}\right) = \frac{1/C - 1/K_{M-1}}{1/C_{2-S} + 1/K_{1-2}} \qquad \ldots\ldots(66)$$

A knowledge of the basic double layer parameters in the absence of specific adsorption (where $(dq'/dq_M) = 0$, and $q' = 0$) can then be applied in the calculation of the various quantities involved in specific adsorption. Devanathan (18) has shown that there is good agreement obtained between calculated and experimental quantities in the systems potassium halide (aqueous) - mercury and aqueous sodium benzene-m-disulphonate - mercury.

Both Grahame's and Devanathan's models, which are based on the same potential relationship, have been criticised recently on the grounds that their basic relationship has severe flaws (20). When the amount of specific adsorption is small, then for a region far removed from any specifically adsorbed ion it will be correct to consider the dielectric constant of the region between the metal and the OHP. to be constant, and also to set the distance of the OHP. equal to x_2. However, in the neighbourhood of a specifically adsorbed ion, the thickness x_1 will consist of contributions from both the metal and the ion, and ϵ_{M-I} will differ appreciably from ϵ_1. Also, it is a reasonable assumption that the specifically adsorbed ion will retain its primary hydration sheath on the side away from the surface, so that the centre of charge of the first diffuse layer (hydrated) ion will be separated from that of the specifically adsorbed ion by approximately two ionic radii plus the diameter of a water molecule. Thus in such a region the distance to the OHP. will be much greater than it is in a region far removed from specifically adsorbed ions, and the OHP. will not be a plane.

The use of continuous charge distributions in the conventional models of both Grahame and Devanathan is equivalent to averaging the above effects. Such averaging

will be a function of the surface coverage, and so $(x_2-x_1)/x_2$ will be found to depend on q_M. The more rigourous approach to the problem given by Macdonald and Barlow (20) is outwith the scope of this section and will not be discussed. It is of interest to note that the results obtained by employing Grahame's and Devanathan's treatments are frequently much better than would be expected on the basis of the criticisms of Macdonald and Barlow.

Bockris and co-workers (32,32a) have suggested a model of the double layer in which specific adsorption of ions is assumed to be electrostatic in nature, and the capacitance hump is thought to arise from a slowdown in the rate of increase of the charge of anions in the IHP. This model has led to good agreement with experiment, both in predicting the dependence of specific adsorption on the electrode charge and in predicting the properties of the hump.

The remainder of this thesis describes the measurement of the differential capacitance of the double layer at the interface between mercury and solutions of the alkali metal chlorides in formamide, together with measurement of the interfacial tension in the same systems. The results of this work are discussed and interpreted in terms of the components of charge of the double layer in formamide, and a model is proposed to explain the independence of cationic specific adsorption on the nature of the cation.

APPARATUS AND EXPERIMENTAL PROCEDURE

APPARATUS AND EXPERIMENTAL PROCEDURE

The three most accessible parameters of the electrical double layer are the interfacial tension, the charge and the capacitance at the interface. Lippmann (2), who used a capillary electrometer to measure interfacial tensions collected most of the early data on the mercury-solution interface. The classic work of Gouy (3,35) was also carried out using this technique, as was more recent work by, for example, Devanathan and Parsons (36). Interfacial tensions have also been measured, at various times, by the drop weight technique, (37,38), Smith (39) having developed a rigourous theoretical relationship between the drop weight and interfacial tension to replace the earlier empirical relationships. While this method sometimes yields inconsistent results, due mainly to solution creep within the capillary of the dropping mercury electrode, the method is of great use for non-aqueous solvents which do not wet glass sufficiently for the more accurate capillary electrometer to be used. Accurate data have also been derived from measurements made on sessile drops (40).

The major limitation of the above methods is that they can be applied only to liquid metal surfaces. Techniques have been developed for the measurment of the interfacial tension at a solid metal surface, but the data are not as accurate as those described above. Frumkin (41)

devised a method based on the variation of the angle of contact of a gas bubble and a metal surface with changing polarisation of the metal. In the present work, a capillary electrometer has been used to measure the interfacial tension between mercury and solutions of potassium and caesium chloride in formamide.

Several methods are available for estimating the charge of the electrical double layer. If an electrode of constant area is used, the amount of electricity required to change the potential by a given amount is fairly readily measured. So long as the electrode remains perfectly polarised, the only process which draws current is the charging of the double layer capacitor. Measurements using both high current density (42) and low density "equilibrium" charging (43) have been made.

If a charging curve can be obtained at constant current, the capacitance of the double layer can be calculated from the slope of the linear portion (44) since

$$C_o = dq/dE = dq/dt \cdot dt/dE$$

$$= i \, dt/dE \qquad \ldots\ldots\ldots(67)$$

where i is the constant current flowing. Using a technique employing equivalent circuit analogues of electrical impedances, McMullen+Hackerman (45) have been able to measure capacitances too large to be determined by the impedance bridge technique.

For a dropping mercury electrode (d.m.e.), if the rate of formation of fresh interface is known, the charge density may be directly determined from the current flow required to maintain the electrode at a constant potential with respect to the solution. At the potential of the electrocapillary maximum, where the charge density is zero, there will be no charging current. This technique has been employed successfully by Philpot (46) and by Frumkin (47). An electronic circuit which displayed differential capacitance-potential curves on a cathode ray oscilloscope was devised by Loveland and Elving(48). Their method is based on the fact that if a linear potential sweep is applied (ie. $dE/dt = K$) then

$$C_o' = {}^{dq}/_{dE} = {}^{dq}/_{dt} \cdot {}^{dt}/_{dE} = {}^{i}/_{K} \qquad \text{.....(68)}$$

for C_o' the total electrode capacitance. If the area of the electrode at the time of measurement is given by A, then the capacitance/unit area C_o is given by

$$C_o = {}^{i}/_{KA} \qquad \text{.....(69)}$$

A display of charging currents against time is therefore equivalent to a plot of differential capacitance against applied potential.

Using an amplifier of high input impedance, and an oscillograph, Proskurnin and Frumkin (4) measured the voltage produced across a test cell by a known alternating current. If it could be assumed that the impedance of the

test cell was solely due to the capacitance of the test electrode, this quantity, inversely proportional to the output voltage, could be measured. Randles (49) improved on this idea by constructing a phase sensitive instrument which gave data on both the resistive and reactive components of the impedance.

Watanabe (50) used a method employing a resonance circuit to measure the resistance and capacitance of the electrical double layer, the unknown values being determined by substitution of standard resistances and capacitances.

The most accurate method of determining the differential capacitance of an electrode is the direct measurement of impedance using an a.c. bridge network. The first such measurements were made by Wien (51). The electrode impedance was determined with a Wheatstone bridge, the capacitance being balanced out by a variable inductance in series with the cell. The a.c. bridge technique uses a cell containing the test electrode, together with an auxilliary electrode of such large area that its impedance may be neglected in comparison with that of the test electrode. The solution resistance is subtracted vectorially from the cell impedance to give the test electrode impedance. Many investigators have included the double layer impedance in a Wheatstone bridge network (52,53,54,55). In the classic

work of D.C.Grahame, the equivalent circuit used to balance the cell impedance was a series combination of resistance and capacitance.

The conventional Wheatstone networks suffer from a number of disadvantages, the most important being that the accuracy is entirely dependent on a large number of impedance standards, and that some form of Wagner earthing is required. In the description of their apparatus, Hills and Payne (55) consider critically all the modifications which must be made to a simple Wheatstone bridge network to ensure the greatest possible accuracy. Another disadvantage of the conventional bridge is that it is difficult to measure large capacitances on it. Nancollas and Vincent (56) showed that the transformer ratio-arm bridge is a much more suitable instrument. Only one resistive and one reactive standard are involved, no special earthing is required, and the impedance of test leads can easily be eliminated.

The Transformer Ratio-Arm Bridge.

The basic circuit of the transformer ratio-arm bridge (57), is shown in figure 2, and in simplified form below.

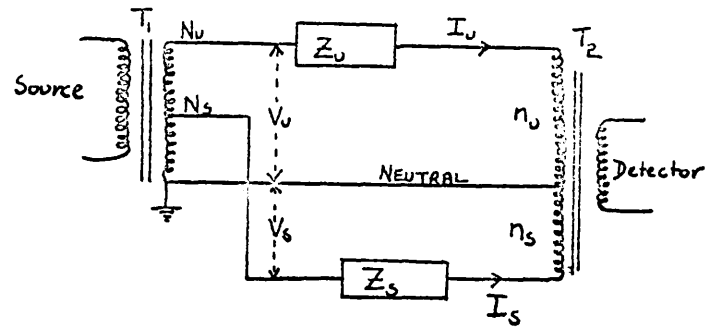

Let Z_u and Z_s be the unknown and standard impedances respectively. T_1 is a voltage transformer, to the primary of which the a.c. source is connected. The secondary winding is tapped to give N_u and N_s turns. T_2 is a current transformer, the primary of which is tapped to give n_u and n_s turns, and the secondary coil is connected to the detector.

Assuming that the transformers are ideal, if the impedance Z_s is adjusted to give a null indication in the detector, zero flux is produced in the current transformer and there is therefore no voltage drop across its windings. The detector sides of both the unknown (Z_u) and standard(Z_s) impedances are therefore at neutral potential. If the voltages across Z_u and Z_s are V_u and V_s respectively,

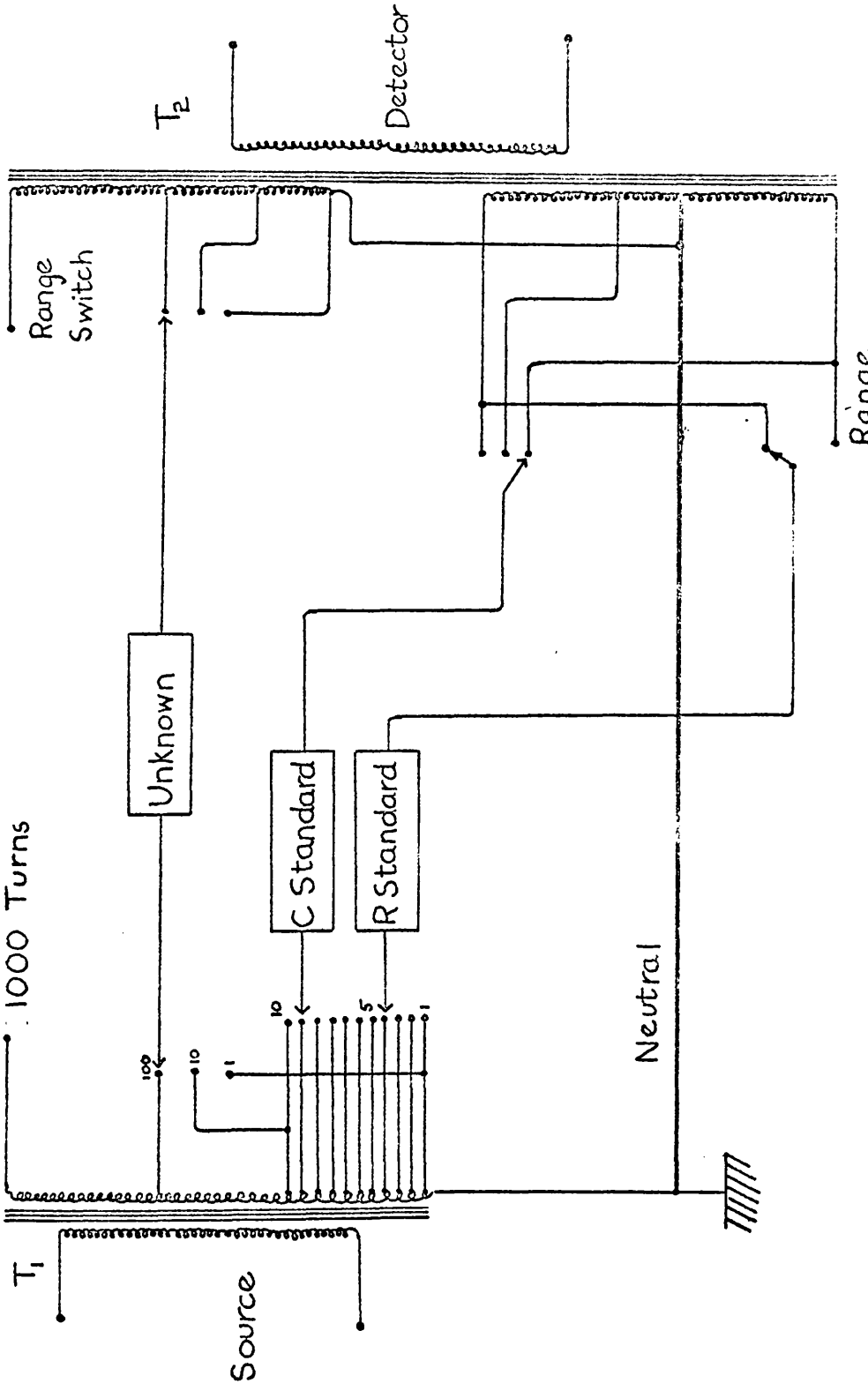

FIG. 2 TRANSFORMER BRIDGE

then the currents through them are given by

$$I_u = V_u/Z_u \quad ; \quad I_s = V_s/Z_s \qquad \text{.....(70)}$$

For zero core flux in T_2, the algebraic sum of the ampere turns must be zero, thus

$$I_u \cdot n_u = I_s \cdot n_s$$

or
$$\frac{V_u \cdot n_u}{Z_u} = \frac{V_s \cdot n_s}{Z_s} \qquad \text{.....(71)}$$

and hence

$$Z_u = \frac{V_u \cdot n_u}{V_s \cdot n_s} \cdot Z_s \qquad \text{.....(72)}$$

For an ideal transformer the voltage ratio is equal to the turns ratio, and hence

$$Z_u = \frac{N_u \cdot n_u}{N_s \cdot n_s} \cdot Z_s \qquad \text{.....(73)}$$

Thus, with suitable tappings on the two transformers, a wide range of measurements can be carried out. Although in practice transformers are not ideal, transmission losses merely reduce the sensitivity. Provided that the coils are precision wound, and that their effective self-resistance is small compared to that of Z_u and Z_s, all the turns embrace the same flux, and hence the ratio of induced voltages is accurately equal to the turns ratio.

Standard impedances may be divided into resistive and reactive components. At balance, both the "in phase" and "quadrature" ampere turns must sum algebraically to zero, and so the resistive and reactive standards must be capable of connection to different tappings to balance out

the currents of the unknown impedance (figure 2). The independance of components is useful in that unwanted impurities in the standards can be balanced out by compensating trimmers in the unknown side of the bridge. An impure capacitor is equivalent to a pure capacitor shunted by a resistance, and the latter can be cancelled by feeding a current, equal to that produced by the resistance impurity, through a fixed trimming resistor into the opposite side of the transformer.

In the Wayne Kerr B221, Universal Bridge used in the present work, transformer tappings are arranged to give two decades, each requiring one resistive and one reactive standard. With a transformer ratio-arm bridge it is possible to add continuously variable controls without detracting from the accuracy of the decade standards. A continuously variable reactance is provided by an air-dielectric capacitor whose residual capacitance is balancedout by a preset trimmer connected to a transformer winding of the opposite sense:

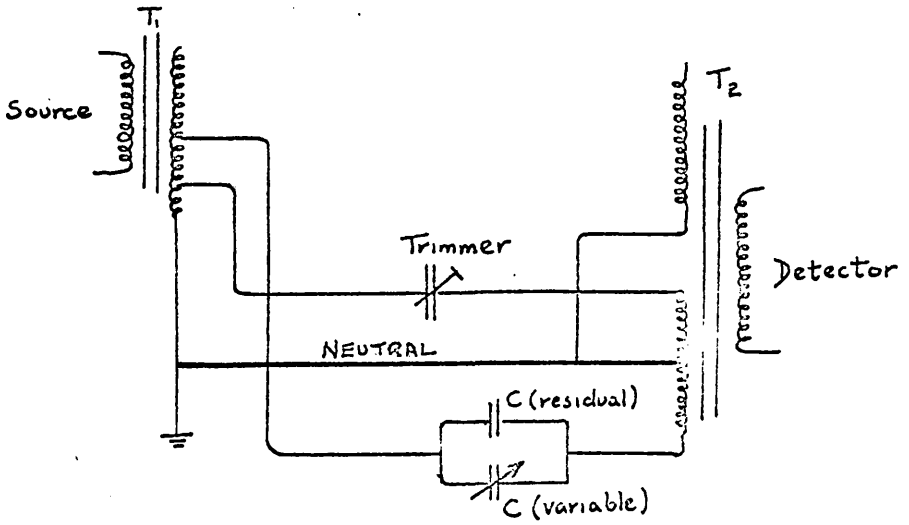

A continuously variable conductance is obtained by connecting a linear potential divider across a few turns of T_1 to produce a variable voltage across a close tolerance resistor:

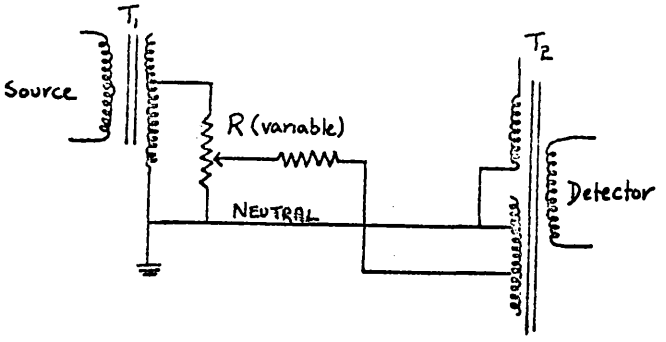

While the voltage transformer is tapped to provide the decade adjustment of each standard, the current transformer is tapped to allow the relative ranges of resistive and reactive standards to be altered. By connecting the unknown to different tappings on both voltage and current transformers, the range of the bridge can be extended above and below that of the standards (figure 2). It should be noted that although one resistive and one reactive standard is required per decade, the transformer ratio may be used to set those in one decade against those in another, so that only one resistive and one reactive fixed standards of known accuracy are required. Finally, in a similar method to that used to purify the standards, any impedance in the external test leads may be compensated. This is an excellent feature of the Wayne Kerr bridge, the "set zero" control

enabling small external impedances in series with the unknown to be trimmed out.

As the transformer ratio-arm bridge operates by summation of currents, it can only measure impedances as a parallel combination of in-phase and quadrature components. Grahame (58) has proposed that the equivalent circuit of the double layer at a polarised d.m.e. is best represented by a resistance and capacitance in series. It is possible to derive an expression relating series and parallel networks, so that results for a parallel network can readily be converted to their series network equivalent. An instrument incorporating a transformer ratio-arm arrangement has been adapted for the measurement of double layer capacitances by Mancollas and Vincent (59) and recently the method has been used by Bockris et al (26).

The Use of an A.C. Bridge for the Measurement of Impedance at a Dropping Mercury Electrode.

A dropping mercury electrode (d.m.e.) consists essentially of a vertical glass capillary tube from which mercury, supplied by a reservoir under a head of about 30cm Hg, issues dropwise. A d.m.e. used as a test electrode has the great advantage over other electrodes that it is constantly renewing its surface, and it is therefore relatively simple to obtain a pure reproducible surface for measurement. The electrode has two major disadvantages in that it requires much more sophisticated electronic techniques to detect bridge balance with an electrode whose impedance is constantly varying with time, and also some method must be developed to evaluate the drop dimensions at the instant of balance. These are related to the time interval between the birth of the drop and the instant of balance. Although this time interval may be measured manually by means of a stop-watch, a more accurate determination is desirable if full use is to be made of the sensitivity of the impedance bridge. A number of methods have been developed for timing this interval, and they fall into two main classes, (1) actual measurement of the interval using a sensitive timing method and (11) adjusting the balance position until the balance occurs exactly at a known time after the birth of the drop.

A number of methods have been described which employ a cathode ray oscilloscope as balance detector. Grahame (53) impressed accurately timed pulses on the time base and thus indirectly measured the time of balance by means of distance on the oscilloscope screen. A similar method was employed by Parsons (60) and Hills and Payne (55) who arranged for the bridge to be balanced at a fixed interval after the birth of the drop. The interval was measured by a crystal controlled electronic timer which emitted a pulse into a double beam cathode ray oscilloscope. By displaying bridge output on the other beam, bridge balance could be made to coincide with the timer output pulse.

Randles (54) used a tapping-off device to give drops of constant lifetime. The relative birth-balance interval as compared with the drop lifetime, was found by adjusting the time constant of a fixed capacitor in such a way that its discharge time could equal either the former or the latter. Here again visual detection of balance was involved. Such procedures have inherent disadvantages in use. In the present work, the apparatus was basically similar to that developed by Nancollas and Vincent (59,61) employing a transformer ratio-arm bridge as the impedance bridge, and electronic circuits which permitted the direct measurement of the birth-balance interval.

Self Timing Bridge Method for Measuring the Impedance of a Dropping Mercury Electrode.

A block diagram of the apparatus is given in figure 3. A d.c. polarising voltage was applied between the d.m.e. and a reference electrode, C. Large blocking capacitors prevented d.c. from entering the transformer ratio-arm bridge, which was connected to the d.m.e. and a platinum mesh sphere of large area which served as an anode. The transformer ratio-arm bridge was used together with a variable frequency audio frequency generator, an amplifier and a " balance detector ", a device which emitted a pulse whenever the bridge was balance. Another unit, the"birth detector " gave out a pulse coincident with the birth of each mercury drop. The pulses were fed into an " interval timer " which accurately measured the time interval between them.

Interval Timer.

The Ericsson interval timer, type 103C, was essentially a device for counting the number of cycles of a known reference frequency occuring during the time interval being measured. Since the maximum error in the counting process is ±1 cycle, the instrumental accuracy is essentially that of the reference frequency. As this was provided by a 100 Kc./sec crystal oscillator with an error of less than 0.005%, a time interval of one second could

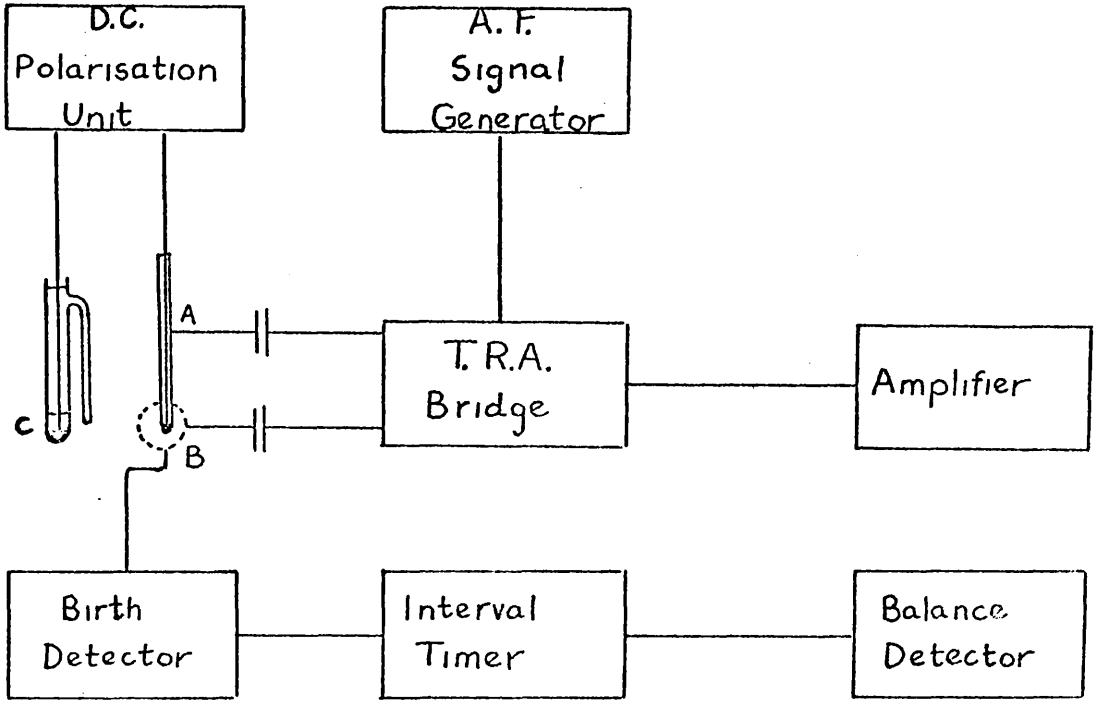

FIG 3 BLOCK DIAGRAM

be measured to within approximately 0.1msec. The start and stop switches were Eccles - Jordan triggers activated by positive and negative pulses of minimum amplitude 10 volts and minimum mean duration 20μsec.

Balance Detection.

The capacitance of a sphere can be expressed in terms of its radius, and it can be shown that for two concentric spheres of almost equal radii, the capacitance is directly proportional to the surface area. This is true when the space between the spheres is filled with a medium of uniform dielectric constant, or whose dielectric constant varies in an identical fashion along any radius. The resistance between two spheres of radius r_1 and r_2 is given by $R = \frac{\sigma}{\pi}(\frac{1}{r_1} - \frac{1}{r_2})$ where σ is a constant. Thus, if r_2 is very large compared to r_1 the resistance is inversely proportional to the radius of the smaller sphere.

Since during the life of a drop of mercury its radius increases as a characteristic function of time, the capacitative component of the double layer increases, while the resistive component decreases, as monotonic functions of time. Thus, as is shown in figure 4, any given balance position can occur at only one instant in the life of the drop, while at any one instant the impedance of the double layer has a unique value.

The bridge source frequency was provided by an

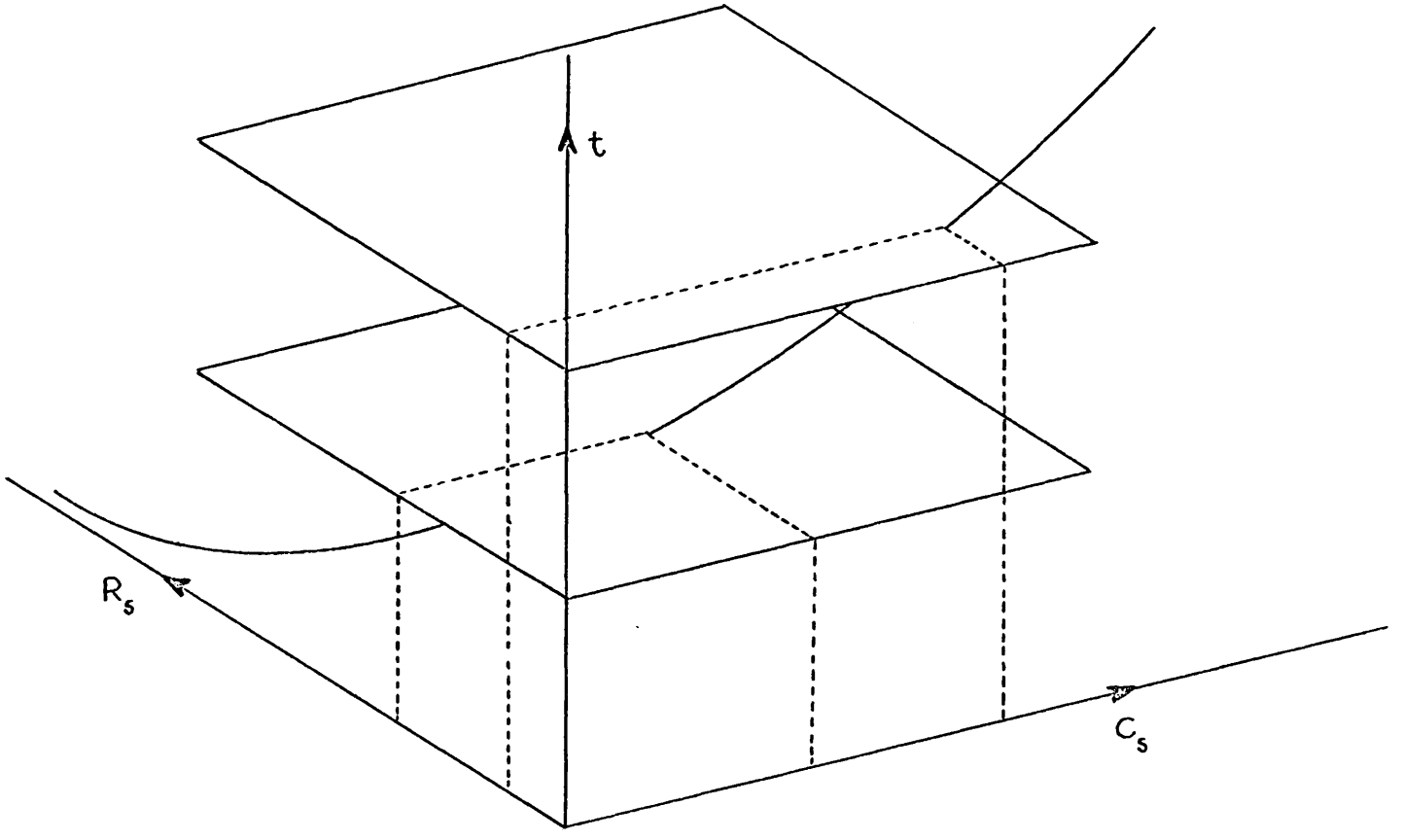

FIG. 4 VARIATION OF ELECTRODE IMPEDANCE WITH TIME

Advance, model H1, variable frequency audio signal generator whose output was controlled so that not more than 10 mv were impressed across the unknown. When the transformer ratio-arm bridge was out of balance a sinusoidal waveform was emitted from the detector, the secondary winding of T_2 (figure 2). As the bridge was brought into balance, the amplitude of this signal decreased from around 0.5 volts to a null of about 5μvolts. Because of the time dependence of the electrode impedance, the bridge gave out an amplitude modulated signal having minima at the instants at which the electrode impedance was closest to the bridge standard impedance. If the bridge was exactly balanced, resistively and reactively, at a point during the life of the drop, the minimum had an amplitude equal in magnitude to the null signal.

The signal output by the bridge required amplification before being fed into the balance detector. The amplifier, built by Elesco Electronics (Development) Ltd., could be accurately tuned to the signal frequency, and had an overall gain of 10^7. It incorporated automatic gain control (A.G.C.) which had a variable threshhold in order to facilitate coarse balancing of the bridge. When the A.G.C. was operative, a high bridge output biased the valves in such a way as to reduce their output, whilst a lower bridge output resulted in less attenuation. By

withholding the A.G.C. bias until the signal had reached a certain level, the region around the balance point could be strongly amplified. The A.G.C. unit consisted of four variable-μ stages with two straight stages providing feedback. To give the amplifier its highly selective frequency response, the A.G.C. amplifier output was fed into a three stage amplifier, tuned to the frequency of the measuring signal by means of feedback through bridged-T networks. A separate cathode-follower input stage and head amplifier was connected by a short coaxial lead to the secondary of the transformer ratio-arm bridge to minimise the loss of bridge output. The output from this unit was then fed into the A.G.C. amplifier. The amplifier was set up by using the A.G.C. threshhold level controls, filter selector, tuners and a feedback control. Three outputs were provided, a high level limited output for use as the trigger potential in the balance detector, a low level output to enable the amplified bridge output to be monitored continuously on a cathode ray oscilloscope, and an unlimited output which could also be used for monitoring purposes. This monitoring provision was of extreme importance in avoiding a false balance, and also enabled bridge balancing to be carried out quickly, as any capacitive or resistive unbalance was readily apparent. Monitoring of the output also gave an immediate

indication of the existence of any noise or harmonics in the output signal, and thus facilitated tuning of the amplifier selectively to the bridge frequency. The three major criticisms of this method put forward by Hills and Payne (55) can thus be avoided easily due to this visual monitoring provision, as the balance can be seen to occur. Since the actual location of the precise balance point is by electronic sensing of the minimum and not simply a process of visual judgement, the accuracy should be greater than that possible by purely visual techniques.

The circuit of the balance detector is given in figure 6. The out-of-balance voltage from the amplifier was fed into a full-wave diode bridge rectifier through a 1:1 balanced and screened transformer, (Sullivan 856), which eliminated any d.c. level in the signal. The crystal diodes were Mullard type OA81. The rectified signal was collected in one of four reservoir capacitors $C_1 - C_4$, chosen to have a suitable time constant for discharge through VR_1. The discharge rate was chosen as in A (figure 5) so that it was not so large that the d.c. level fell off to the null value between signal cycles (B in figure 5) giving a false balance indication, nor so small that the real balance point was missed (C in figure 5). The selection of the time constant, using S_1 and VR_1 (figure 6) was governed by:

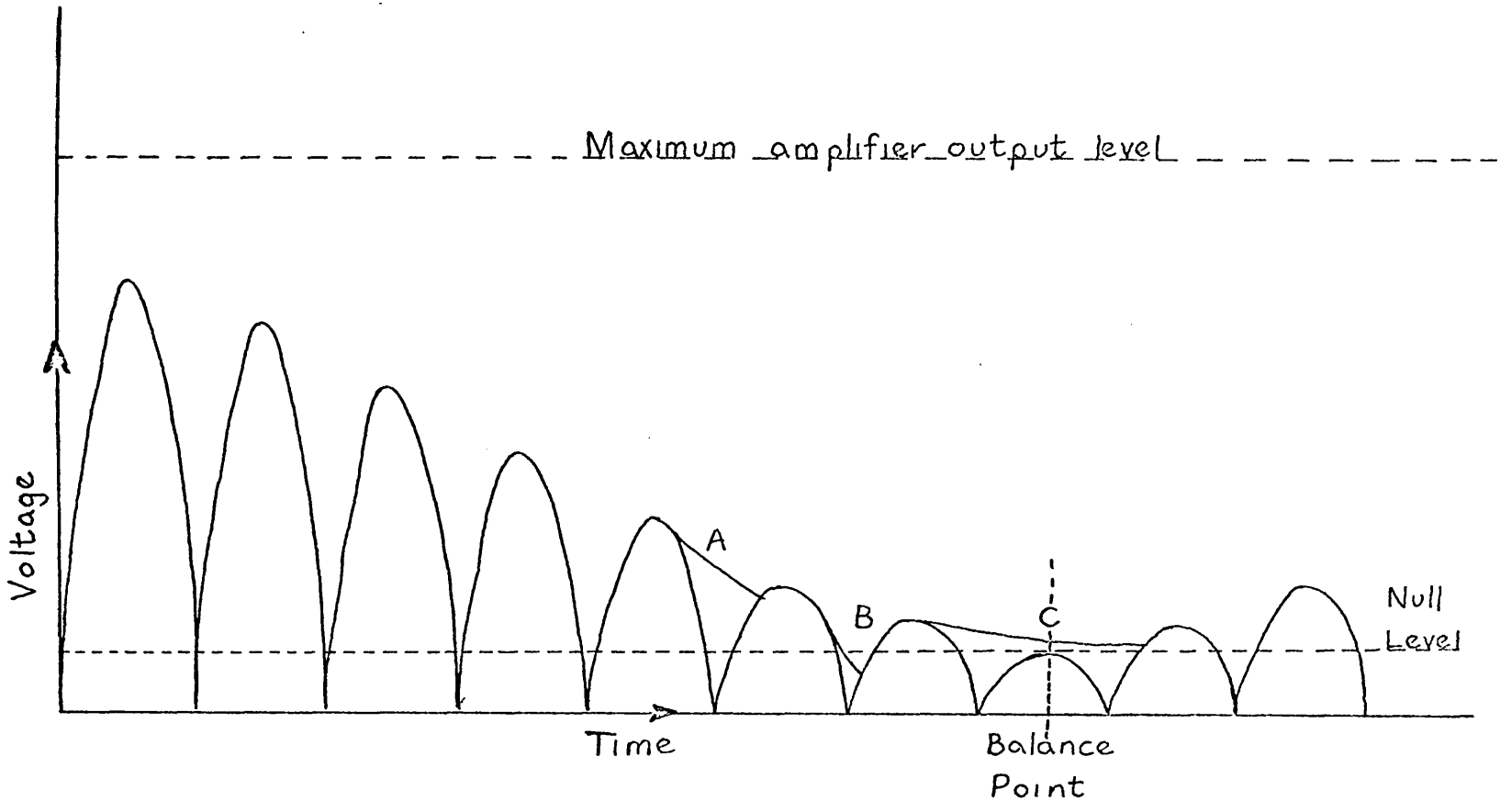

FIG. 5 RECTIFIED AMPLIFIER OUTPUT NEAR BRIDGE BALANCE.

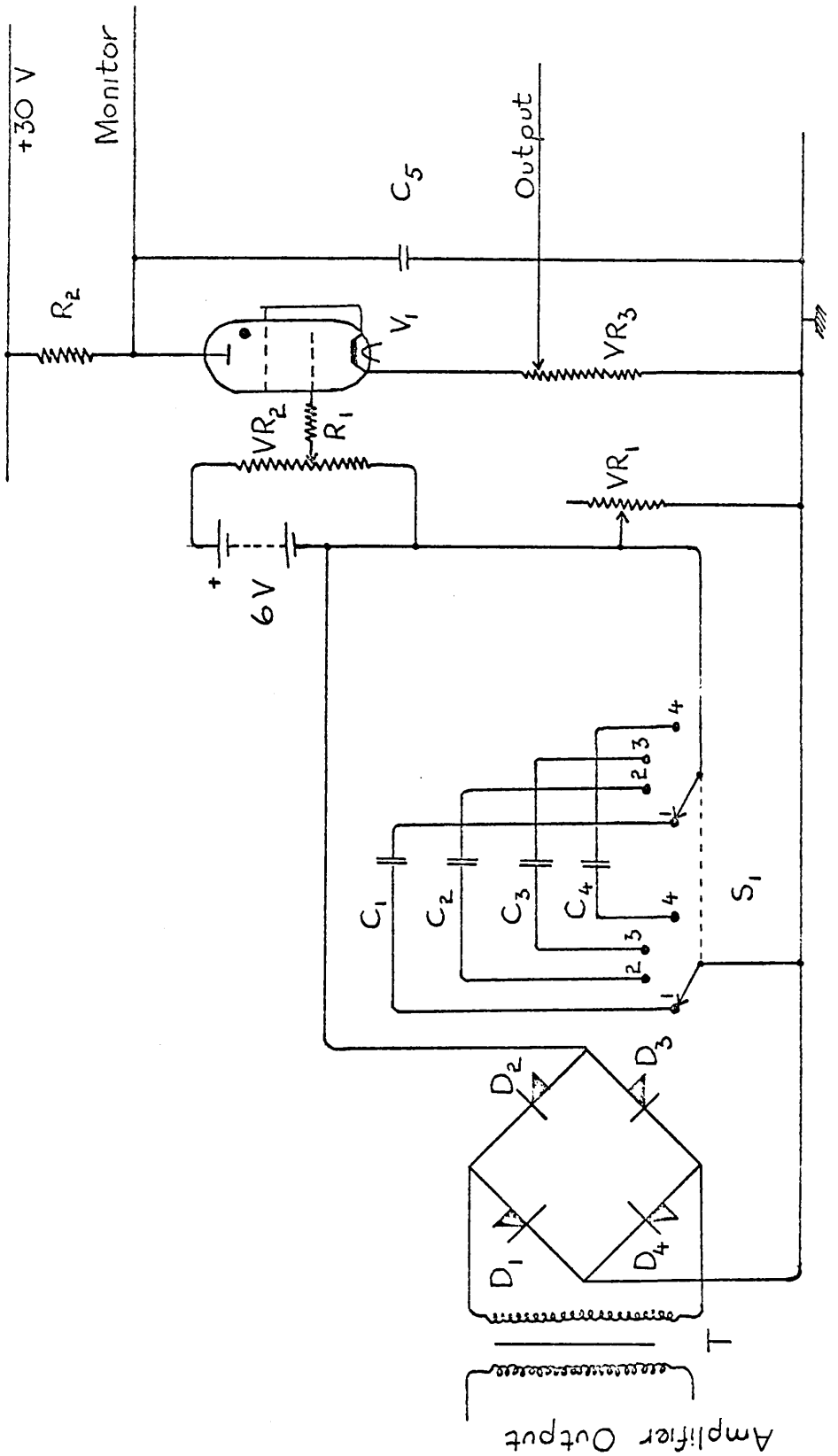

FIG. 6 BALANCE DETECTOR

Figure 6. BALANCE DETECTOR.

Components.

R_1 : 10 KΩ

R_2 : 4.7 KΩ

VR_1 : 152-506 KΩ

VR_2 : 0-100 KΩ

VR_3 : 0-100 Ω

C_1 : 700 pF

C_2 : 0.002 μF

C_3 : 0.005 μF

C_4 : 0.01 μF

C_5 : 0.5 μF

V_1 : CV 4018

$D_1 - D_4$: OA 81

T : 1:1 Sullivan (856).

(a) The frequency of the bridge measuring signal and
(b) the rate of change of electrode impedance.

The d.c. signal was then applied to the thyratron control grid in series with a backing potential provided by the potential divider VR_2 connected across a 6 volt dry battery. A grid stopper R_1 of resistance 10KΩ sharpened the critical point of the valve. Once a thyratron has struck, the grid loses control, and to halt discharge the anode voltage must be reduced to below about 10 volts. This was accomplished by controlling the anode H.T. supply by means of an R-C combination of relatively long time constant ($R_2 - C_5$: 2.5msec). In effect, this part of the circuit is a monostable multivibrator. The stable state occurred when the anode voltage was below the striking value for the applied grid voltage, and the capacitor C_5 was charged to H.T. potential.

When the grid potential was made more positive, the thyratron struck, discharged C_5, causing it to extinguish and return to its stable state. Since the discharge current was limited mainly by the small cathode resistor, VR_3, of 100Ω, the discharge time for C_5 was short. A sharp pulse was therefore obtained from VR_3 which was suitable for activation of the stop gate of the interval timer. The thyratron was a CV4018 with the screen grid connected to the cathode. The H.T. supply was 32 volts, obtained

by transforming mains a.c., rectifying with a full wave silicon rectifier, and smoothing with a π filter to give less than 100mv of 50 c.p.s. ripple.

Bridge Standardisation.

Since it was necessary to polarise the d.m.e. with respect to the solution, the transformer ratio-arm bridge had to be isolated from the d.c. polarisation circuit. This was accomplished by placing a 1000μF blocking capacitor in each measuring arm, in series with the cell impedance (figure 7). The error so introduced can be computed, but it was more convenient to compensate for the blocking capacitors, and, at the same time, for the impedance of the coaxial leads, by using the bridge trimmers. An accurate parallel combination of resistance and capacitance, (1.003 KΩ, 0.4732μF) maintained at 25°C ± 0.05°C could be connected to the bridge through coaxial leads identical to those leading to the cell. The bridge readings were then set exactly to the value of the standard impedance, and a null was obtained using the trimming controls on the bridge. The potential divider VR_2 (figure 6) was adjusted so that the thyratron just struck. By altering the main bridge controls in either direction, it could be confirmed that the thyratron ceased conduction on both sides of balance. It was possible to confine the "in-balance" signal to a region smaller than 0.05% of the total

impedance measured. As an added precaution, the standard impedance could also be connected to the bridge by means of very short leads. This enabled its impedance to be checked against the bridge primary standards at monthly intervals to guard against any drift due to ageing.

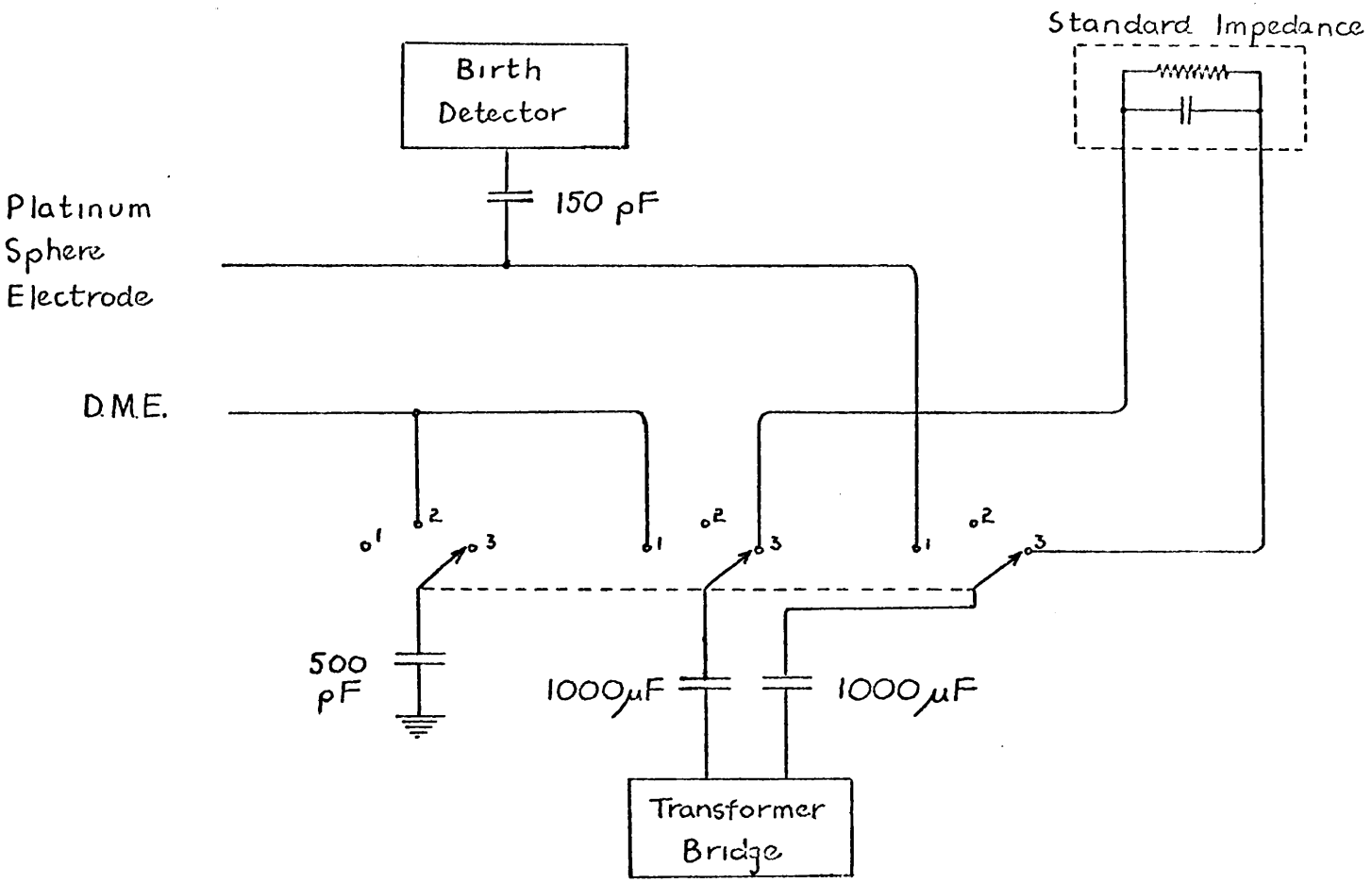

FIG. 7 BRIDGE STANDARDISATION

Drop Birth Detector.

The drop birth detector (figure 8) consisted of a 4.5Mc/sec Hartley oscillator, the coil of which had a secondary winding connected through a 150pF capacitor to the platinum gauze electrode in the cell. While the mercury drop was growing, the oscillator was damped by the relatively low internal impedance of the cell. At the moment of drop detachment, however, the impedance of the dropping circuit rose instantaneously to a very high value, and a rapid burst of oscillations resulted. A radio frequency path to earth was provided by a 500pF capacitor connected to the d.m.e. (bridge selector switch, position 2, figure 7). This was disconnected when the electrode impedance was being measured (switch position 1, figure 7). When the bridge selector switch was in position 2, the transformer ratio-arm bridge was disconnected from the electrodes, a necessary precaution during birth detection since otherwise there was a low impedance radio frequency path to earth through the bridge. The surge of oscillations resulting from drop detachment was amplified by a pentode with tuned anode, the anode coil being transformer coupled to the diode V_2. C_5 and R_3 were a decoupling circuit. After being rectified by V_2 the radio frequency component of the signal was filtered out by the C_7-R_6-R_7 network, and then applied by C_8

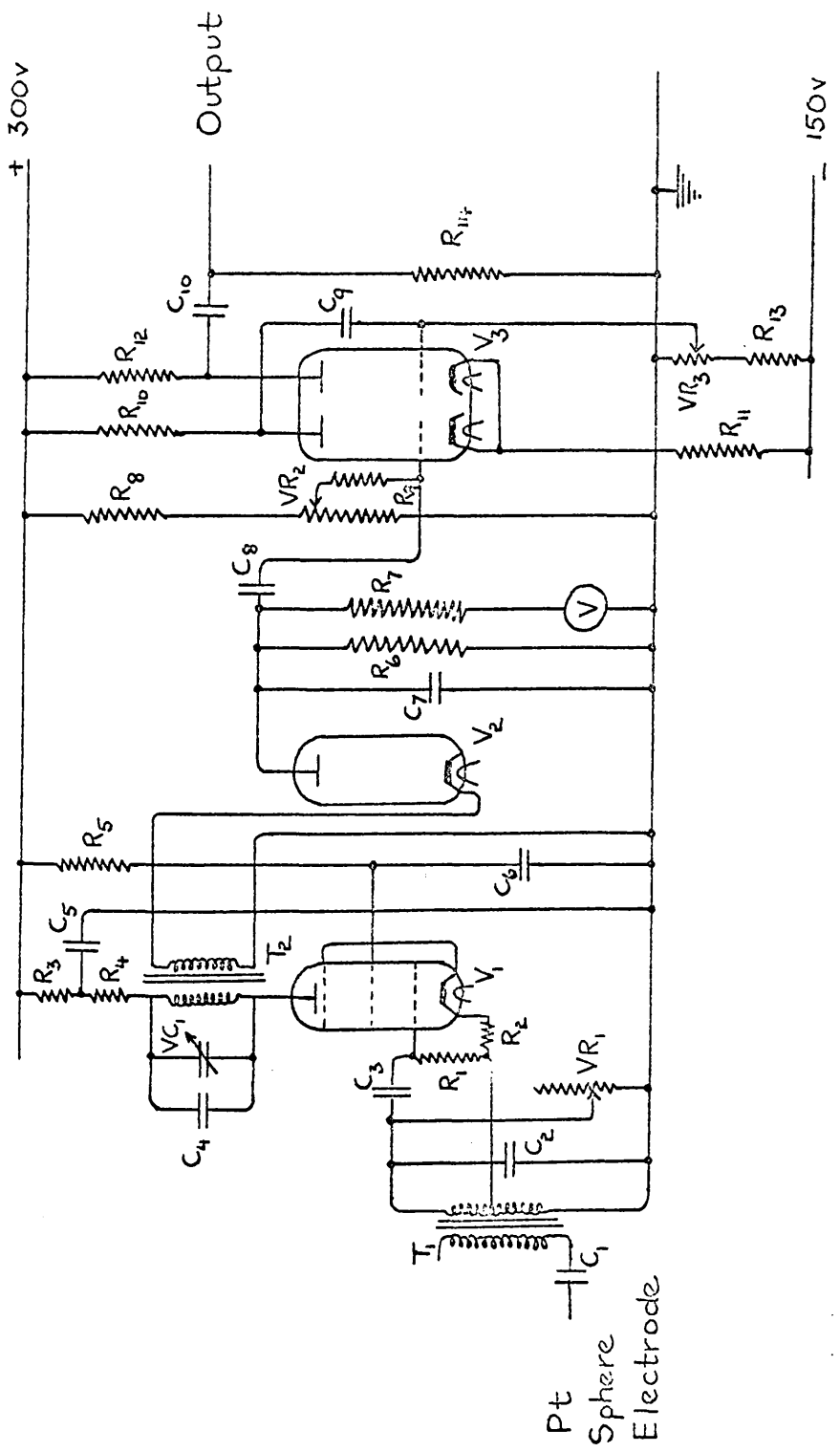

FIG. 8 DROP BIRTH DETECTOR

Figure 8. BIRTH DETECTOR.

Components.

R_1 : 10 KΩ	R_7 : 33 KΩ	R_{13} : 47 KΩ
R_2 : 330 Ω	R_8 : 560 KΩ	R_{14} : 100 KΩ
R_3 : 100Ω	R_9 : 33 KΩ	VR_1 : 0-550 KΩ
R_4 : 100 KΩ	R_{10} : 1.2 KΩ	VR_2 : 0-100 KΩ
R_5 : 47 KΩ	R_{11} : 20 KΩ	VR_3 : 0-50 KΩ
R_6 : 33 KΩ	R_{12} : 10 KΩ	

C_1 : 150 pF	C_5 : 0.01 μF	C_9 : 0.47 μF
C_2 : 150 pF	C_6 : 0.005 μF	C_{10} : 500 pF
C_3 : 100 pF	C_7 : 470 pF	VC_1 : 0-200 pF
C_4 : 100 pF	C_8 : 0.01 μF	

V_1 : CV 4014

V_2 : CV 4007

V_3 : CV 4024

T_1 : 32 turns, ferrite core, 1 cm diam. Polythene former.

T_2 : 32 turns, ferrite core, 1 cm diam. Polythene former.

to a control grid of the double triode V_3. This valve operated as a monostable multivibrator, and gave out a sharp pulse. A final differentiation circuit, C_{10}-R_{14}, then limited the pulse width to 50μsec, ensuring that it would activate only the start gate of the timer if both start and stop gates were linked. In this condition, the timer was used to measure accurate drop lifetimes by making use of two successive pulses from the birth detector. A three position switch allowed selection of stop signals.

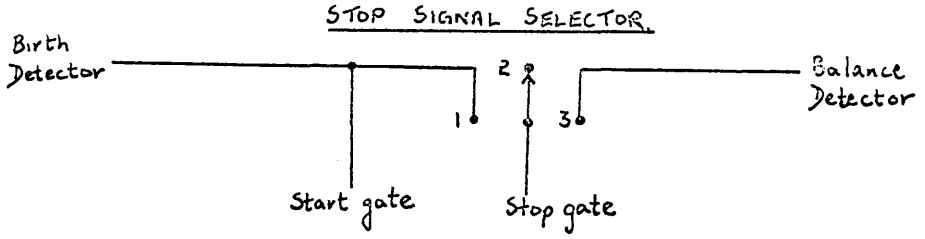

Position	1	Drop Lifetime
"	2	Stop small gate open
"	3	Birth-balance interval.

VR_1 acted as an internal oscillation damping control, and was set in accordance with the impedance of the cell solution. Incorporation of a voltmeter facilitated the setting of VR_1, and also provided a useful visual check of proper d.m.e. function.

D.C. Polarisation Unit.

The circuit used to charge the growing mercury drops to a fixed static potential with respect to a reference electrode is shown in figure 9. A twelve volt bank of lead-accumulators was connected to a linear 1000Ω Helipot in series with a linear 50Ω potential divider. Two 150 H chokes were placed between the electrodes and the charging circuit to isolate bridge a.c. from the latter. While the error in measured electrode impedance caused by neglecting this parallel d.c. circuit was less than 0.05% at a bridge frequency of 1Kc/sec, measurements at lower frequencies would require allowance to be made for it. The circuit also incorporated a microammeter so that any deviation from perfect polarisation, caused by an electrode reaction such as reduction of ions or solvent decomposition, could be detected: the maximum charging current was of the order of 1μA. Because of the large inductive impedance of the microammeter, it was necessary to ensure that it was not in circuit during measurement of the electrode impedance.

The polarisation potential could be applied between the d.m.e. and either a reference electrode or a mercury pool anode. Accurate adjustment of the applied potential was made by switching in a potentiometer as shown in figure 9. The potentiometer, Tinsley type 3387B, was used in

conjunction with an Electronic Instruments Ltd. Vibron Electrometer (model 33B) as null detector. This electrometer was especially useful when the internal impedance of the cell was high. Although it could be used directly for measuring potentials of 0.0 - 1.0 volts in its least sensitive range, it was normally used as a null instrument with 100m volt or 300m volt full scale deflection, in conjunction with a "backing potential" provided by the Tinsley potentiometer. The latter was standardised with a saturated Weston cell (Sangamo Weston Ltd., model S134) of internal resistance 600Ω and mean e.m.f. 1.0186 volts at 20°C. Since the a.c. voltage across the cell never exceeded 10m volts, there was effectively no interference with the applied polarisation potential.

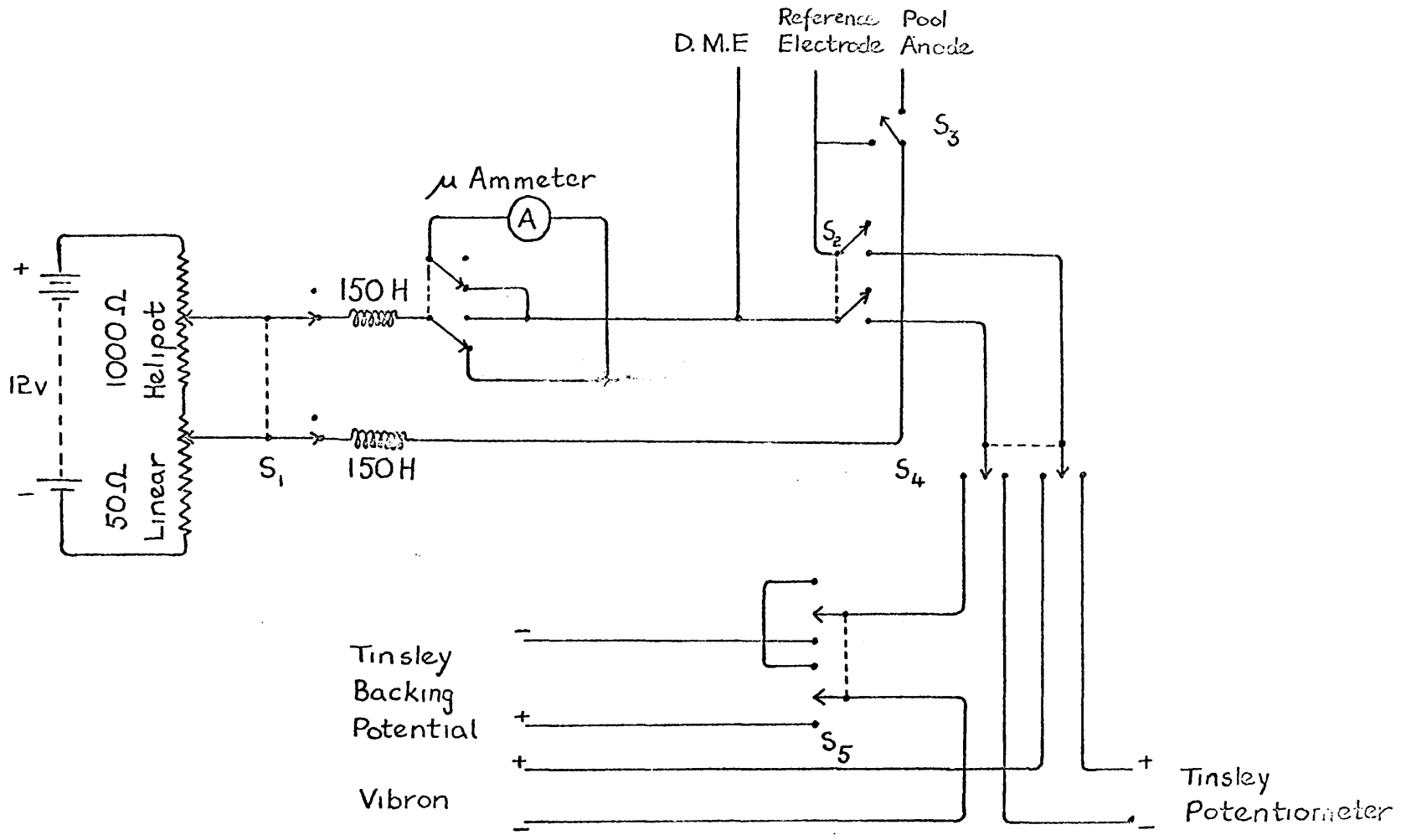

FIG. 9. D.C. POLARISATION UNIT.

Audio Frequency Standardisation.

The frequency of the audio signal generator, required for the parallel to series conversion, was standardised by comparing it with the sub-standard frequencies generated by the crystal oscillator in the interval timer. The latter produced pulses at rates of 10^n p.p.s. where n is an integer between -1 and +5. Initially, a generator signal frequency was chosen close to 10^n c.p.s. This was displayed together with the signal from the interval timer on a double beam oscilloscope whose time base was synchronised with the timer pulses. The model used, Cossor 1035, has a common time base for both beams, and thus both traces appeared stationary when the generator frequency was identical to the pulse repetition rate of the timer signal. As the audio generator became very stable after several hours running, it was possible to obtain a frequency accurate to within 0.01% of the standard frequency. If required, the long term stability could be checked by feeding the generator output into the "External Frequency" channel of the interval timer and thus counting the number of cycles over a long period. Though the stability of the generator was verified by the above tests, under normal circumstances the frequency was checked periodically during a run.

Pulse Counter.

This instrument, which could count pulses with a low repetition rate was used:
(1) to extend the range of the interval timer above 10sec by making use of the pulse given out by every 10sec.
(11) to enable drop count to be made, using the 'one pulse per drop' produced by the drop birth detector.

The circuit of the counter (figure 11) consisted of a thyratron trigger unit, a Post Office electromechanical relay and associated power supplies. The counter was able to register up to 9999 drops, and extend the range of the interval timer by a factor of 10^4. The trigger circuit was activated by positive pulses such as those produced by the interval timer. Since the birth detector emitted negative pulses, however, (as opposed to balance pulses which were positive) it was necessary to invert the phase before using them to activate the counter. A complete circuit of the phase invertor and pulse switching unit is given in figure 10.

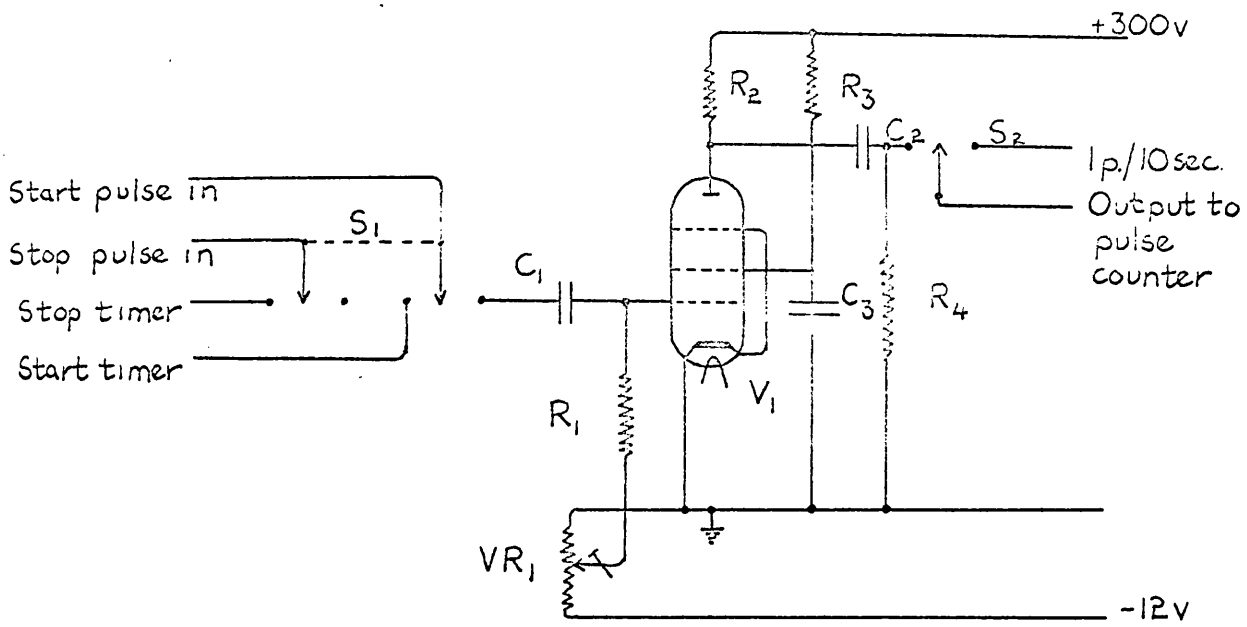

FIG. 10 PHASE INVERTOR AND PULSE SELECTOR

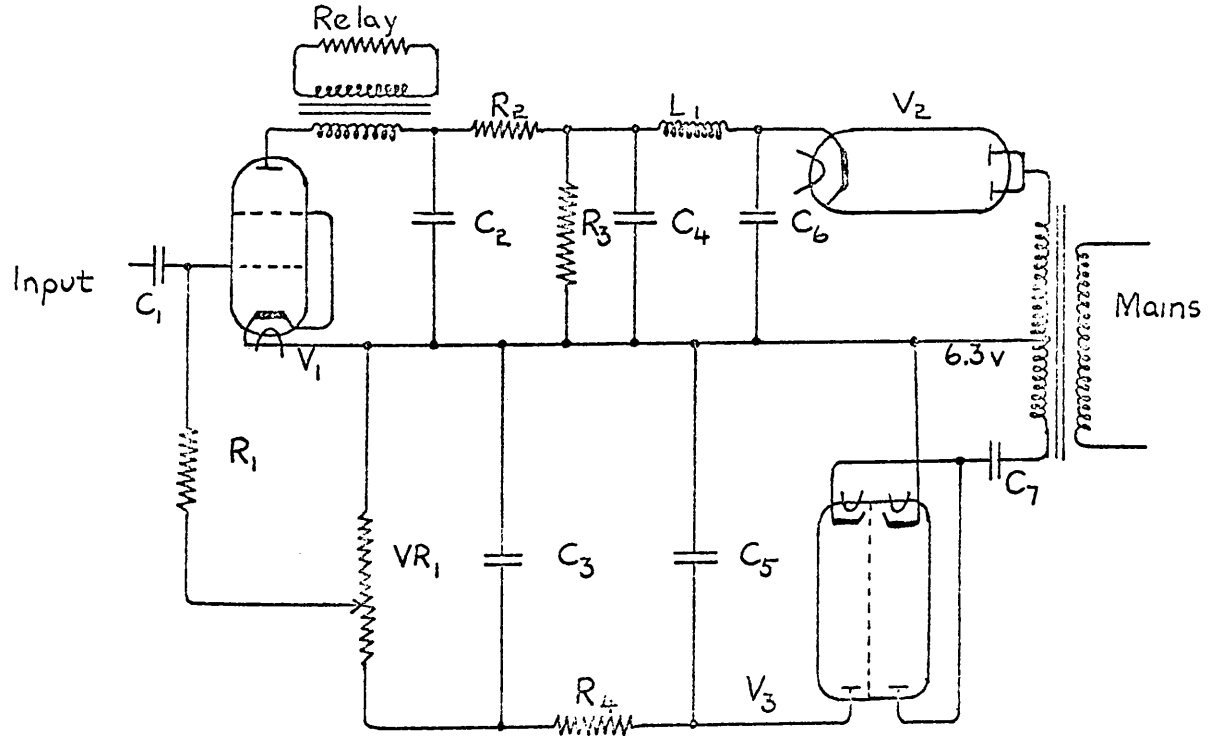

FIG. 11 PULSE COUNTER

Figure 10. PHASE DETECTOR AND PULSE SELECTOR.

Components.

R_1 : 470 KΩ
R_2 : 22 KΩ
R_3 : 120 KΩ
R_4 : 100 KΩ
VR_1 : 5 KΩ

C_1 : 0.1 μF
C_2 : 0.047 μF

V_1 : CV 4014

Figure 11. PULSE COUNTER.

Components.

R_1 : 100 KΩ
R_2 : 1.5 MΩ
R_3 : 47 KΩ
R_4 : 2 KΩ
VR_1 : 2 KΩ
V_1 : CV 4018
V_2 : CV 4005
V_3 : CV 140 (283)

C_1 : 0.15 μF
C_2 : 0.5 μF
C_3 : 25 μF
C_4 : 24 μF
C_5 : 25 μF
C_6 : 16 μF
C_7 : 25 μF
L_1 : 10 H.

Monitoring.

During an experiment the amplifier output and balance detector signal voltages were monitored continuously on a Solartron double beam cathode-ray oscilloscope (type CD10142). It was also found convenient to monitor certain other signals periodically. This was done on a Cossor (type 1035) cathode-ray oscilloscope, and an input selector was built for this to facilitate rapid checking.

C.R.O. INPUT SELECTOR.

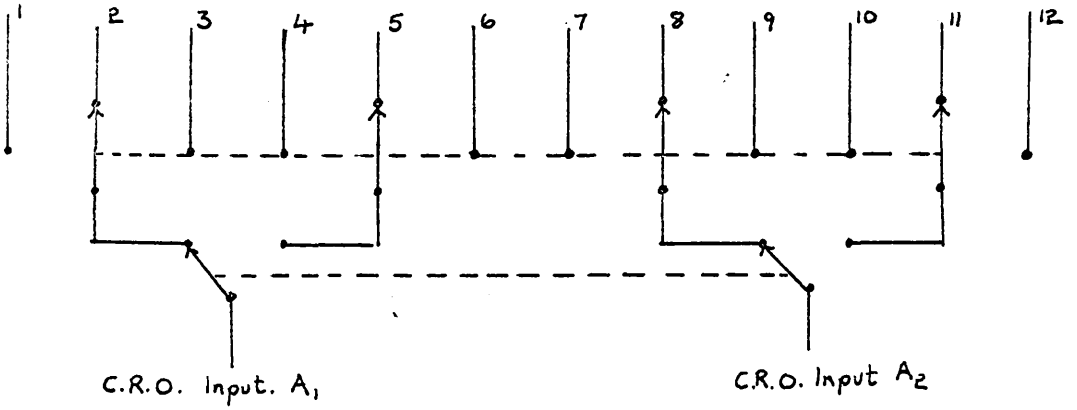

1. 10^3 p.p.s.
2. Unlimited amplifier o/p
3. 10^4 p.p.s.
4. Birth pulse
5. -
6. Unlimited amplifier o/p
7. A.F. signal generator o/p.
8. Balance Pulse
9. A.F. signal generator o/p
10. Balance pulse
11. Unlimited amplifier o/p
12. -

The Differential Capacitance Cell.

The cell, illustrated in figure 12 and plate 1 was constructed of pyrex glass, and had a capacity of about 75 ml. The cathode was a fine glass capillary from which mercury issued in the form of drops at the centre of a hollow spherical anode of platinum gauze. This made contact with the exterior by means of a platinum wire sealed into the glass and extending into the side arm E (figure 12) which was filled with mercury. Two small holes in the sphere, 180° apart, allowed for the insertion of the capillary at the top, and the escape of mercury at the bottom. The mercury fell into cup H, which could be emptied into a collection vessel I by turning the Teflon tap J. The mercury collection vessel was attached to the main part of the cell by a B10 joint and was held in position by two springs attached at one end to a brass collar, and at the other to the outside of the tap. Mercury in the collection vessel could be transferred to a weighing bottle G by pumping air down the side arm F. Solutions in the cell were de-oxygenated by bubbling pre-saturated, oxygen-free nitrogen through the cell from arms A or B and allowing the gas to escape through a conventional bubbler attached to side arm C. Provision was made for use of a mercury pool anode: the mercury occupied the annular region around cup H and electrical contact was

made with it by way of a glass-sealed platinum wire inserted in arm A. Side arm D was used to house the reference electrode or salt bridge, and all side arms terminated in B10 sockets.

Fine capillaries, external radius $\sim 3 \times 10^{-2}$ cm, internal radius $\sim 2 \times 10^{-3}$ cm were drawn from thick walled pyrex tubing which had been cleaned in a mixture of nitric and sulphuric acid, washed thoroughly with conductivity water and then dried in an oven. Suitable capillaries gave a droprate of over 5 sec in conductivity water when under a 30 cm head of mercury. Acceptable capillaries were then joined to B14 air bleeds in an atmosphere of dust free nitrogen. A B14 - B34 adaptor completed the connection to the top of the cell, and the mercury reservoir (capacity 4Kg) was attached to the capillary at K by means of a short length of carefully cleaned polythene tubing to facilitate insertion and withdrawal of the capillary. The reservoir was connected to a long vertical tube of bore 1 cm to enable the height of the mercury head to be determined. An illuminated screen was placed behind this tube and the mercury head observed on a cathetometer reading to ± 0.001 cm. In order to maintain a constant height of mercury, a special clamp was used to attach the reservoir to the clamp stand. A very fine screw control allowed fine adjustments to be made to the mercury level. Electrical

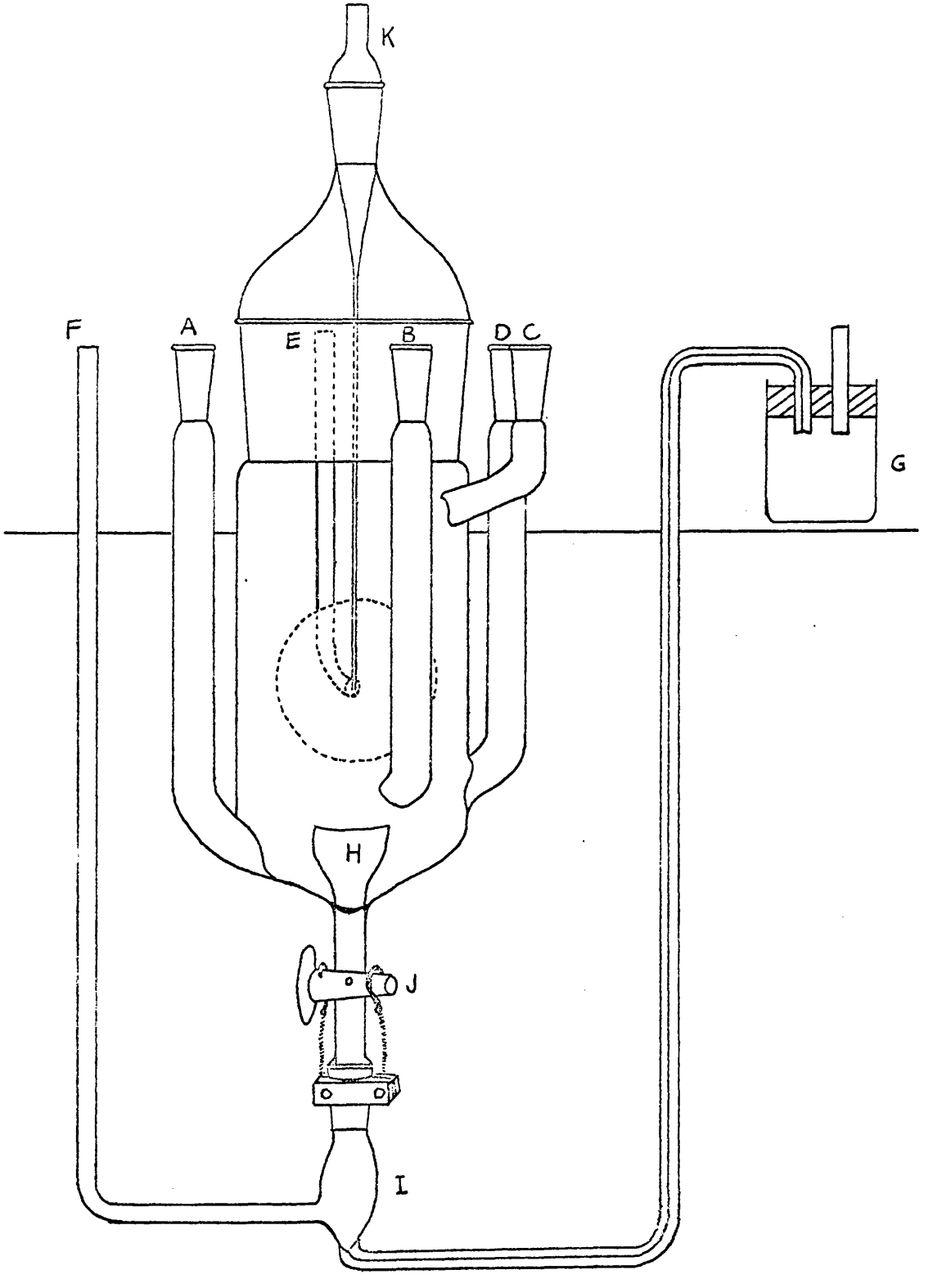

FIG. 12 THE CAPACITANCE CELL

contact was made with the mercury by means of a platinum wire sealed in glass.

Temperature Control.

The cell was immersed in a tank of water thermostated with a "Circotherm" thermostatic unit which maintained the tank within ±0.05°C of the required temperature. For work at low temperatures, a copper coil through which refrigerant could be passed was immersed in the tank. The thermostat was switched off during an actual measurement to prevent any effects due to vibration.

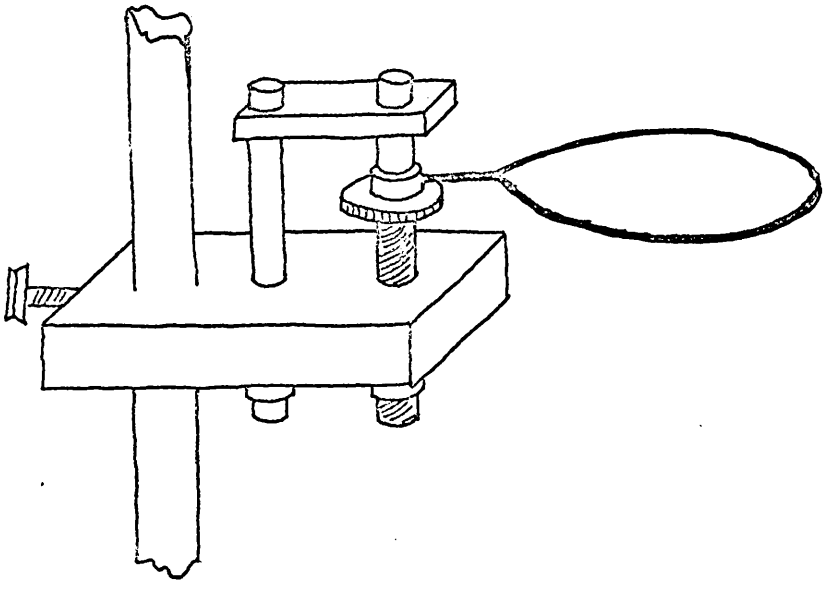

Reservoir clamp.

PLATE 1.

THE DIFFERENTIAL CAPACITANCE CELL.

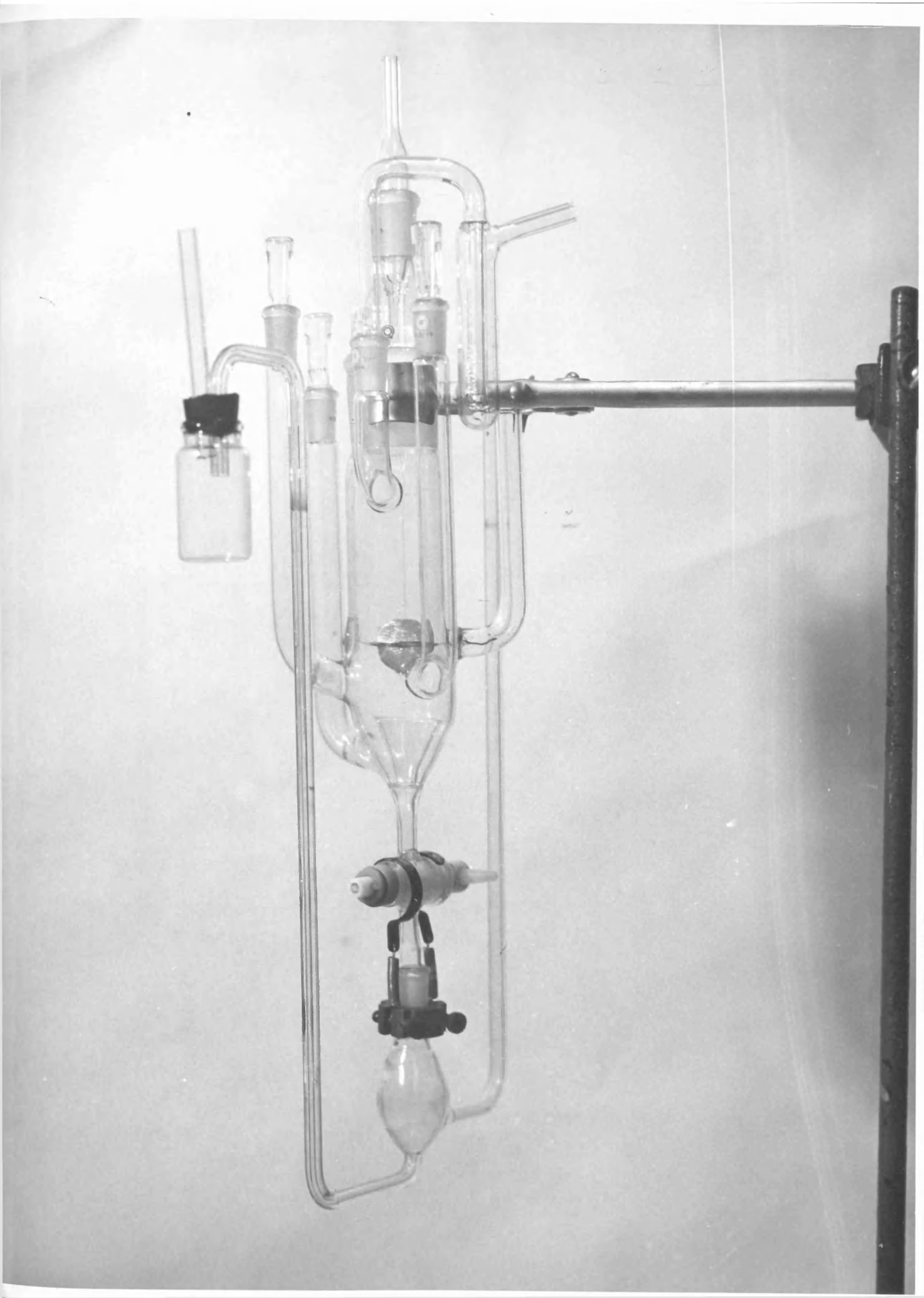

Electrocapillary Apparatus.

The capillary electrometer is basically a very simple apparatus which requires little more than a source of d.c. polarising voltage, a mercury capillary, a pressurising system for the mercury and some means of determining the pressure required to maintain the mercury in the capillary at some convenient reference point. In recent years a considerable amount of work has been carried out using the capillary electrometer. Conway and Barradas (62) give much useful information on the optimum operating conditions. In the present work, the following apparatus, shown schematically in figure 13 was used.

D.C. Polarisation.

The d.c. polarisation was provided by a twelve volt bank of lead accumulators connected to a linear 1000 Ω Helipot in series with a 50Ω linear potential divider. The circuit also incorporated a microammeter so that any deviation from perfect polarisation could be detected. When the mercury was allowed to drop freely, the maximum charging current was of the order of 1μA. When measurements were being performed, the microammeter was switched out of the circuit. Accurate adjustment of the potential was made by switching in a potentiometer (figure 13). The potentiometer used was a K3 Leeds and Northrup

Universal Potentiometer, used with a Leeds and Northrup D.C. Null Detector. The high resistance of the null detector effectively prevented any polarisation due to this circuit.

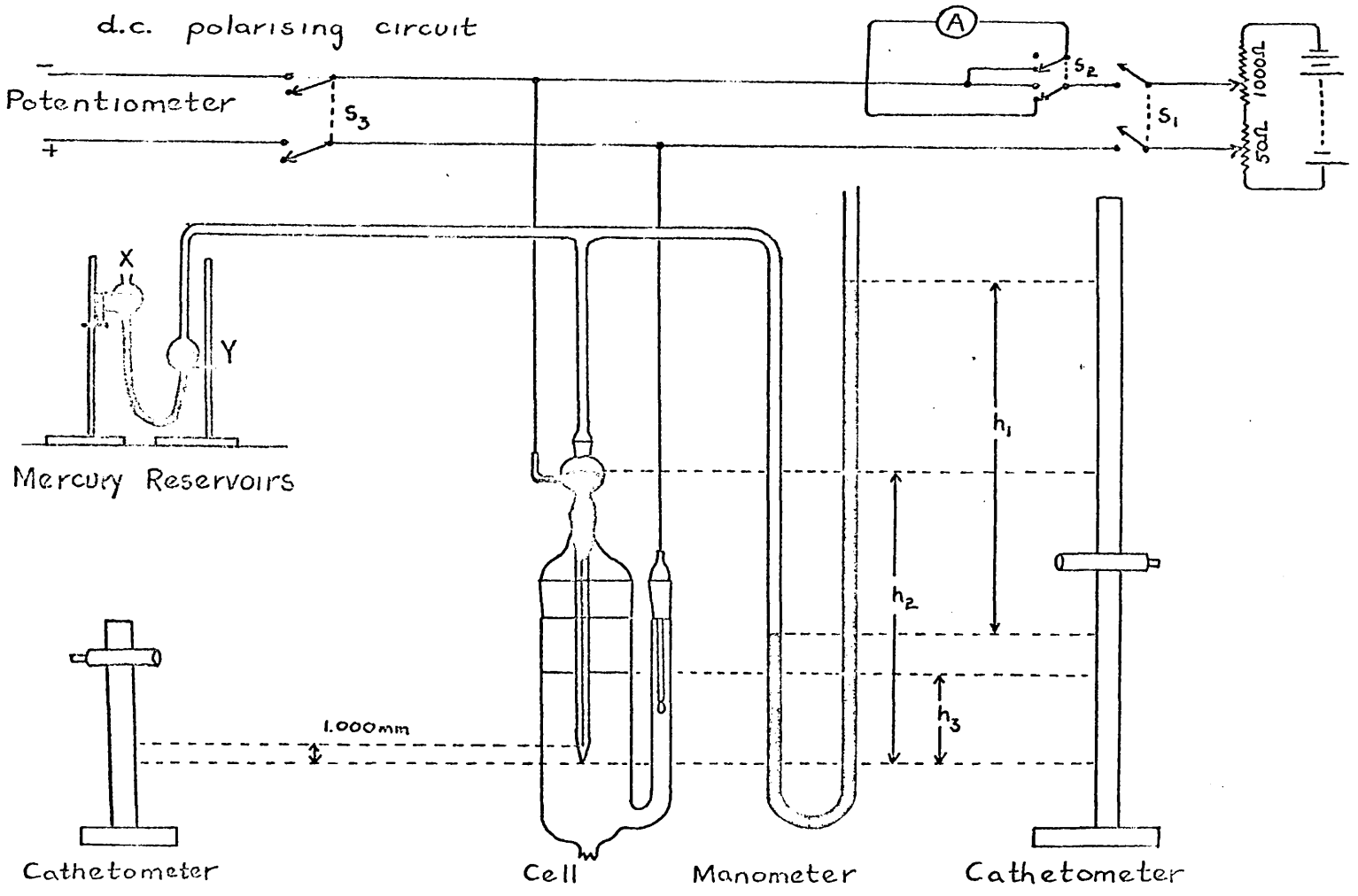

FIG. 13 CAPILLARY ELECTROMETER APPARATUS (SCHEMATIC)

The Capillary Electrometer Cell.

The cell, shown in figure 14 and plate 2 had a capacity of about 75 ml, and was constructed of pyrex glass. Side arm A was provided to allow bubbling out of the solution in the cell. Pre-saturated, oxygen-free nitrogen was passed into the cell and allowed to escape through a conventional bubbler in side arm B or C. The reference electrode was placed in side arm D. Tube F allowed excess mercury to be removed from the cell when required.

The mercury capillary was constructed in a manner similar to that described by Conway and Barradas (62). 0.3mm pyrex tubing, previously cleaned in a HNO_3-H_2SO_4 mixture was washed many times with conductivity water, and dried in an oven. The capillary was then drawn down in a gentle taper over the last half inch of its length, and finally the end was drawn down again to a very small diameter in a cool flame. A good capillary necessitated a very gentle taper over the last 5mm of its length, and a sufficiently small diameter to support an open column of mercury at least 8 inches high. The capillary was mounted at one end of a B14 male joint, the other end of which was joined to a 25ml reservoir. The reservoir and capillary could be inserted into the cell through a B14-B34 adaptor head, as shown in the diagram. The upper

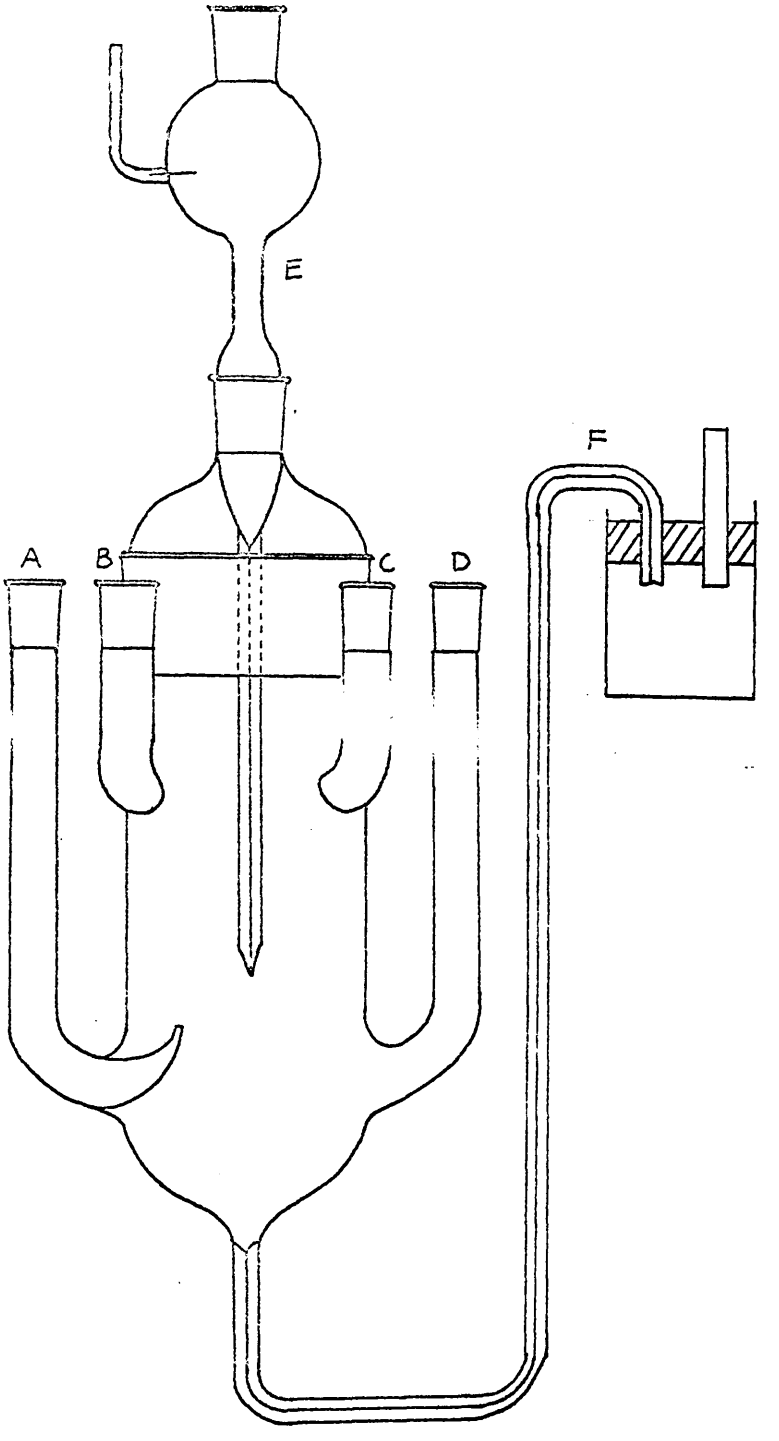

FIG. 14. THE CAPILLARY ELECTROMETER CELL.

end of the reservoir was connected by a gas line to the pressurising device, and also to a mercury manometer. The pressurising system consisted of two large mercury reservoirs, one of which was connected to the capillary reservoir and the manometer. The pressure in the system could be sensitively controlled by raising and lowering reservoir X by means of a screw adjuster similar to that used in the differential capacitance apparatus. The cell and manometer were enclosed in an air thermostat maintained at 25° C ± 0.2° C.

In an experiment, the total length of column of mercury supported by interfacial tension when the meniscus had been brought to the reference point 1.000mm from the tip of the capillary was

$$h_{corr} = h_1 + h_2 - \frac{(h_3 - 0.100)d_T}{D} - 0.100 \quad \text{cm of mercury}$$

(see figure 13) where $(h_3 - 0.100)d_T/D$ is the mercury head equivalent to the solution above the meniscus, d_T is the solution density, D the density of the mercury, and h_1, h_2, h_3, measured by the cathetometer, are expressed in cm.

Electrocapillary Maximum Apparatus.

Electrocapillary maximum potentials were determined by method V described by Grahame and hid co-workers (63). The capillary electrometer cell, supported in a thermostat controlled to ± 0.05° C was fitted with a relatively wide capillary which permitted the mercury to stream in

fine droplets from the tip when under a head of mercury of approximately 30cm. The system was protected from electrical interference by capacitors connecting both streaming and reference electrodes to ground. The cell solution was de-oxygenated with pre-saturated, oxygen-free nitrogen, passed for several hours after the electrode streaming had been commenced, and the potential between the streaming and reference electrodes measured at intervals using a K3 Leeds and Northrup Universal Potentiometer with a Leeds and Northrup D.C. Null Detector. The highest attainable potential was taken as that of the electrocapillary maximum.

PLATE 2.

THE CAPILLARY ELECTROMETER CELL.

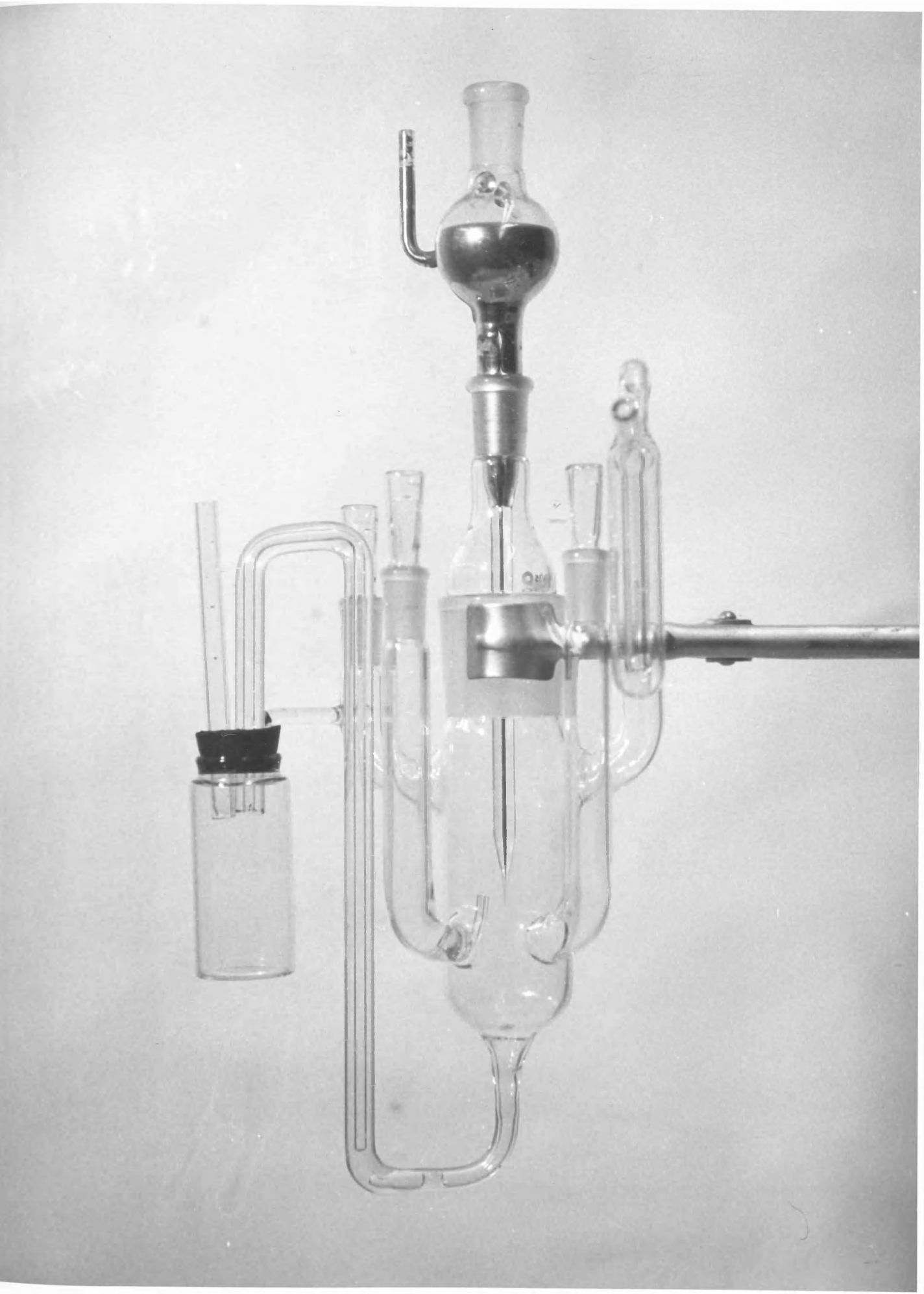

Experimental.

(1) Preparation of materials.

Mercury.

Mercury was thoroughly washed with water by vigourous shaking and decantation. It was then filtered through a finely perforated filter paper and washed with acetone. After being sprayed in a fine stream down a 100cm column of 10% nitric acid, the mercury was allowed to stand under concentrated sulphuric acid for 24 hours before being thoroughly washed with water and dried with acetone. It was finally distilled three times under vacuum, with stringent precautions being taken to prevent the entry of impurities into the system. The mercury was stored under pressure in an atmosphere of nitrogen. It was difficult to assess the purity of themercury, although it has been found (64) that a pure specimen, on shaking with conductivity water, gives rise to a "foam" lasting for over 15sec, while impure samples give foams lasting for considerably shorter periods.

Formamide.

Gaseous ammonia was added to B.D.H. "98%" formamide until it was slightly alkaline. Any ammonium formate present was filtered off. The formamide was distilled six times under reduced pressure using an efficient spray trap, the fraction retained distilling over below 60°C.

The pure formamide had a melting point of 2.5°C (literature value 2.55°C). It was found that the polarisation range the solvent could sustain without succumbing to electrolytic dissociation was markedly dependent on the number of distillations. The maximum stable range was attained in formamide which had been distilled at least five times. The purified solvent was stored under dry nitrogen.

Alkali Metal Chlorides.

AnalaR potassium, sodium, rubidium and caesium chlorides were recrystallised three times from conductivity water and dried at 300°C just prior to use. Lithium chloride was recrystallised three times from dry ethanol, and the ethanol removed by gentle heating in a stream of dry nitrogen. The solid was heated to constant weight at 120°C and stored under dry nitrogen. Just before use it was heated again to 240°C.

(2) Preparation of Solutions.

Since traces of moisture were likely to affect measurements made in a non-aqueous solvent system, all solutions were made up by weight in a dry box filled with dry nitrogen. The solutions were stored in 500ml flasks with standard taper necks, and a special head fitted the latter enabling the solution to be blown over into the cell by dry nitrogen without coming into contact with the atmos-

phere. The solution densities were determined using a pycnometer.

(3) Reference Electrodes (figure 15).

The silver-silver chloride electrodes used with the chloride solutions in formamide were similar to those described by Harned (65), McAuley (66) and in detail by Vincent (61). A platinum wire was wound in a helix and sealed into one end of a pyrex tube, the other end of which was attached to a Quickfit B10 cone. The helix was filled with a thick paste of spectroscopically pure silver oxide in conductivity water. The electrode, after having been dried at 100°C was heated at 400°C in a muffle furnace until the metallic oxide had completely decomposed to grey, lustrous silver. Another coating of the oxide was applied and the electrode heated as before. This process was repeated until none of the platinum was visible through the silver. An epoxy resin was then cast in the electrode tube to ensure a good pyrex-platinum seal. The electrode was then chloridised, using a platinum cathode on the absence of light, by electrolysis in normal aqueous hydrochloric acid, at a current density of approximately lamp/cm^2 for three hours. Finally, after having been washed thoroughly with a formamide solution of potassium chloride, the electrode was allowed to age in the dark for several weeks in a similar solution. Before a run, the electrode was washed several times in cell solution. Electrodes prepared in this fashion were

found to be reproducible to better than 1mv.

The 0.1M calomel reference electrode was prepared by a method similar to that described by Vincent (61). It was connected to the capillary electrometer cell by a salt bridge containing 0.1M aqueous potassium chloride solution. When not in use the salt bridge was protected by a guard tube.

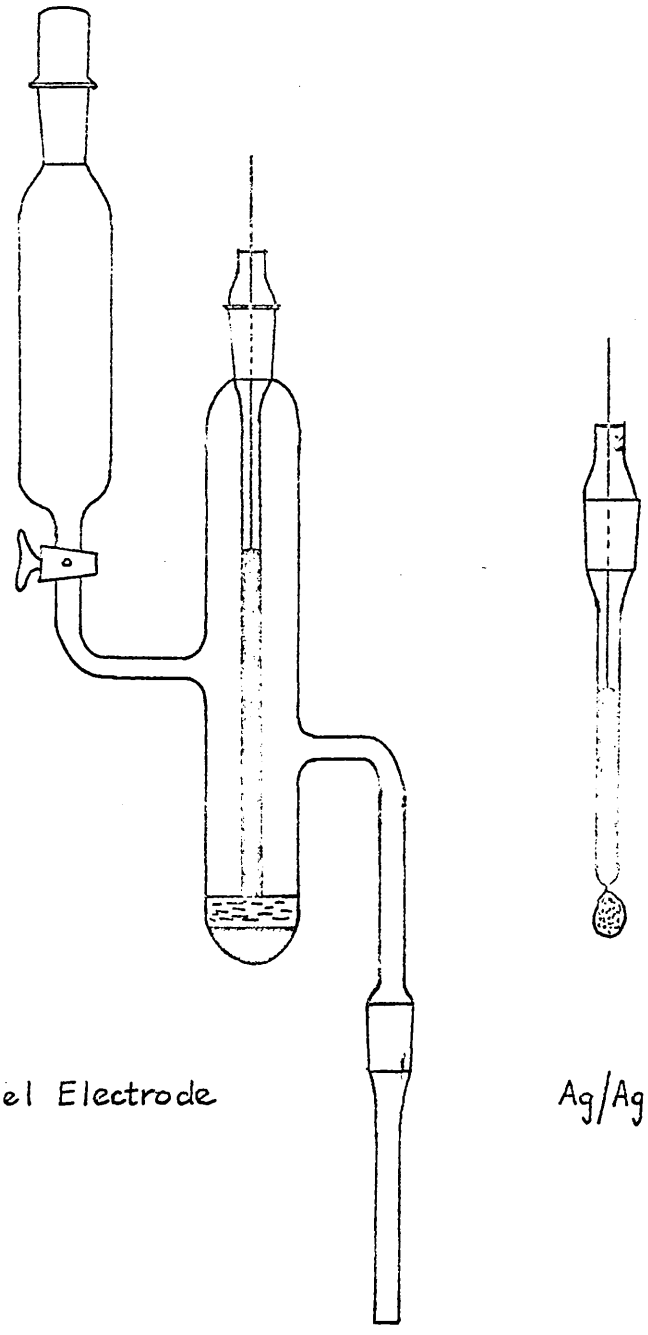

Calomel Electrode

Ag/AgCl Electrode

FIG. 15. REFERENCE ELECTRODES.

(4) General Run Procedure, Differential Capacitance Measurement.

Before an experiment, the batteries were discharged for one hour in order to stabilise the e.m.f. Mercury flow was started before transferring the test solution to the cell, which was done in the absence of air. The cell was placed in the thermostat, the solution de-oxygenated by passing pre-saturated oxygen-free nitrogen for three hours. After the first hour, the dropping mercury electrode was polarised cathodically to a potential just below that of solvent decomposition until the reduction current was negligible, removing any reducible material. The birth detector was then set up using VR_1 and VC_1 (figure 8) with the impedance selector in the "Off" position (position 2, figure 7) and the cathode ray oscilloscope connected to "Start Pulse". When the amplifier had been tuned to the bridge frequency, the balance detector was made ready as follows. With the impedance selector at "Standardise" (position 3, figure 7) and the amplifier output and signal generator output set for maximum sensitivity, the transformer ratio-arm bridge was adjusted to read the correct value of the standard impedance, and the test lead impedance balanced out by means of the trimmers. After selection of the discharge constant for the reservoir capacitor (VR_1, S_1), VR_2 could

be set to allow the thyratron to strike (figure 6). It was essential to check that the thyratron ceased conduction within the prescribed limits on either side of bridge balance.

For a given polarisation voltage, a birth-balance interval could be determined once a balance position had been accurately located. With the interval timer stop signal selector set at "Birth-balance" and the impedance selector at "Off", the timer was reset, and the birth detector allowed to start it. The impedance selector was then turned to "Unknown" (position 1, figure 7) in time for the balance detector pulse to stop the timer. The reading on the latter was noted, together with the bridge settings.

When the stop signal selector was set at "Drop lifetime", and the impedance selector at "Off", successive pulses from the birth detector enabled the interval timer to record t_g, the length of time between the birth of successive drops.

At frequent intervals during a run, checks were made on the mercury level in the reservoir, the standardisation of the potentiometer and the frequency of the signal generator.

The mean mercury flow rate was determined at a fixed potential in the following manner. Tap J (figure 12) was opened to allow any mercury in H to fall into I, the

interval timer was started manually and tap J closed simultaneously at the birth of a drop. The mercury in I was blown into G and discarded. After maintaining constant the applied potential and mercury head for thirty to sixty minutes, all the mercury in H was allowed to flow through J into I, and the interval timer was stopped and J closed simultaneously at the birth of a drop. The mercury in I was then blown over into G, and subsequently washed, dried and weighed. Since the mass of mercury flowing in a fixed interval of time was known, the mean flow rate could be calculated. In a normal experiment, the flow rate was measured both immediately before and immediately after the capacitance determinations. This provided a check on the constancy of the characteristics of the capillary.

After a run, the outside of the capillary was washed with conductivity water, dried in a stream of dust-free air and enclosed in a glass guard tube before the mercury flow was stopped.

(5) General Run Procedure, Interfacial Tension Measurement.

Before a run, the battery was discharged for one hour to stabilise the e.m.f. The capillary was placed in position in the test cell, and the test solution transferred in the absence of air. The cell was placed in the thermostat and the solution de-oxygenated by passing pre-saturated oxygen-free nitrogen for the duration of the experiment. Due to the slow attainment of thermal equilibrium in an air thermostat, the test cell was allowed to equilibrate overnight at 25°C. When the cell was properly equilibrated, the mercury in the capillary electrode was pressurised to an extent sufficient to cause drop formation, and the electrode polarised cathodically to a potential just below that of solvent decomposition until the reduction current was negligible, removing any reducible material. The pressure was released to stop drop formation, and the observing microscope set to a position 1.000mm above the capillary tip. At each potential investigated the illuminated mercury meniscus was brought to this mark by adjusting the applied pressure. At least four determinations of the pressure required to bring the mercury to the reference point were made at each potential, and the resulting mean value of h_{corr} used to evaluate γ, the interfacial tension. A drop of mercury was expelled between each measurement. The heights of the

mercury columns were measured with an accuracy of 0.02% on a cathetometer, and the capillary was calibrated by measuring interfacial tensions in 0.1M aqueous potassium chloride solution, using a 0.1M calomel electrode as reference, and comparing the results with those of Devanathan and Peries (67).

After a run, the mercury was again started dropping and the outside of the capillary washed with conductivity water, dried in a stream of dust-free air and enclosed in a glass guard tube before the drop formation was stopped.

(6) General Run Procedure, Electrocapillary Maximum Determination.

Before a run, the cell was purged with nitrogen and the electrode streaming commenced prior to the transfer of the test solution, which was carried out in the absence of air. The cell was placed in the thermostat and the solution was de-oxygenated by passing pre-saturated oxygen-free nitrogen for the duration of the experiment. The e.m.f between the streaming electrode and the reference electrode was measured at fifteen minute intervals after the attainment of thermal equilibrium, and the highest potential recorded was taken as that of the electrocapillary maximum. After a run, the electrode was cleaned and stored in the usual way.

RESULTS

RESULTS

The differential capacitance at applied potentials E_-, for the solutions being studied were computed from the impedance data using the method developed by Mancollas and Vincent (61,68). The average rate of flow of mercury $\bar{m}_t$ mg/sec up to time t in the life of the drop could be calculated once the height of the mercury column h_b equivalent to the back pressure was known. This was given by

$$h_b = 2\gamma / gDr_t$$

$$= \gamma / 172.73\, w_t^{1/3} \quad \text{at } 25^\circ C \quad \ldots\ldots(74)$$

where D was the density of the mercury, g the gravitational constant and r_t the radius of the growing drop of mass w_t mg at time t sec.

Writing M as the constant rate of flow that would be obtained with the same head of mercury, h, if there were no back pressure, then if it is assumed that the rate was proportional to the effective pressure,

$$m_t / M = (h - h_b)/h \quad \ldots\ldots(75)$$

and thus

$$m = \frac{dw}{dt} = M\left(1 - \frac{h_b}{h}\right)$$

$$= M\left(1 - \gamma / \left[172.73\, h\, w_t^{1/3}\right]\right) \quad \ldots\ldots(76)$$

Usually $h \gg h_b$, and this expression could be simplified to(39)

$$\frac{dw}{dt} = \frac{M}{\left(1 + \frac{h_b}{h} + \frac{h_b^2}{h^2}\right)} = \frac{M}{\left[1 + \frac{\gamma}{172.73\, h\, w_t^{1/3}} + \frac{\gamma^2}{(172.73h)^2 w_t^{2/3}}\right]} \quad \ldots\ldots(77)$$

which gave on integration

$$Mt = w_t + \frac{3}{2}\frac{\gamma w_t^{2/3}}{172.73h} + \frac{3\gamma^2 w_t^{1/3}}{(172.73h)^2} \qquad \ldots\ldots(78)$$

The integration constant here was ignored since w_t was negligible when t = 0. Smith (39) showed that inversion of equation (78) by means of approximations in which terms in $(\gamma/h)^3$ were considered negligible yielded

$$w_t = Mt - \frac{1.5\, M^{2/3} t^{2/3}\gamma}{172.73h} - \frac{1.5\, M^{1/3} t^{1/3}\gamma^2}{(172.73h)^2} \qquad \ldots\ldots(79)$$

Equation (79) was valid only when $t \geq 0.05$sec since terms which were important when t was small had been neglected.

Since the impedance bridge measured impedances as a parallel combination, the results obtained were transformed into the series equivalents. The required transforms were

$$R_s = G_p^{-1}\left(1 + \omega^2 C_p^2/G_p^2\right)^{-1} \qquad \ldots\ldots(80)$$

$$C_s = C_p\left(1 + G_p^2/\omega^2 C_p^2\right) \qquad \ldots\ldots(81)$$

where G_p and C_p were the parallel impedance components of conductance and capacitance respectively, R_s and C_s the series impedance components of resistance and capacitance and ω the frequency. $\bar{m}$, the average rate of flow of mercury in mg/sec up to time t_g, the drop time, was measured by weighing the mercury collected over a known time interval at a fixed potential. At this potential the drop mass $w_g = \bar{m}t_g$.

To evaluate the constant M, the experimental values of w_g and t_g were substituted into equation (78). The

value of γ, the interfacial tension at the potential of measurement of t_g and w_g was also required for this calculation. Since this was not readily available for non-aqueous solutions, an approximate value of sufficient accuracy for use in the calculation was computed from the relationship of Harkins and Brown (69)

$$\gamma = \frac{\alpha \cdot g \cdot 10^{-3} \cdot w_g}{\rho}\left(0.159 + \frac{5.706\,\rho}{w_g^{1/3}}\right) \qquad \ldots\ldots(82)$$

where $\alpha = [(D-d_T)/D]$ and d_T = density of the solution at T°C. ρ was the capillary orifice radius in cm. At any given potential, if w_g was known, γ could be calculated by direct substitution in equation (82). The radius ρ was determined from drop weight measurements carried out under conditions of known interfacial tension.

The drop mass w_t at time t was required for the determination of the surface area of the drop at that instant. In the derivation of equation (78) Smith set $w_{t=0} = 0$. In the calculation of w_t employed in the present work, w_t was taken as being the sum of an empirical time independent component w_o and a time dependent component f(t) where

$$f(t) = Mt - \frac{1.5 M^{2/3} t^{2/3} \gamma}{172.73\,h} - \frac{1.5 M^{1/3} t^{1/3} \gamma^2}{(172.73\,h)^2} \qquad \ldots\ldots(83)$$

i.e. $$w_t = w_o + f(t) \qquad \ldots\ldots(84)$$

Since Smith (39) and MacNevin and Balis (70) have demon-

strated the mercury drop to be spherical except near the beginning and end of its life, the drop area could be calculated from

$$A = K\left\{w_o + f(t)\right\}^{2/3} \qquad \text{where } K = (4\pi)^{1/3}.(3/D)^{2/3}\,10^{-2}.$$

Here, however, the small screened area A_s where the mercury column in the capillary joins the drop was not considered. A more precise value for the area of the drop at time t was

$$A_t = K\left\{w_o + f(t)\right\}^{2/3} - A_s \qquad \ldots\ldots(85)$$

Since by definition $C_s = C_o A_t$ then

$$C_s = C_o\left[K\left\{w_o + f(t)\right\}^{2/3} - A_s\right] \qquad \ldots\ldots(86)$$

and $$(C_s + C_o A_s)^{3/2} = (C_o K)^{3/2} w_o + (C_o K)^{3/2} f(t) \qquad \ldots\ldots(87)$$

To evaluate f(t), γ had to be known at the potential of measurement, and since w_g was not known, except at the potential of flow rate measurement, the following procedure was adopted. An approximate value for γ was substituted in (79) and the resulting w_g value used in (82) to calculate a more accurate value. By using an iteration technique, constant values for γ and w_g were obtained. f(t) was then computed from equation (83), and equation (87) solved, neglecting initially the term in A and obtaining an approximate value for C_o from the linear plot of $C_s^{3/2}$ against f(t). Using this value, $(C_s + C_o A_s)^{3/2}$ was calculated, and plotted against f(t) to give a more accurate value of C_o, which was further improved by iteration. The intercept of the final $(C_s + C_o A_s)^{3/2}$ vs f(t) plot was used in the calculation of w_o,

and it was found that in formamide solutions w_o was not a constant for a given capillary under changing conditions of polarisation, in marked contrast to the observed behaviour of w_o in aqueous solutions (68).

The complete calculation required to evaluate C_o from the impedance bridge data was carried out with the aid of an English Electric Leo KDF9 computer. The programme employed is given in **appendix 1**, and a typical calculation is shown in table 1.

Differential capacitances at different potentials E_-, measured against a silver-silver chloride reference electrode in the same solution, were determined for the following solutions: 0.100 m lithium, sodium, rubidium and caesium chlorides and 0.050, 0.071, 0.100 and 0.500 m potassium chloride at 25° C. 0.100 m solutions of potassium and caesium chlorides were also studied at 5° and 45° C. The results, which were reproducible to about ± 0.1% are given in tables 2-13.

The interfacial tension γ was given by

$$\gamma = \frac{h_{corr} \cdot g \cdot \rho}{2} \qquad \ldots\ldots(88)$$

where ρ was the radius of the capillary at the reference point and h_{corr} the head of mercury which was being supported

by the interfacial tension when the mercury meniscus was at the reference point. ρ was evaluated by carrying out determinations of h_{corr} under conditions of known interfacial tension. The results of the calibration are listed in table 14. Interfacial tensions at different potentials E_-, measured against a silver-silver chloride reference electrode in the same solution, were determined for the following solutions in formamide: 0.050 m and 0.100 m potassium chloride and 0.050, 0.0889, 0.100 and 0.179 m caesium chloride at 25°C. The results, given in tables 15-20, were reproducible to ± 0.2 dynes/cm except at extreme cathodic potentials, where reproducibility was ± 0.5 dynes/cm. Table 21 compares the interfacial tension results for 0.050 m potassium chloride obtained by direct measurement with those from double integration of the capacity-potential curve.

The potential of the electrocapillary maximum was measured for every solution studied by the differential capacitance technique. The results, which were reproducible to ± 1mv are reported in table 22.

q_M, the charge on the dropping mercury electrode, given by

$$q_M = \int_{E^{cm}}^{E} C_o \cdot dE$$

was calculated by integration of the capacitance-potential curves. An electronic computer was used to fit the experimental data to a polynomial of any chosen degree, and the closeness of fit verified by comparing a plot of the polynomial with the experimental points. The polynomial was then integrated by the computer, the necessary integration constants being obtained from the e.c.m. potentials. The programme required for the curve-fitting and integration operation is given in appendix 2.

It was found that the maximum cathodic polarisation which could be achieved before decomposition of the formamide, and accompanying current flow, depended markedly on the purity of the solvent. A minimum of five fractional distillations at reduced pressure and a temperature below 60°C was required before the maximum polarisation range could be sustained by the solvent. In the present work the dropping mercury electrode was studied at charges of $-20\mu C/cm^2$ in contrast to the maximum value of $-14\mu C/cm$ achieved by Payne (71).

Plots of the differential capacitance against charge are given in figures 16, 17, 18 and in figures 19, 20 the interfacial tension is plotted against the potential for potassium and caesium chloride solutions at 25°C.

SAMPLE 1

Sample calculation, part of run 33.

INPUT DATA

$D = 13.5340$, $d = 1.14846$, $f = 1.000 \times 10^3$, $K = 8.52833 \times 10^{-3}$,

$h = 36.166$, $\rho = 2.843 \times 10^{-3}$, $w_g = 7.42955$, $t_g = 4.35079$.

E_-	t_g	$C_p \times 10^6$	$G_p \times 10^3$	t_b
volts	sec	F	mho	sec
-0.500	4.34020	0.2327	0.800	1.18071
		0.3026	1.200	1.95545
		0.3354	1.400	2.39518
-0.600	4.31803	0.3486	1.400	2.79905
		0.3173	1.200	2.32173
		0.2473	0.800	1.44102
-0.700	4.27203	0.2479	0.800	1.48530
		0.3194	1.200	2.40422
		0.3527	1.400	2.90288
-0.800	4.19666	0.3524	1.400	2.89429
		0.3192	1.200	2.39461
		0.2476	0.800	1.47238
-0.900	4.15824	0.2480	0.800	1.52836
		0.3214	1.200	2.49986
		0.3067	1.100	2.25989
-1.000	4.03936	0.3334	1.200	2.85828
		0.2586	0.800	1.76116
		0.3168	1.100	2.55175

TABLE 1

RESULTS

N = 1.79301

γ = 392.8

E_-	γ	$C_o(a)$	$C_o(f)$	$A_o \times 10^4$
volts	dynes/cm	μF/cm	μF/cm	cm^2
-0.500	391.3	22.0676	22.0783	16.93
-0.600	389.4	20.3699	20.3758	6.52
-0.700	385.5	19.9454	19.9539	7.17
-0.800	379.0	19.8960	19.9044	11.57
-0.900	375.7	19.3709	19.3794	16.02
-1.000	365.5	18.0875	18.0947	17.78

(a) value after first cycle.

(f) final value.

TABLE 2

0.050 m KCl in formamide at 25° C.

	Run 30	Run 31	Run 38	Mean	
E_-	C_o	C_o	C_o	C_o	q_m
volts	$\mu F/cm^2$	$\mu F/cm^2$	$\mu F/cm^2$	$\mu F/cm^2$	$\mu C/cm^2$
-0.200	38.94	39.06	39.03	39.01	6.64
-0.300	26.29	26.12	26.15	26.19	3.46
-0.400	19.50	19.45	19.51	19.49	1.20
-0.500	15.75	15.66	15.76	15.72	-0.54
-0.600	14.68	14.64	14.76	14.69	-2.04
-0.700	15.35	15.38	15.39	15.37	-3.53
-0.800	16.93	16.85	16.89	16.89	-5.14
-0.900	18.15	18.15	18.17	18.16	-6.90
-1.000	18.31	18.26	18.24	18.27	-8.72
-1.100	16.86	16.89	16.97	16.91	-10.50
-1.200	16.07	16.14	16.10	16.10	-12.16
-1.300	14.95	14.97	14.93	14.95	-13.69
-1.400	14.00	14.09		14.05	-15.14
-1.500	13.54	13.47		13.50	-16.53
-1.600	13.28	13.30		13.29	-17.85

TABLE 3

0.071 m KCl in formamide at 25° C

	Run 45	Run 46	Run 47	Mean	
E_-	C_o	C_o	C_o	C_o	q_M
volts	$\mu F/cm^2$	$\mu F/cm^2$	$\mu F/cm^2$	$\mu F/cm^2$	$\mu C/cm^2$
-0.200	38.62	38.66	38.81	38.70	6.79
-0.300	27.12	27.16	27.18	27.15	3.55
-0.400	20.59	20.53	20.45	20.52	1.21
-0.500	16.41	16.36	16.40	16.39	-0.61
-0.600	15.45	15.35	15.46	15.42	-2.18
-0.700	15.95	15.92	15.92	15.93	-3.74
-0.800	17.38	17.38	17.30	17.35	-5.40
-0.900	18.35	18.36	18.33	18.35	-7.19
-1.000	18.29	18.25	18.23	18.26	-9.03
-1.100	17.04	17.06	17.13	17.08	-10.81
-1.200	15.81	15.82	15.81	15.81	-12.47
-1.300	14.87	14.79	14.78	14.81	-14.00
-1.400	13.94	14.02	13.99	13.98	-15.43
-1.500	13.44	13.39		13.42	-16.81
-1.600	13.20	13.25		13.23	-18.13

TABLE 4

0.100 m KCl in formamide at 25° C

	Run 19	Run 28	Run 29	Mean	
E_-	C_o	C_o	C_o	C_o	q_M
volts	$\mu F/cm^2$	$\mu F/cm^2$	$\mu F/cm^2$	$\mu F/cm^2$	$\mu C/cm^2$
-0.200	38.34	38.42	38.45	38.40	6.95
-0.300	28.09	28.00	28.04	28.04	3.65
-0.400	21.31	21.22	21.21	21.25	1.22
-0.500	17.09	17.08	17.16	17.11	-0.68
-0.600	16.13	16.21	16.10	16.15	-2.32
-0.700	16.49	16.54	16.46	16.50	-3.94
-0.800	17.74	17.81	17.85	17.80	-5.66
-0.900	18.56	18.59	18.51	18.55	-7.48
-1.000	18.39	18.44	18.44	18.42	-9.33
-1.100	17.16	17.16	17.10	17.14	-11.12
-1.200	15.86	15.87	15.85	15.86	-12.78
-1.300	14.70	14.78	14.67	14.72	-14.30
-1.400	14.00	14.02	13.95	13.99	-15.72
-1.500		13.34	13.35	13.35	-17.10
-1.600		13.26	13.16	13.21	-18.43
-1.700		13.16	13.20	13.18	-19.73

TABLE 5

0.500 m KCl in formamide at 25°C

	Run 33	Run 34	Mean	
E_-	C_o	C_o	C_o	q_M
volts	$\mu F/cm^2$	$\mu F/cm^2$	$\mu F/cm^2$	$\mu C/cm^2$
-0.300	32.32	32.24	32.28	4.30
-0.400	25.90	25.94	25.92	1.40
-0.500	22.08	22.20	22.14	-0.98
-0.600	20.38	20.40	20.39	-3.09
-0.700	19.95	19.85	19.90	-5.10
-0.800	19.90	19.86	19.88	-7.09
-0.900	19.38	19.42	19.40	-9.06
-1.000	18.09	18.15	18.12	-10.93
-1.100	16.63	16.53	16.58	-12.67
-1.200	15.11	15.22	15.17	-14.26
-1.300	14.20	14.32	14.26	-15.72
-1.400	13.49	13.48	13.49	-17.12

TABLE 6

0.100 m KCl in formamide at 5°C

	Run 54	Run 55	Mean	
E_-	C_o	C_o	C_o	q_M
volts	$\mu F/cm^2$	$\mu F/cm^2$	$\mu F/cm^2$	$\mu C/cm^2$
-0.200	39.87	39.84	39.86	7.54
-0.300	28.86	28.96	28.91	4.16
-0.400	22.56	22.68	22.62	1.61
-0.500	18.64	18.68	18.66	-0.44
-0.600	17.14	17.15	17.15	-2.21
-0.700	17.65	17.79	17.72	-3.94
-0.800	18.94	18.91	18.93	-5.77
-0.900	19.89	19.82	19.86	-7.72
-1.000	19.83	19.82	19.83	-9.72
-1.100	18.37	18.32	18.35	-11.63
-1.200	16.25	16.33	16.29	-13.36
-1.300	15.12	15.10	15.11	-14.93
-1.400	14.35	14.24	14.30	-16.39
-1.500	14.12	14.07	14.10	-17.81
-1.600	14.21	14.18	14.20	-19.22

TABLE 7

0.100 m KCl in formamide at 45°C

	Run 50	Run 51	Mean	
E_-	C_o	C_o	C_o	q_M
volts	$\mu F/cm^2$	$\mu F/cm^2$	$\mu F/cm^2$	$\mu C/cm^2$
-0.200	41.20	41.32	41.26	6.46
-0.300	26.36	26.26	26.31	3.22
-0.400	21.66	21.72	21.69	0.86
-0.500	17.94	17.85	17.90	-1.10
-0.600	16.41	16.50	16.46	-2.83
-0.700	16.89	17.01	16.95	-4.48
-0.800	17.73	17.78	17.76	-6.20
-0.900	18.63	18.64	18.64	-8.02
-1.000	18.07	18.15	18.11	-9.88
-1.100	17.46	17.53	17.50	-11.68
-1.200	15.88	15.84	15.86	-13.53
-1.300	14.80	14.81	14.81	-14.86
-1.400	14.35	14.41	14.38	-16.32
-1.500	13.92	13.92	13.92	-17.74
-1.600	13.50	13.59	13.55	-19.09

TABLE 8

0.100 m LiCl in formamide at 25°C

	Run 21	Run 24	Run 36	Mean	
E_-	C_o	C_o	C_o	C_o	q_m
volts	$\mu F/cm^2$	$\mu F/cm^2$	$\mu F/cm^2$	$\mu F/cm^2$	$\mu C/cm^2$
-0.200	40.78	40.89	40.84	40.84	7.37
-0.300	30.40	30.44	30.37	30.40	3.81
-0.400	21.48	21.46	21.42	21.45	1.24
-0.500	17.47	17.49	17.51	17.49	-0.68
-0.600	16.14	16.27	16.28	16.23	-2.33
-0.700	16.54	16.46	16.51	16.50	-3.96
-0.800	17.36	17.28	17.30	17.31	-5.66
-0.900	17.93	17.92	17.89	17.91	-7.43
-1.000	17.79	17.73	17.74	17.77	-9.21
-1.100	16.78	16.86	16.85	16.83	-10.94
-1.200	16.00	15.96	16.06	16.01	-12.59
-1.300	15.04	15.06	15.05	15.05	-14.14
-1.400		14.44	14.36	14.40	-15.61
-1.500		13.90	13.87	13.89	-17.02
-1.600		13.86	13.87	13.87	-18.41
-1.700		13.88	13.92	13.90	-19.80

TABLE 9

0.100 m NaCl in formamide at 25° C.

	Run 41	Run 42	Mean	
E_-	C_o	C_o	C_o	q_m
volts	$\mu F/cm^2$	$\mu F/cm^2$	$\mu F/cm^2$	$\mu C/cm^2$
-0.200	42.39	42.54	42.52	7.08
-0.300	27.99	28.00	28.00	3.66
-0.400	21.31	21.38	21.35	1.23
-0.500	17.41	17.46	17.44	-0.69
-0.600	16.45	16.42	16.44	-2.37
-0.700	16.68	16.73	16.71	-4.00
-0.800	17.75	17.71	17.73	-5.73
-0.900	18.58	18.48	18.53	-7.57
-1.000	18.50	18.59	18.55	-9.44
-1.100	17.04	17.11	17.08	-11.23
-1.200	16.12	16.10	16.11	-12.89
-1.300	14.78	14.69	14.74	-14.43
-1.400	14.03	13.95	13.99	-15.87
-1.500	13.60	13.57	13.59	-17.23

TABLE 10

0.100 m RbCl in formamide at 25°C.

	Run 39	Run 40	Run 44	Mean	
E_-	C_o	C_o	C_o	C_o	q_m
volts	$\mu F/cm^2$	$\mu F/cm^2$	$\mu F/cm^2$	$\mu F/cm^2$	$\mu C/cm^2$
-0.200	40.16	40.13	40.09	40.13	7.21
-0.300	29.30	29.28	29.20	29.26	3.77
-0.400	21.67	21.62	21.58	21.62	1.25
-0.500	17.71	17.79	17.79	17.76	-0.69
-0.600	16.62	16.63	16.61	16.62	-2.39
-0.700	16.96	17.10	17.03	17.03	-4.05
-0.800	17.89	17.80	17.82	17.84	-5.81
-0.900	18.98	18.94	19.01	18.98	-7.66
-1.000	18.81	18.70	18.73	18.75	-9.54
-1.100	17.32	17.27	17.32	17.30	-11.35
-1.200	16.30	16.34	16.24	16.28	-13.04
-1.300	14.84	14.87	14.91	14.87	-14.59
-1.400		14.28	14.19	14.24	-16.04
-1.500		13.65	13.70	13.68	-17.43
-1.600		13.73	13.85	13.79	-18.81
-1.700		14.54	14.57	14.56	-20.21

TABLE 11

0.100 m CsCl in formamide at 25° C.

	Run 25	Run 37	Run 35	Mean	
E_-	C_o	C_o	C_o	C_o	q_M
volts	$\mu F/cm^2$	$\mu F/cm^2$	$\mu F/cm^2$	$\mu F/cm^2$	$\mu C/cm^2$
-0.300	27.86	27.90	27.83	27.86	3.60
-0.400	20.68	20.68	20.57	20.64	1.20
-0.500	17.56	17.64	17.64	17.61	-0.68
-0.600	16.54	16.48	16.52	16.51	-2.36
-0.700	16.90	16.92	16.91	16.91	-4.03
-0.800	18.13	18.04	18.06	18.08	-5.79
-0.900	18.60	18.60	18.66	18.62	-7.62
-1.000	18.36	18.30	18.35	18.34	-9.47
-1.100	17.49	17.43	17.50	17.47	-11.26
-1.200	16.25	16.20	16.25	16.23	-12.96
-1.300	15.43	15.33	15.35	15.37	-14.54
-1.400	14.91	14.85	14.97	14.91	-16.04
-1.500	14.90	15.05	15.03	14.99	-17.52
-1.600	15.71	15.76	15.64	15.70	-19.05
-1.700	18.20	18.08		18.14	-20.74
-1.800	20.85	20.76		20.81	-22.67

TABLE 12

0.100 m CsCl in formamide at 5°C.

	Run 52	Run 53	Mean	
E_-	C_o	C_o	C_o	q_m
volts	$\mu F/cm^2$	$\mu F/cm^2$	$\mu F/cm^2$	$\mu C/cm^2$
-0.300	28.42		28.42	4.07
-0.400	21.99	21.87	21.93	1.58
-0.500	18.80	18.76	18.78	-0.43
-0.600	17.16	17.19	17.18	-2.21
-0.700	17.63	17.57	17.60	-3.95
-0.800	19.23	19.23	19.23	-5.79
-0.900	19.84	19.90	19.87	-7.74
-1.000	19.98	20.04	20.01	-9.74
-1.100	18.75	18.73	18.74	-11.69
-1.200	17.39	17.38	17.39	-13.51
-1.300	16.04	16.00	16.02	-15.17
-1.400	15.27	15.30	15.29	-16.72
-1.500	15.31	15.19	15.25	-18.35
-1.600	15.94	15.86	15.90	-19.81
-1.700	18.22	18.34	18.28	-21.48

TABLE 13

0.100 m CsCl in formamide at 45°C

	Run 48	Run 49	Mean	
E_-	C_o	C_o	C_o	q_M
volts	$\mu F/cm^2$	$\mu F/cm^2$	$\mu F/cm^2$	$\mu C/cm^2$
-0.300	27.63		27.63	3.30
-0.400	21.44	21.39	21.42	0.86
-0.500	18.23	18.15	18.19	-1.09
-0.600	16.77	16.80	16.79	-2.83
-0.700	17.27	17.34	17.31	-4.53
-0.800	17.82	17.85	17.84	-6.28
-0.900	18.14	18.21	18.18	-8.09
-1.000	17.85	17.77	17.81	-9.89
-1.100	17.03	16.92	16.98	-11.64
-1.200	16.23	16.15	16.19	-13.30
-1.300	15.62	15.71	15.67	-14.88
-1.400	15.36	15.31	15.34	-16.43
-1.500	15.54	15.52	15.53	-17.98
-1.600	16.05	16.10	16.08	-19.55

TABLE 14

Calibration of capillary using 0.100 M aqueous KCl.

E_-	h_{corr}	γ *	$\rho \times 10^3$
volts	cm	dynes/cm	cm
-0.100	47.486	388.0	1.2318
-0.200	49.228	401.5	1.2295
-0.300	50.624	413.6	1.2316
-0.400	51.523	421.5	1.2333
-0.500	52.078	425.5	1.2317
-0.600	52.327	426.0	1.2273
-0.700	52.001	424.0	1.2292
-0.800	51.364	419.5	1.2312
-0.900	50.562	413.1	1.2317
-1.000	49.678	404.6	1.2278
-1.100	48.463	395.0	1.2287

Mean radius $(1.2303 \pm 0.0019) \times 10^{-3}$ cm

* Interpolated data of Devanathan and Peries (67)

TABLE 15

Interfacial tensions in 0.050 m KCl in formamide at 25° C.

	Run 61	Run 62	Mean
E_-	γ	γ	γ
volts	dynes/cm	dynes/cm	dynes/cm
-0.200	375.2	375.8	375.5
-0.300	380.3	380.1	380.2
-0.400	382.4	382.2	382.3
-0.467	382.7	382.6	382.7
-0.500	382.6	382.6	382.6
-0.600	381.1	381.5	381.3
-0.700	378.4	378.6	378.5
-0.800	374.2	374.1	374.2
-0.900	368.4	368.0	368.2
-1.000	360.1	360.3	360.2
-1.100	349.5	348.8	349.2
-1.200	338.0	338.6	338.3
-1.300	326.5	326.0	326.3
-1.400	311.2	312.0	311.6
-1.500	297.7	296.8	297.2
-1.600	280.5	281.3	280.9

TABLE 16

Interfacial tensions in 0.100 m KCl in formamide at 25° C

	Run 63	Run 64	Mean
E_-	γ	γ	γ
volts	dynes/cm	dynes/cm	dynes/cm
-0.200	373.5	374.3	373.9
-0.300	378.9	379.1	379.0
-0.400	381.1	381.0	381.1
-0.462	381.4	381.6	381.5
-0.500	381.2	381.3	381.3
-0.600	379.9	379.6	379.8
-0.700	376.8	376.4	376.6
-0.800	371.7	372.0	371.9
-0.900	365.6	365.0	365.3
-1.000	356.5	356.9	356.7
-1.100	344.9	345.6	345.3
-1.200	333.8	333.6	333.7
-1.300	321.0	321.4	321.2
-1.400	306.3	305.5	305.9
-1.500	290.1	291.0	290.6
-1.600	274.2	273.6	273.9

TABLE 17

Interfacial tensions in 0.050 m CsCl in formamide at 25° C.

	Run 70	Run 71	Mean
E_-	γ	γ	γ
volts	dynes/cm	dynes/cm	dynes/cm
-0.200	381.7	382.5	382.1
-0.300	387.3	386.9	387.1
-0.400	388.7	389.0	388.9
-0.500	389.1	388.9	389.0
-0.600	387.4	387.6	387.5
-0.700	384.4	384.3	384.4
-0.800	380.5	380.0	380.3
-0.900	374.6	374.1	374.4
-1.000	365.6	366.0	365.8
-1.100	355.4	356.0	355.7
-1.200	344.5	344.1	344.3
-1.300	330.7	331.1	330.9
-1.400	316.2	315.5	315.9
-1.500	300.0	300.6	300.3
-1.600	284.3	284.7	284.5

TABLE 18

Interfacial tensions in 0.0889 m CsCl in formamide at 25° C.

	Run 77	Run 79	Mean
E_-	γ	γ	γ
volts	dynes/cm	dynes/cm	dynes/cm
-0.200	380.1	381.0	380.6
-0.300	386.0	385.6	385.8
-0.400	387.5	387.9	387.7
-0.500	388.1	387.9	388.0
-0.600	386.7	386.6	386.7
-0.700	383.1	383.5	383.3
-0.800	378.0	378.3	378.2
-0.900	372.5	371.9	372.2
-1.000	363.1	363.6	363.4
-1.100	352.9	352.7	352.8
-1.200	340.0	340.6	340.3
-1.300	326.5	327.3	326.9
-1.400	311.2	312.2	311.7
-1.500	295.8	295.0	295.4
-1.600	279.1	278.7	278.9

TABLE 19

Interfacial tensions in 0.100 m CsCl in formamide at 25° C.

	Run 67	Run 68	Mean
E_-	γ	γ	γ
volts	dynes/cm	dynes/cm	dynes/cm
-0.200	380.3	380.9	380.6
-0.300	385.9	385.5	385.7
-0.400	387.6	387.6	387.6
-0.500	387.8	387.6	387.7
-0.600	386.0	386.4	386.2
-0.700	383.1	382.9	383.0
-0.800	378.3	377.7	378.0
-0.900	371.6	371.9	371.8
-1.000	362.9	362.3	362.6
-1.100	352.1	352.5	352.3
-1.200	339.3	340.2	339.8
-1.300	326.3	325.7	326.0
-1.400	310.8	310.0	310.4
-1.500	293.9	294.6	294.3
-1.600	277.6	278.0	277.8

TABLE 20

Interfacial tensions in 0.179 m CsCl in formamide at 25 C.

	Run 73	Run 74	Mean
E_-	γ	γ	γ
volts	dynes/cm	dynes/cm	dynes/cm
-0.200	379.4	379.8	379.6
-0.300	384.9	384.7	384.8
-0.400	386.6	387.0	386.8
-0.500	387.0	387.0	387.0
-0.600	384.9	384.6	384.8
-0.700	381.1	380.9	381.0
-0.800	376.4	375.8	376.1
-0.900	369.0	369.4	369.2
-1.000	359.1	359.7	359.4
-1.100	348.1	348.6	348.4
-1.200	335.9	335.5	335.7
-1.300	321.6	321.0	321.3
-1.400	305.3	306.1	305.7
-1.500	288.9	288.2	288.6
-1.600	271.0	271.5	271.3

TABLE 21

Comparison between γ from double integration and γ experimental for 0.050 m KCl in formamide, at 25° C.

E_-	γ_1	γ_2
volts	dynes/cm	dynes/cm
-0.200	375.5	375.1
-0.300	380.2	380.0
-0.400	382.3	382.3
-0.500	382.6	382.6
-0.600	381.3	381.3
-0.700	378.5	378.5
-0.800	374.2	374.0
-0.900	368.2	368.2
-1.000	360.2	360.4
-1.100	349.2	350.7
-1.200	338.3	339.4
-1.300	326.3	326.4
-1.400	311.6	311.9
-1.500	297.2	295.9
-1.600	280.9	279.3

γ_1 Experimental values for interfacial tension.

γ_2 Integrated values for interfacial tension.

TABLE 22

Potentials of the e.c.m. in formamide solutions

Solution	Temperature T°C	$E^{e\,cm}$ volts
0.050 m KCl	25	-0.467
0.071 m KCl	25	-0.465
0.100 m KCl	25	-0.462
0.500 m KCl	25	-0.457
0.100 m LiCl	25	-0.462
0.100 m NaCl	25	-0.462
0.100 m RbCl	25	-0.462
0.100 m CsCl	25	-0.462
0.100 m KCl	5	-0.477
0.100 m KCl	45	-0.442
0.100 m CsCl	5	-0.477
0.100 m CsCl	45	-0.442

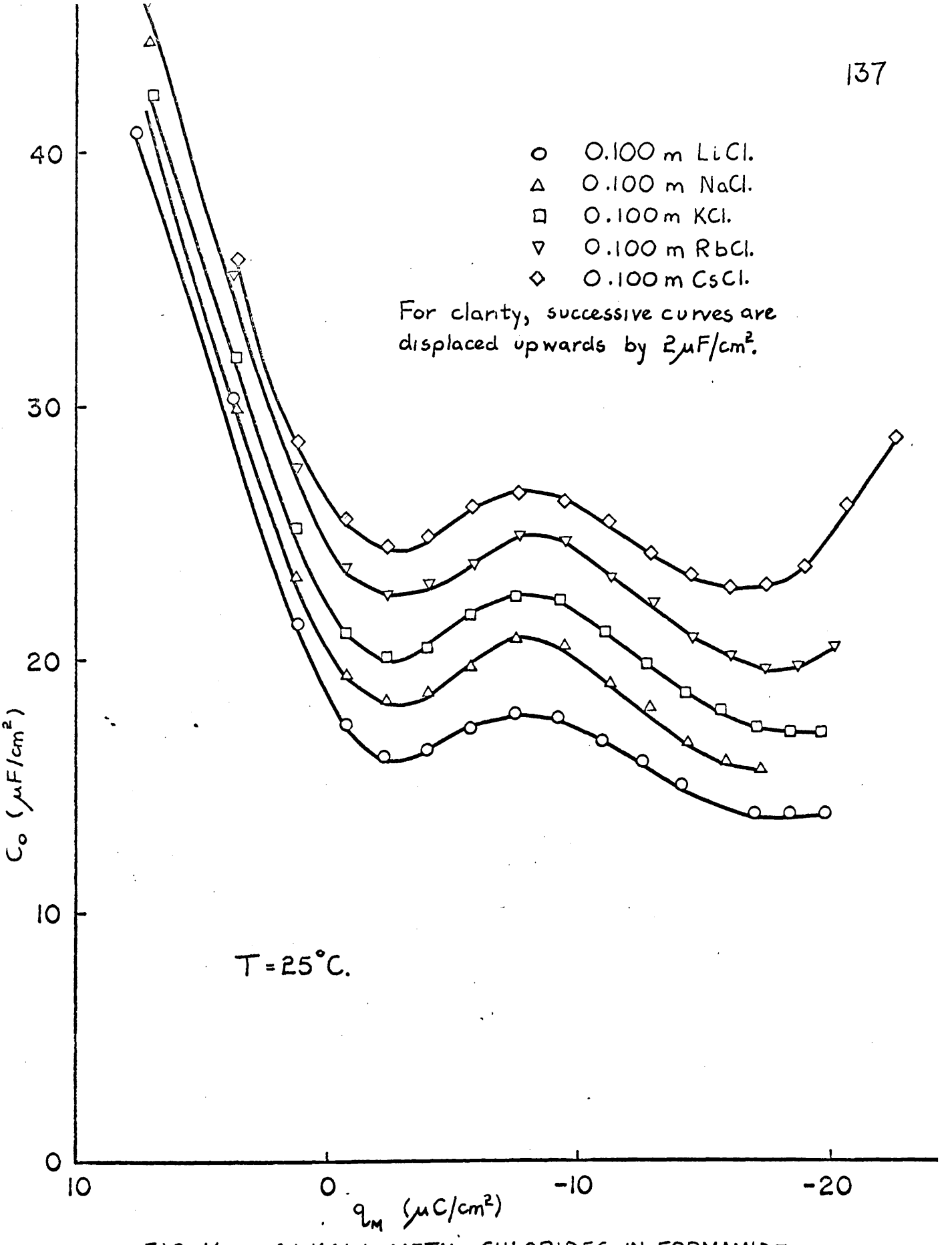

FIG. 16. ALKALI METAL CHLORIDES IN FORMAMIDE.

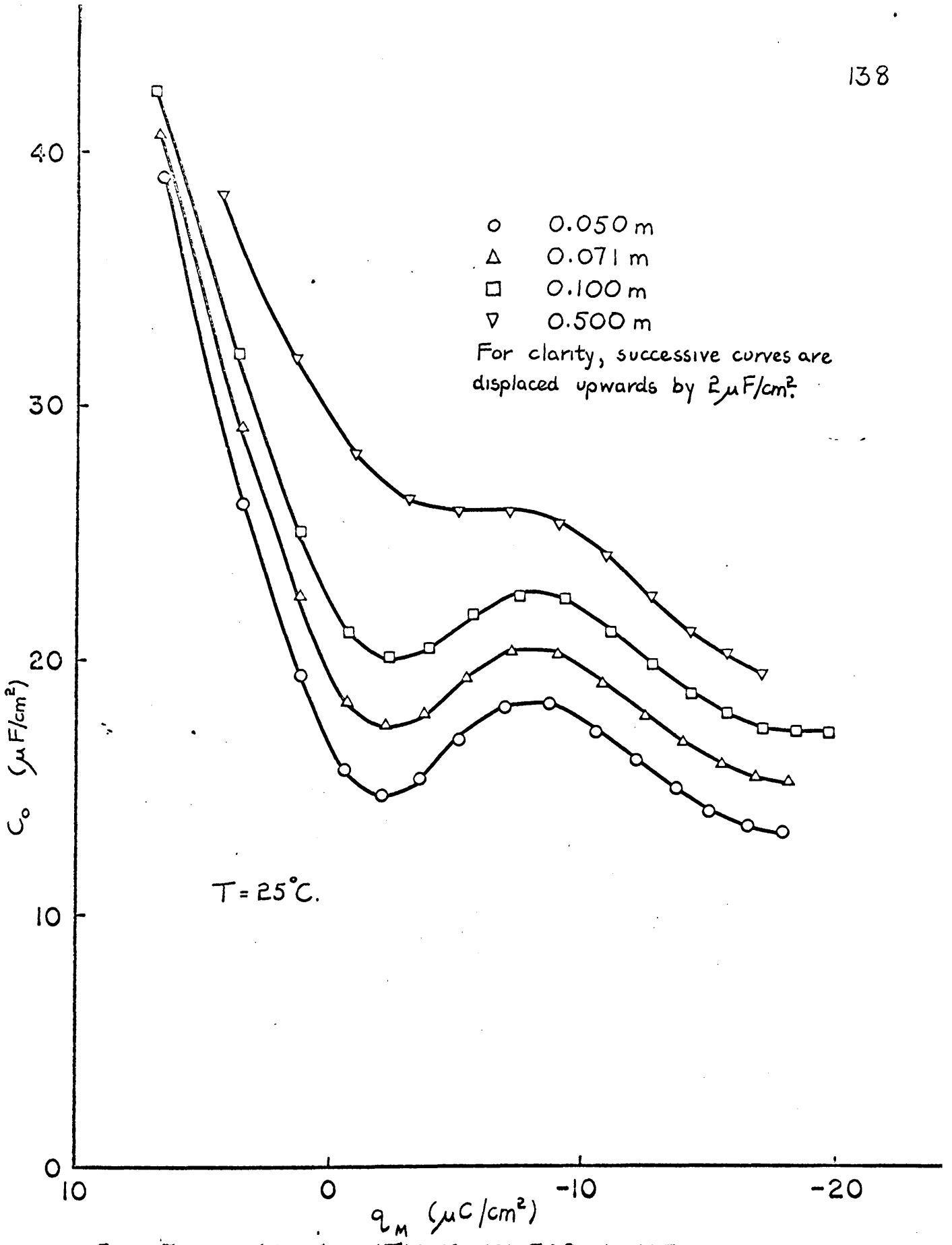

FIG. 17. KCl SOLUTIONS IN FORMAMIDE.

0.100m KCl	0.100m CsCl	T°C
d	a	5
e	b	25
f	c	45

The left ordinate scale refers to KCl.

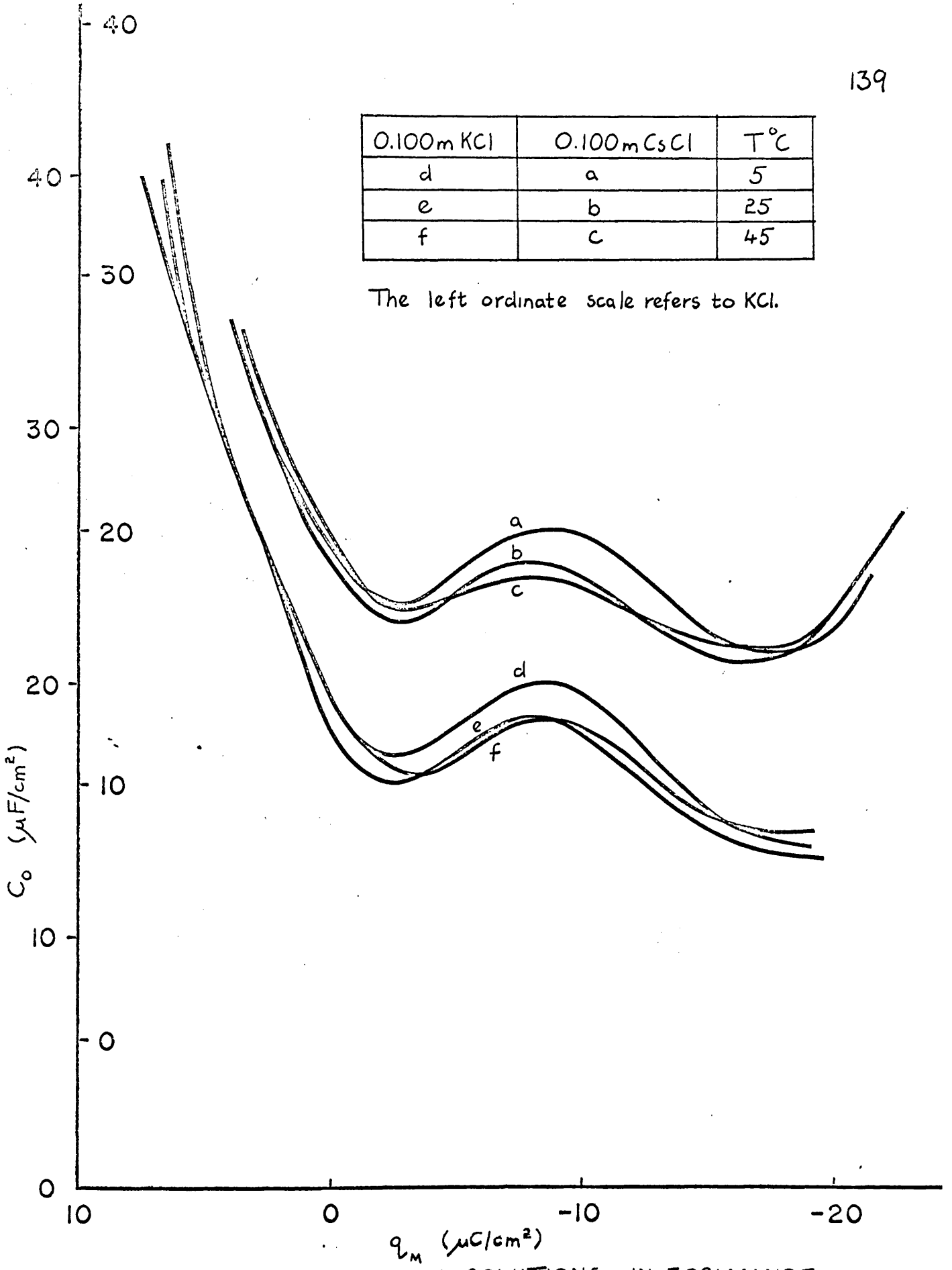

FIG. 18. KCl AND CsCl SOLUTIONS IN FORMAMIDE.

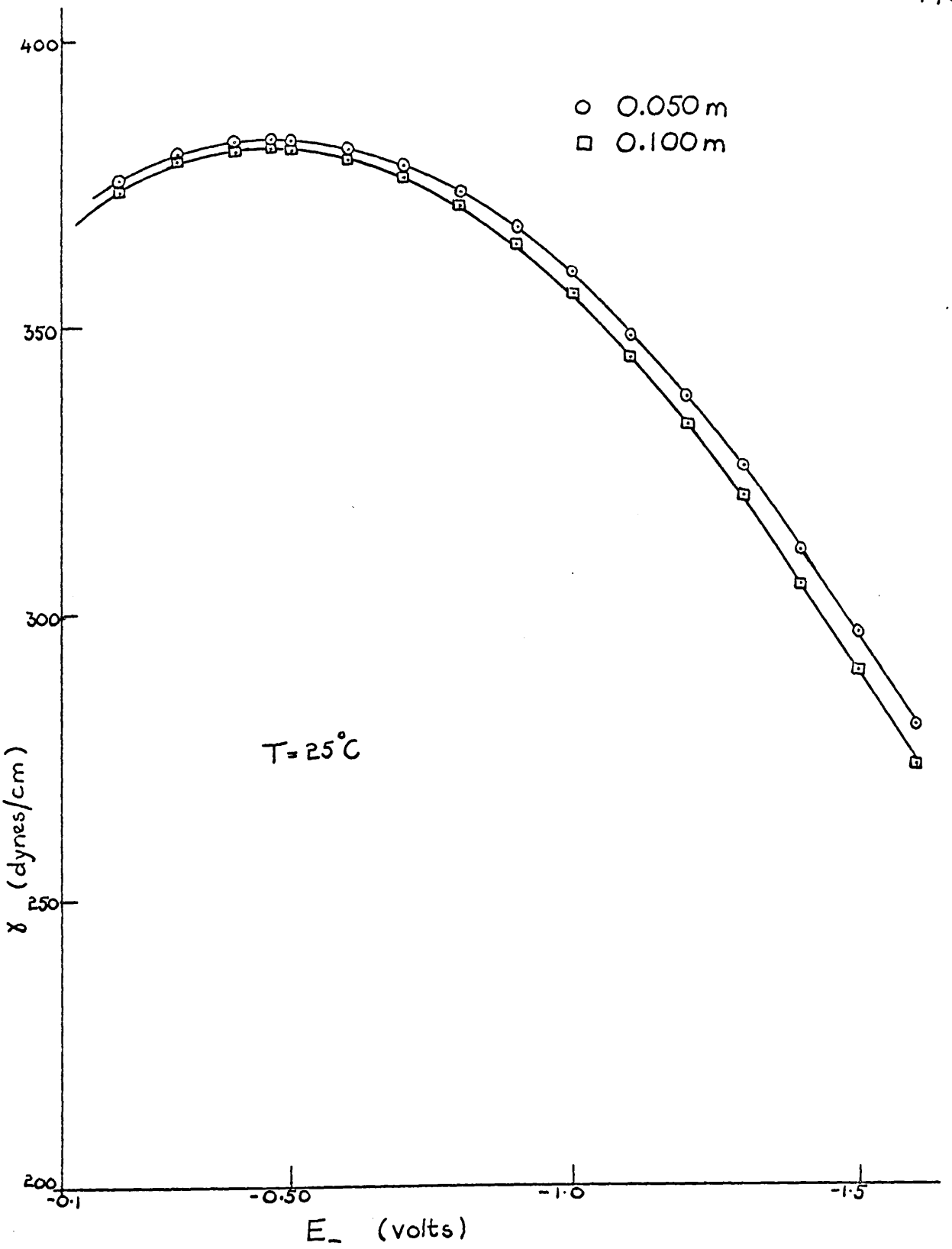

FIG. 19 KCl SOLUTIONS IN FORMAMIDE

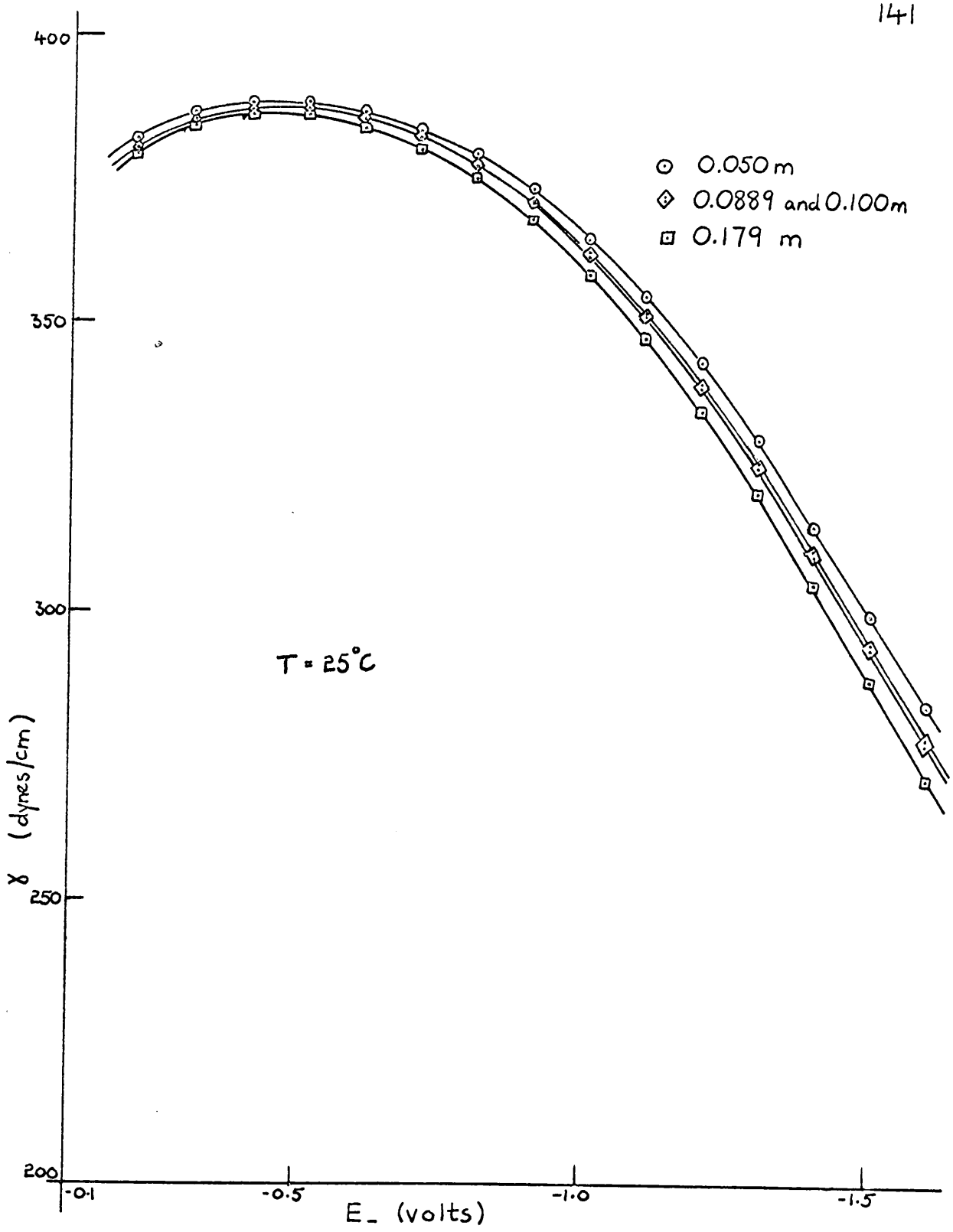

FIG. 20 CsCl IN FORMAMIDE

DISCUSSION

DISCUSSION.

The differential capacitance vs. charge plots (figures 16, 17, 18) have the same general appearance as those obtained from studies in aqueous systems. There is a rise in capacitance on both the anodic and cathodic sides, with a characteristic capacitance hump at intermediate potentials, and it is convenient to discuss the shapes of these curves within these three regions of potential.

Anodic Region.

As has been found to be the case in aqueous systems (72), the cation does not have any noticeable effect on the capacitance on the anodic side of the e.c.m. This is to be expected, as the cations will occupy only the diffuse layer in this polarisation range, and thus a change in cation size will not affect appreciably the positions of the IHP. and OHP. The concentration has only a small effect on the capacitance of the double layer in this region, especially at potentials far removed from the e.c.m. This would indicate that specific adsorption of anions, which will provide the main contribution to the capacitance in this region, is primarily a function of the electrode charge, and has only a small dependence on the concentration.

On the anodic side the capacitance increases with increasing temperature, as has been found in aqueous systems

(13,73). There is no completely satisfactory explanation for this at present, but Macdonald and Barlow (17) have suggested that it may be due to an increase in temperature making available more sites for anionic specific adsorption. If it is assumed that the specifically adsorbed ions are held at the electrode surface by very strong forces when at the extremes of polarisation, then the extent of desorption of the more weakly held solvent will be such that though the fractional coverage by specifically adsorbed ions falls, the actual coverage will rise due to the large increase in available sites. At lower field strengths it is probable that the increase in sites might no longer compensate for the reduction in fractional coverage by the specifically adsorbed ion, resulting in this case in a decrease in actual coverage. As yet this model of the temperature dependence of specific adsorption has not been expressed in a quantitative mathematical form.

The Region of the Hump.

It is seen in figures 16, 17, 18 that the capacitance vs. charge curves have a well-defined hump at charges considerably more cathodic than the corresponding humps in aqueous solutions (72,74). Similar observations have been made for potassium iodide (71) and potassium fluoride (75) solutions in formamide, and Damaskin and co-workers (76)

obtained results in 0.1 N solutions of some alkali halides in formamide at 20°C. It should be pointed out that the results of Minc and co-workers (77) for potassium fluoride solutions, while qualitatively similar, appear to be consistently low, perhaps as a result of insufficient solvent purification.

In the case of potassium chloride (figure 17) the effect of the electrolyte concentration on the hump can be clearly seen. As might be expected, at the lower concentrations variation of the concentration has very little effect on the appearance of the hump, and not until a concentration of 0.50 m is reached do we find the hump being masked by specific adsorption. This is in marked contrast to the behaviour of aqueous solutions of potassium chloride, in which the hump is masked out at a solution concentration of about 0.1 M, suggesting that either the forces involved in specific adsorption in formamide are weaker, or that the formamide molecule is more strongly held at the interface than is the water molecule.

The effect on the hump of changing the temperature can be seen in figure 18. For both potassium and caesium chlorides there is a general lowering of the hump with increase in temperature. This result is not unexpected, and closely parallels the corresponding situation in aqueous systems, though in that case the hump has disappeared at

temperatures higher than about 30° C (74). If solvent dipole orientation is responsible for the capacitance hump such a temperature dependence would be predicted. On this theory, the position of the hump would suggest that the formamide molecule has its most stable orientation with the positive pole of the solvent dipole directed away from the mercury surface. This is consistent with the orientation expected to be most stable on a consideration of the structure of the formamide molecule (78,79), namely that in which the oxygen atom is directed towards the mercury surface.

At the potential of the hump there is no marked effect of cation on the capacitance, except in the case of lithium chloride, which has a markedly lower capacitance. Further information as to the components of the doublelayer in this particular region is required before any explanation can be advanced.

The Far Cathodic Region.

In the far cathodic region there is a very pronounced effect of cation on the capacitance. The capacitance values at the most cathodic potentials reached were in the order $K^+ \approx Na^+ < Li^+ < Rb^+ < Cs^+$. It is interesting to note that in every case a minimum could be observed in the capacitance curves at large cathodic potentials before the onset

of solvent decomposition. The capacitances of caesium chloride and rubidium chloride rise much more rapidly than that of lithium chloride, whilst the capacitance rises have barely begun for sodium chloride and potassium chloride. A similar rise has been observed in aqueous solutions (13) though in this case the capacitances are in the order $Li^+ < Na^+ < K^+ < Rb^+ < Cs^+$. It is possible that this rise is dependent to some extent on specific adsorption, and accordingly any discussion will be postponed until the appropriate section. Damaskin and co-workers observed a similar effect in their studies of the alkali halides in N-methyl formamide (80) and more recently in formamide (76). Payne (71) in his investigation of formamide solutions of potassium iodide did not achieve applied potentials sufficiently negative to observe this rise.

Figure 18 shows that there is a small tendency for the capacitance to rise with increasing temperature, more clearly seen in the curves for caesium chloride. It is difficult to understand this increase unless it is due to an effect similar to that put forward by Macdonald and Barlow (17) to explain the temperature dependence of the capacitance in the anodic region. The positive electrode charges at which this temperature dependence occurs are of much lower magnitude than the negative charges at which it also occurs. Since the extent of specific adsorption of

anions at a given positive charge density is much greater than the corresponding adsorption of cations at an equivalent negative charge density, this serves to reinforce the view that the effect is due to an increase in available adsorption sites, and a resulting increase in specific adsorption.

Examination of the effect of concentration on the capacitance, in this region, in potassium chloride solutions (figure 17) shows that there is only a small dependence on concentration. Over most of the region the capacitance falls, probably as a result of dielectric saturation which would be concentration independent. The small concentration dependence even at the capacitance rise would indicate that any specific adsorption occurring is almost independent of concentration.

The Electrocapillary Maximum Region.

A minimum is apparent in most of the capacitance vs. charge plots slightly to the cathodic side of the e.c.m. If no specific adsorption was occurring, this minimum would be expected to be at the e.c.m. The nature of the cation has very little effect on this minimum, but discussion of the effect requires a knowledge of the components of charge in the double layer, and will therefore be postponed until the appropriate section. As with the hump, specific adsorption at high electrolyte concentrations

masks this minimum. It also has a complex dependence on temperature, the capacitances falling in the order 5°> 45°> 25° C. If the solvent capacitance is considered on the basis of the Watts-Tobin theory (15), as it is modified to apply to formamide (page 180), it would be expected that at the hump the order of capacitances would be 5°> 25°> 45° C, and at the minimum, which is about 0.4v removed from the hump, 45°> 25°> 5° C. Just such dependences have been observed in aqueous solutions, e.g. by Frumkin et al (73). It would appear that the 5° curve is anomalous , and this is possibly due to an increase in specific adsorption. This fits in well with the model proposed by Macdonald and Barlow (17) if we remember that the minimum is close to the e.c.n., and thus the interaction forces between a specifically adsorbed ion and the electrode will be much lower than at the anodic or cathodic extremes, since the electrostatic interaction will be much smaller. The decrease in specific adsorption with temperature in this region must be more than compensated for by the increase in solvent capacitance in the case of the 45° C curve, resulting in the temperature dependence observed at the capacitance minimum.

Comparison of the capacitance results for potassium chloride obtained in this work with the preliminary results reported by Vincent (61) shows discrepancies to occur over

a large part of the potential range (table 23). These are believed to be due to three main factors.

(1) An irregular drift in the capacitance of the standard impedance used by Vincent (81). It was for this reason that the impedance standard used in this work was designed in such a way as to enable its resistance and capacitance to be readily checked against the primary standards of the transformer ratio-arm bridge , the drift in the standard was found to be negligible throughout the period of the investigation.

(2) Insufficient purification of the formamide used by Vincent. In the present work it was shown that a minimum of six distillations at below 60° C was required to obtain solvent of sufficient purity for a double layer capacitance investigation. The formamide used by Vincent was only distilled twice at a temperature of 110° - 120° C.

(111) The calculation employed in the preliminary work used data for only one balance position at each potential, and assumed w_o to be constant. Apart from the uncertainty involved in using only one data set, the assumption of constant w_o has been shown to be false in the present work (page111).

The electrocapillary curves, figures 19,20, show the expected decrease in interfacial tension with increas-

TABLE 23

Comparison of results obtained in this work with those of Vincent (61) for 0.100 m KCl in formamide.

E_- volts	C_o(a) $\mu F/cm^2$	C_o(b) $\mu F/cm^2$
-0.200	38.40	37.72
-0.300	28.04	26.27
-0.400	21.25	19.83
-0.500	17.11	16.34
-0.600	16.15	15.01
-0.700	16.50	15.30
-0.800	17.80	16.21
-0.900	18.55	17.09
-1.000	18.42	17.41
-1.100	17.14	17.06
-1.200	15.86	16.10
-1.300	14.72	14.80
-1.400	13.99	13.92
-1.500	13.35	13.53
-1.600	13.21	13.36

(a) this work

(b) Vincent (61)

ing concentration. Double integration of the capacitance vs potential results was found, in each case, to yield values for the interfacial tensions in good agreement with the measured values (table 21, page 135). It can be seen that the drop in interfacial tension with increasing concentration grows larger as the potential becomes more cathodic, corresponding to a large surface excess concentration of cations. The potential of the maximum in the curves is in good agreement with the potential of the e.c.m. as measured by the streaming mercury technique.

From table 22 (page 136) it is seen that the e.c.m. potential is independent of the nature of the cation, and shows some dependence on temperature and on concentration. To study the effect of concentration further, an Esin and Markov plot (page 30) was constructed for the four concentrations of potassium chloride studied at 25°C, the activity coefficients being estimated from the work of Povarov and co-workers (82) with sodium chloride in formamide at 25°C, making the assumption that sodium and potassium chlorides would have the same activity. The activity of the 0.50m solution was estimated by extrapolation. The resulting Esin and Markov plot was a set of parallel straight lines of gradient 1.15 (figure 21) for charges more negative than $-10\mu C/cm^2$, indicative of cationic specific adsorption.

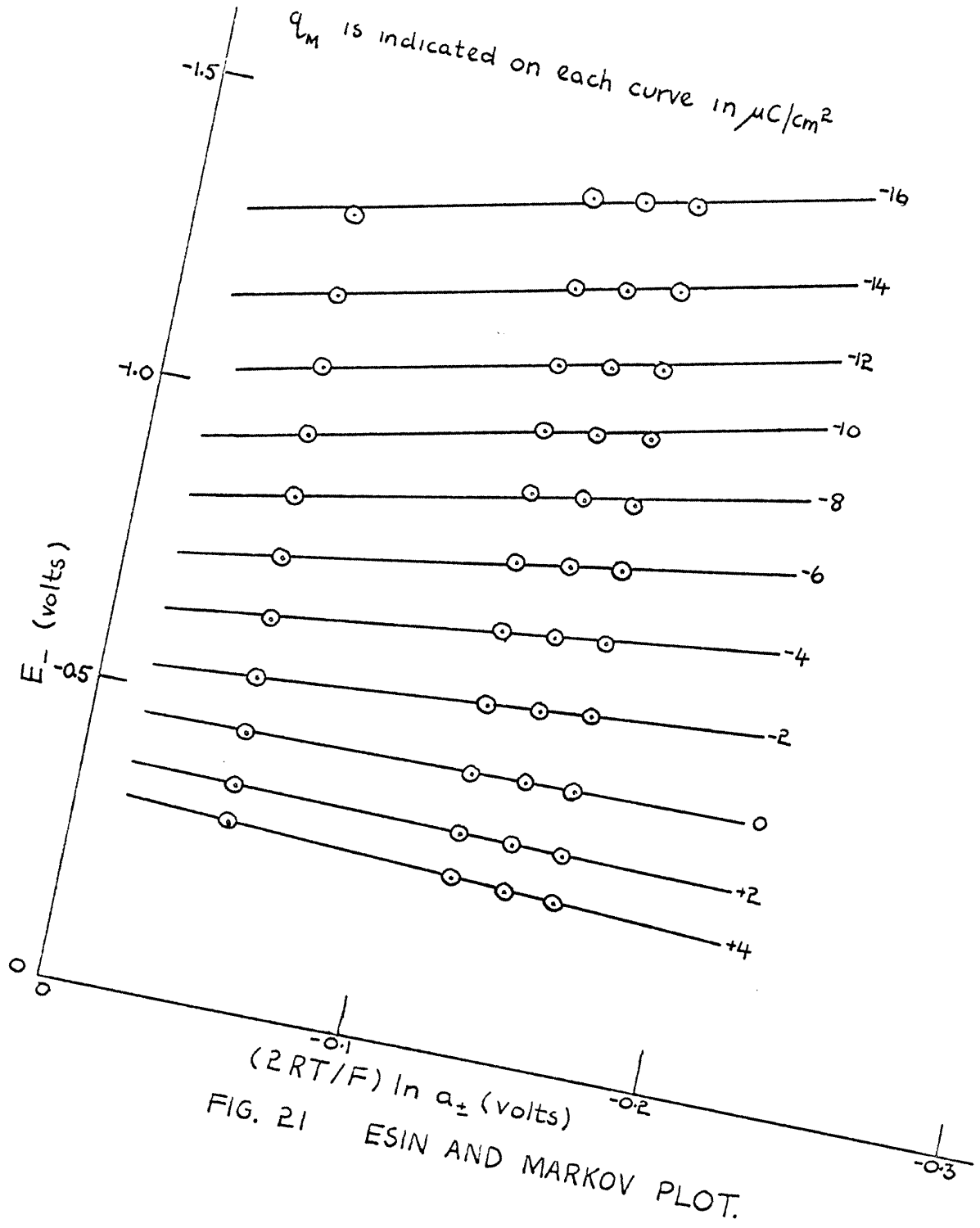

FIG. 21 ESIN AND MARKOV PLOT.

Since both anions and cations appear to play an important role in the double layer at a mercury electrode in formamide, it is of interest to attempt to evaluate the components of charge in the double layer. This can be done by evaluating the relative surface excesses of anions (Γ_-) and (Γ_+) cations followed by analysis into their components. With this in mind, the relative surface excesses were calculated both for 0.071m potassium chloride solution and for 0.100m caesium chloride solution.

Potassium chloride.

Γ_- and Γ_+ in 0.071m potassium chloride solution were calculated by the method of Grahame and Soderberg (21). The part of the differential capacitance due to cations was obtained by integration of $(\Delta C_o/\Delta \log a_\pm)_{E_-}$ with respect to E_-, using the mean activities given by Povarov and co-workers (82) to evaluate the mean activity $a_\pm$. Since specific adsorption of the cation was suspected, the integration constant was obtained from the calculated value of C_+ at the e.c.m. obtained from equation (36)

$$C_+ = FC_o^{ecm}\left(\frac{\partial E_-}{RT\partial \ln a_\pm^2}\right)^{ecm}$$

C_- was computed from $C_o = C_+ + C_-$. Plots of C_+ and C_- vs E_- are given in figure 22.

Γ_+ was obtained by integration of the C_+ vs E_- curve, the integration constant being evaluated from the inter-

facial tension data at the e.c.m. (equation 37)

$$(\partial\gamma/\partial\mu)^{ecm} = -\Gamma_{salt} = -\Gamma_+ = -\Gamma_- \qquad \text{(for a 1:1 electrolyte)}$$

and Γ_- resulted from the relationship

$$-q_M = z_+F\Gamma_+ + z_-F\Gamma_- \qquad \text{.....(89)}$$

The results are shown in table 24, and plots of $z_+F\Gamma_+$ and $z_-F\Gamma_-$ as a function of E_- are given in figure 23. As a check, the surface excesses at several potentials were calculated from the interfacial tension data for 0.050m and 0.100m potassium chloride solutions, and the results were found to be in good agreement with those calculated by the Grahame and Soderberg method.

Caesium Chloride.

The surface excesses Γ_+ and Γ_- at a mercury electrode in a 0.100m solution of caesium chloride in formamide were evaluated from the variation of the interfacial tension with the chemical potential at constant E_-, using the relationship,

$$\Gamma_+ = -\left(\frac{\partial\gamma}{\partial\mu}\right)_{E_-} = -\left(\frac{\partial\gamma}{RT\,\partial\ln a_\pm^2}\right)_{E_-}$$

The quantity on the R.H.S. was evaluated at 0.100m by plotting γ against $4.606RT\log a_\pm$ at constant E_- for all the caesium chloride concentrations studied. Mean activities were interpolated from the data of Povarov and co-workers (83). Smooth curves were drawn through the experimental points, and the gradients of the tangents

to the curves at the points corresponding to 0.100m gave the required quantity. The results are given in table 25, and plots of $z_+F\Gamma_+$ and $z_-F\Gamma_-$ as a function of E_- are shown in figure 24. In both determinations, the relative surface excesses are calculated to an accuracy of $\pm 0.6\mu C/cm^2$, except at the cathodic extremes, where the uncertainty is somewhat larger.

From the general appearance of the surface excess plots (figures 23,24), it can be concluded that specific adsorption of cations is occurring in the far cathodic region, since the surface excess of anions reaches a minimum value, and then increases again as the potential becomes more cathodic. As the electrode charge is growing increasingly negative, this increase in the anionic surface excesses must reflect specific adsorption of the cation. Even the minimum value of $z_-F\Gamma_-$ corresponds to an excess of anions in the double layer, so simultaneous specific adsorption would appear to be taking place. This conclusion is reinforced by the failure of an attempted analysis of the components of charge using the technique outlined previously for systems in which specific adsorption of only one type of ion is taking place in the region under study.

TABLE 24

Grahame and Soderberg Calculation (21).

Surface excesses in 0.071 m KCl in formamide at 25° C.

E_-	C_+	$z_+F\Gamma_+$	q_M	$z_-F\Gamma_-$	$z_+F\Gamma_+$ *
volts	$\mu F/cm^2$	$\mu C/cm^2$	$\mu C/cm^2$	$\mu C/cm^2$	$\mu C/cm^2$
-0.400	-0.18	3.4	1.2	-4.6	3.5
-0.465	2.57	3.5	0	-3.5	3.5
-0.500	4.05	3.6	-0.6	-3.0	3.8
-0.600	8.09	4.2	-2.2	-2.0	4.4
-0.700	11.80	5.2	-3.7	-1.5	5.6
-0.800	14.80	6.5	-5.4	-1.1	6.8
-0.900	16.89	8.1	-7.2	-0.9	8.5
-1.000	18.18	9.9	-9.0	-0.9	10.3
-1.100	18.87	11.7	-10.8	-0.9	11.5
-1.200	19.02	13.6	-12.5	-1.1	13.5
-1.300	18.81	15.5	-14.0	-1.5	15.0
-1.400	18.42	17.4	-15.4	-2.0	16.8
-1.500	17.98	19.2	-16.8	-2.4	19.4
-1.600	17.52	21.0	-18.1	-2.9	20.6

$C_+^{ecm} = 2.57\ \mu F/cm^2$ $\qquad$ $z_+F\Gamma_+^{ecm} = 3.5\ \mu C/cm^2$

0.050 m KCl $\log a_\pm = -1.073$ $\qquad$ 0.100 m KCl $\log a_\pm = -1.361$

* Evaluated from interfacial data for 0.100 m and 0.050 m KCl in formamide.

TABLE 25

Surface excesses in 0.100 m CsCl in formamide at 25° C.

E_-	$z_+F\Gamma_+$	q_M	$z_-F\Gamma_-$
volts	$\mu C/cm^2$	$\mu C/cm^2$	$\mu C/cm^2$
-0.400	3.7	1.2	-4.9
-0.500	3.6	-0.6	-3.0
-0.600	4.4	-2.3	-2.1
-0.700	5.6	-4.0	-1.6
-0.800	6.9	-5.7	-1.2
-0.900	8.5	-7.6	-0.9
-1.000	10.3	-9.5	-0.8
-1.100	12.1	-11.3	-0.8
-1.200	13.9	-13.0	-0.9
-1.300	15.7	-14.5	-1.2
-1.400	17.5	-16.0	-1.5
-1.500	19.3	-17.5	-1.8
-1.600	21.6	-19.1	-2.5

m	0.050	0.0889	0.100	0.179
$\log a_\pm$	-1.367	-1.131	-1.083	-0.851

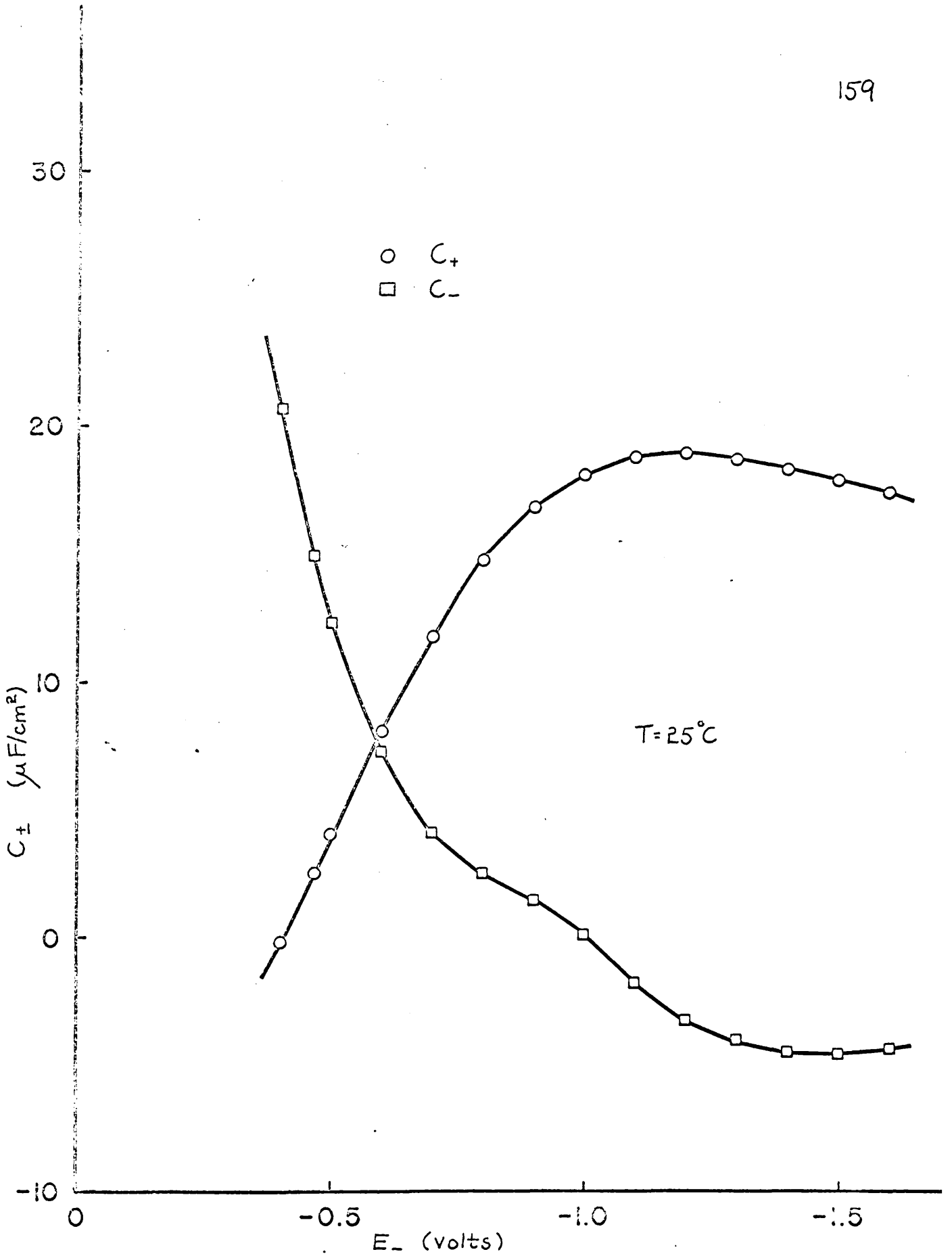

FIG. 22. CAPACITANCE CONTRIBUTIONS IN 0.071m KCl.

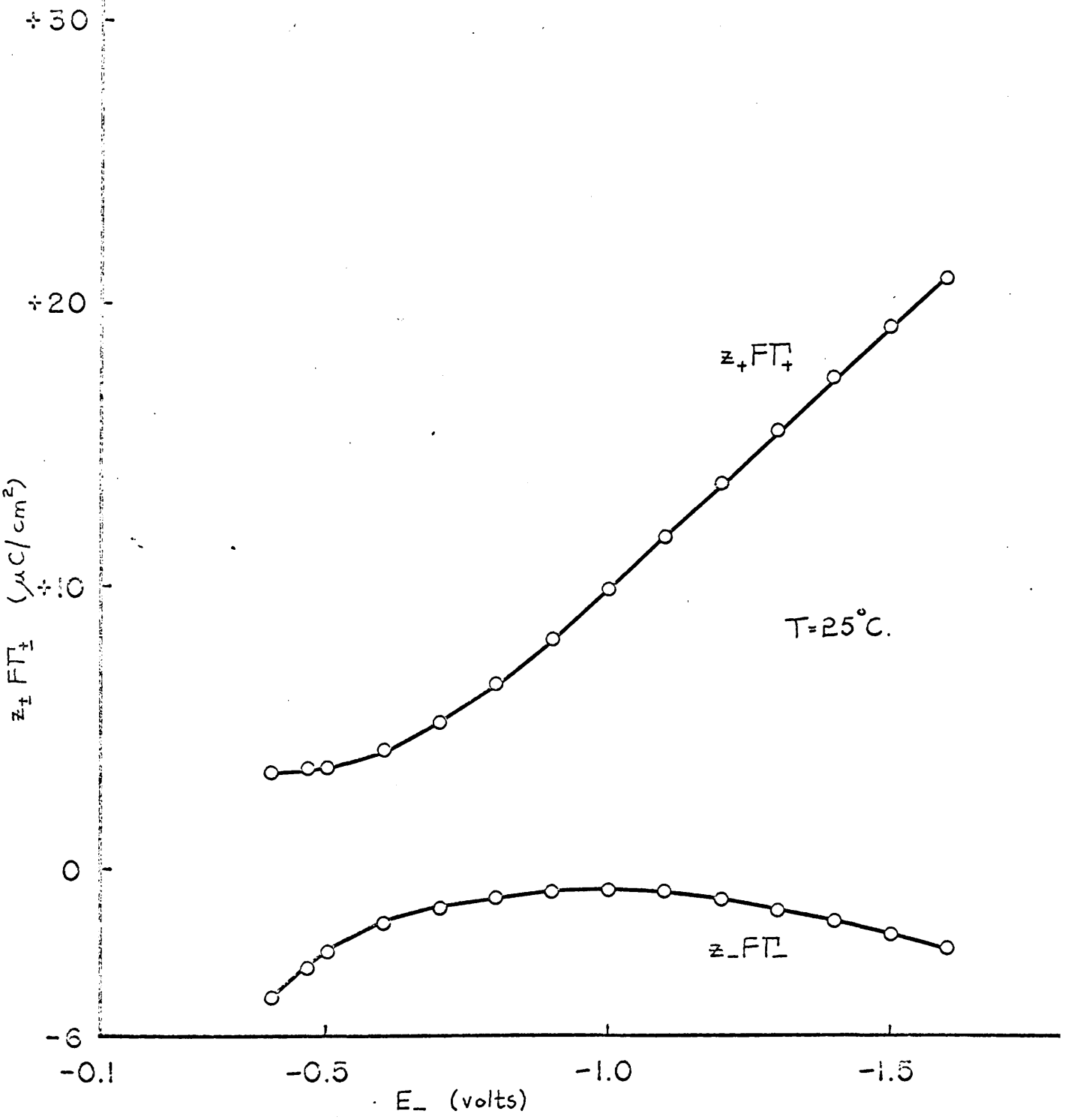

FIG. 23. SURFACE EXCESSES IN 0.071m KCl.

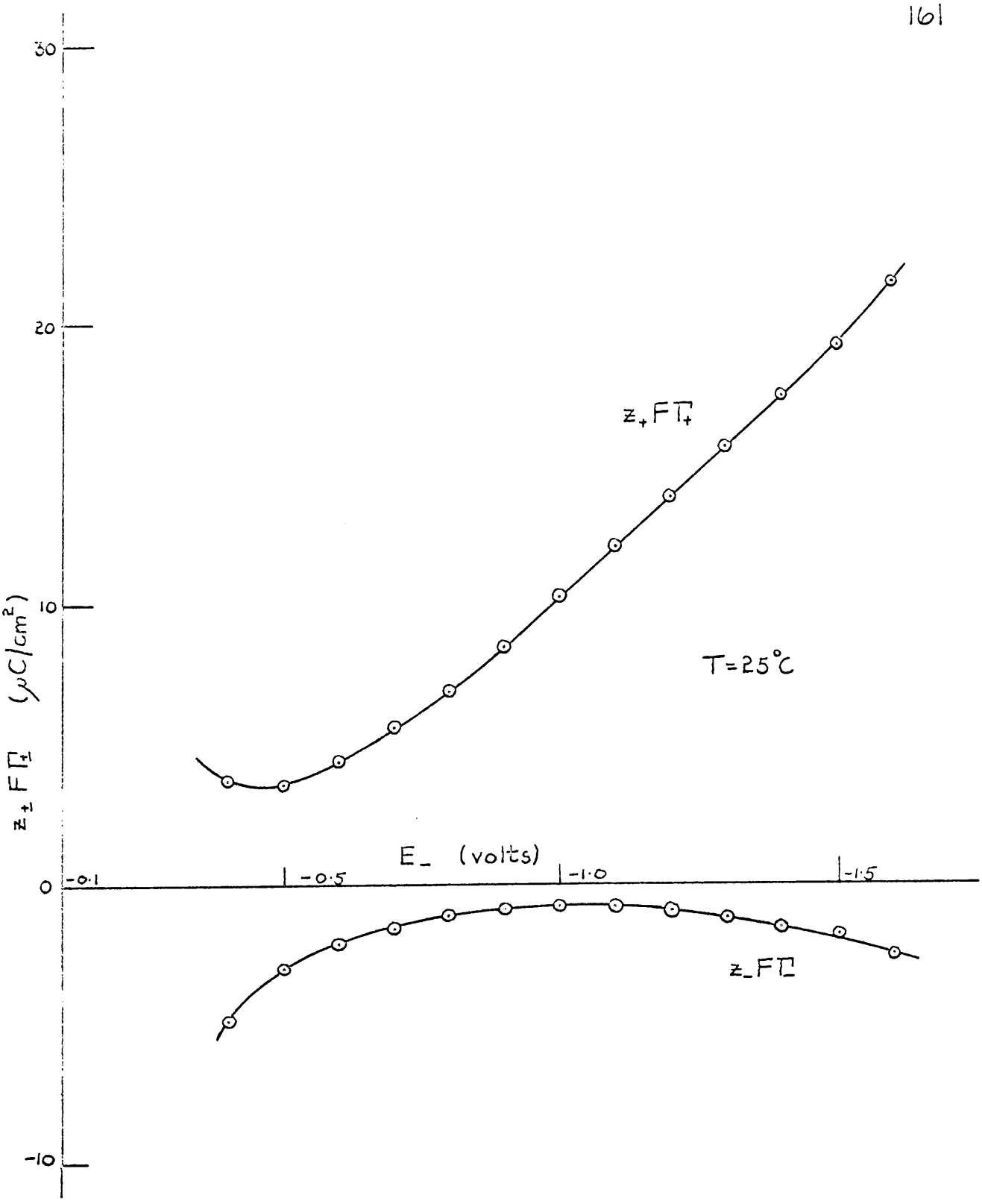

FIG. 24 SURFACE EXCESSES IN 0.100m CsCl.

In the theoretical section it was pointed out that there was no reliable method available for the evaluation of the components of charge in a region of simultaneous specific adsorption. A tentative analysis of the components of charge under such conditions has therefore been developed, and applied to both systems. Calculations of the surface excesses in formamide (71) indicate that iodide ions are not specifically adsorbed at electrode charges more negative than $-10\mu C/cm^2$. Since chloride ions would be adsorbed to a smaller extent than are iodide ions at any given value of the surface charge, it is therefore reasonable to assume that at potentials more negative than -1.2v there will be no anionic specific adsorption occurring. On the basis of this assumption, φ_2, q_+^{2-s}, and q_+' can be calculated from the surface excess results for 0.071m potassium chloride in formamide at -1.3,-1.4,-1.5 and -1.6v using the relationships

$$q_-^{2-s} = z_-F\Gamma_- \qquad \ldots\ldots(90)$$

$$q_-^{2-s} = -1.96\left(e^{19.46\varphi_2}-1\right) \qquad \ldots\ldots\ldots(91)$$

$$q_+^{2-s} = 1.96\left(e^{-19.46\varphi_2}-1\right) \qquad \ldots\ldots\ldots(92)$$

$$q_+' = z_+F\Gamma_+ - q_+^{2-s} \qquad \ldots\ldots\ldots(93)$$

A plot of q_+' against E_- is linear and can be extrapolated to give values of q_+' at other potentials. Essentially linear plots have also been obtained in aqueous systems, plotting q_-' against q_M or E for specifically adsorbed

anions (19,67). Having thus evaluated q'_+ at different potentials, φ_2 and q'_- can be readily evaluated using the relationships

$$q_+^{2-s} = z_+ F\Gamma_+ - q'_+ \qquad \ldots\ldots(94)$$

$$q'_- = z_- F\Gamma_- - q_-^{2-s} \qquad \ldots\ldots(95)$$

together with equations (91) and (92) above. The results are given in table 26, figure 25 shows the relationship between φ_2 and E_-, and figure 26 plots of q'_+ and q'_- vs E_-.

A similar analysis can be carried out on the surface excess results for 0.100m caesium chloride in formamide, the relationships required being equation (90) at potentials more negative than -1.1v, equations (93),(94),(95) and

$$q_-^{2-s} = -2.32\,(e^{19.46\varphi_2} - 1) \qquad \ldots\ldots(96)$$

$$q_+^{2-s} = 2.32\,(e^{-19.46\varphi_2} - 1) \qquad \ldots\ldots(97)$$

The results are given in table 27, a plot of φ_2 vs E_- in figure 25 and of q'_+ and q'_- vs E_- in figure 27.

Before considering these results, it is interesting to note that an alternative method for analysis of simultaneous specific adsorption which is based on a simple electrostatic model of the double layer has recently been put forward by Delahay(84). This method employs six independent equations with six unknowns which can be solved by iteration provided some of the parameters are known. The analysis of the aqueous thallium nitrate system carried out by Delahay by this method yields a linear plot of

TABLE 26

Components of charge analysis.

0.071 m KCl in formamide at 25°C.

E_-	q_-^{2-S}	q_+^{2-S}	q_-^{1}	q_+^{1}	ϕ_2
volts	$\mu C/cm^2$	$\mu C/cm^2$	$\mu C/cm^2$	$\mu C/cm^2$	volts
-1.600	-2.8	-1.2	0*	22.1	0.046
-1.500	-2.4	-1.1	0*	20.3	0.041
-1.400	-2.0	-1.0	0*	18.4	0.036
-1.300	-1.5	-0.9	0*	16.4	0.030
-1.200	-1.3	-0.8	0.1	14.4#	0.026
-1.100	-1.1	-0.7	0.2	12.5#	0.024
-1.000	-0.9	-0.6	0.1	10.5#	0.020
-0.900	-0.6	-0.5	-0.3	8.5#	0.013
-0.800	-0.1	-0.1	-1.0	6.6#	0.002
-0.700	0.4	0.5	-1.8	4.7#	-0.011
-0.600	0.8	1.4	-2.8	2.8#	-0.023

* assumed zero.

\# extrapolated values.

TABLE 27

Components of charge analysis.

0.100 m CsCl in formamide at 25° C.

E_-	q_-^{2-S}	q_+^{2-S}	q_-'	q_+'	ϕ_2
volts	$\mu C/cm^2$	$\mu C/cm^2$	$\mu C/cm^2$	$\mu C/cm^2$	volts
-1.600	-2.5	-1.2	0*	22.0	0.038
-1.500	-1.8	-1.0	0*	20.3	0.030
-1.400	-1.5	-0.9	0*	18.4	0.025
-1.300	-1.2	-0.8	0*	16.5	0.021
-1.200	-0.9	-0.7	0*	14.6	0.017
-1.100	-0.8	-0.6	0	12.7#	0.015
-1.000	-0.6	-0.5	-0.2	10.8#	0.013
-0.900	-0.5	-0.4	-0.4	8.9#	0.010
-0.800	-0.1	-0.1	-1.1	7.0#	0.002
-0.700	0.4	0.5	-2.0	5.1#	-0.010
-0.600	0.7	1.2	-3.0	3.2#	-0.021

* assumed zero.

extrapolated values.

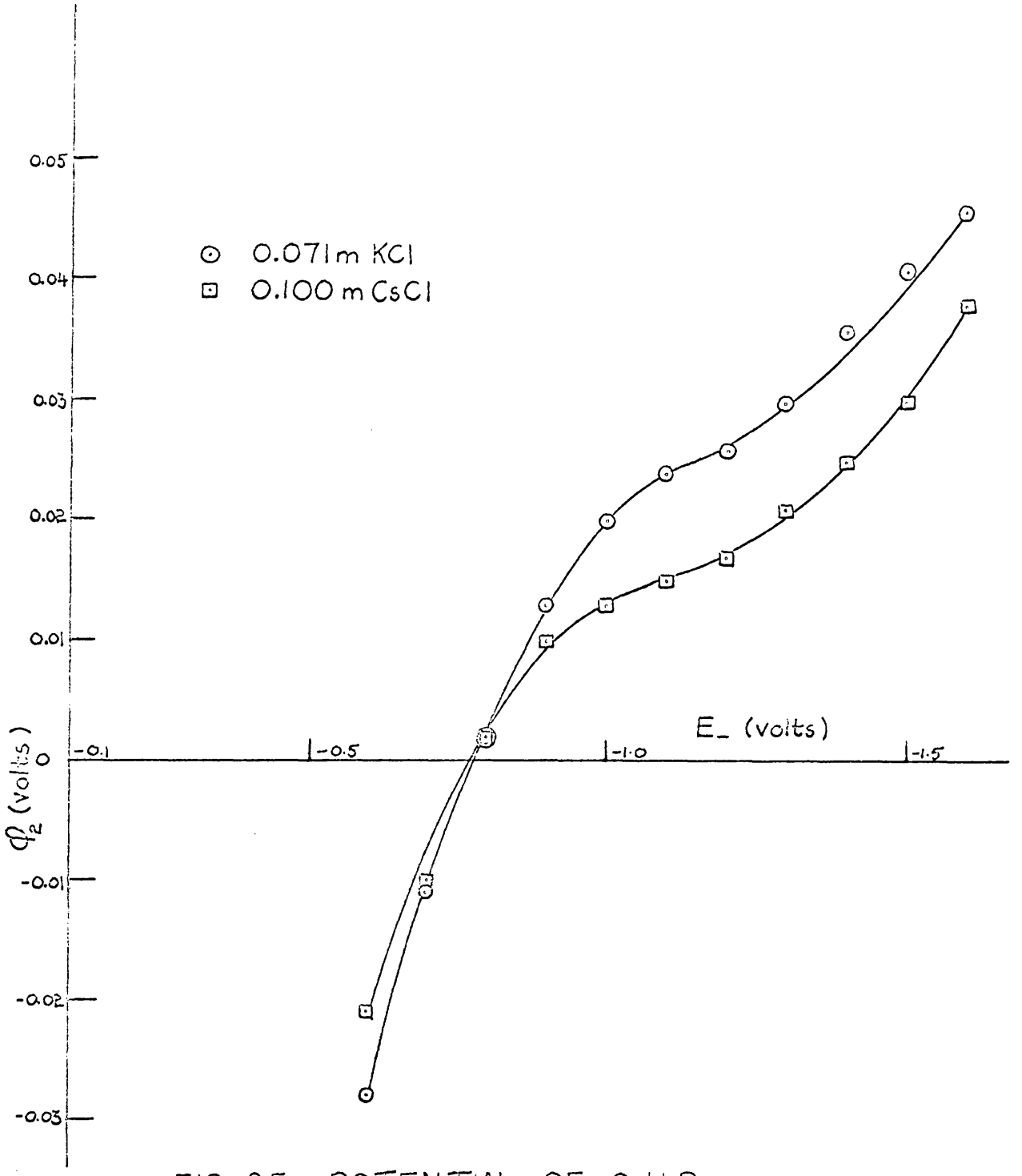

FIG. 25. POTENTIAL OF O.H.P.

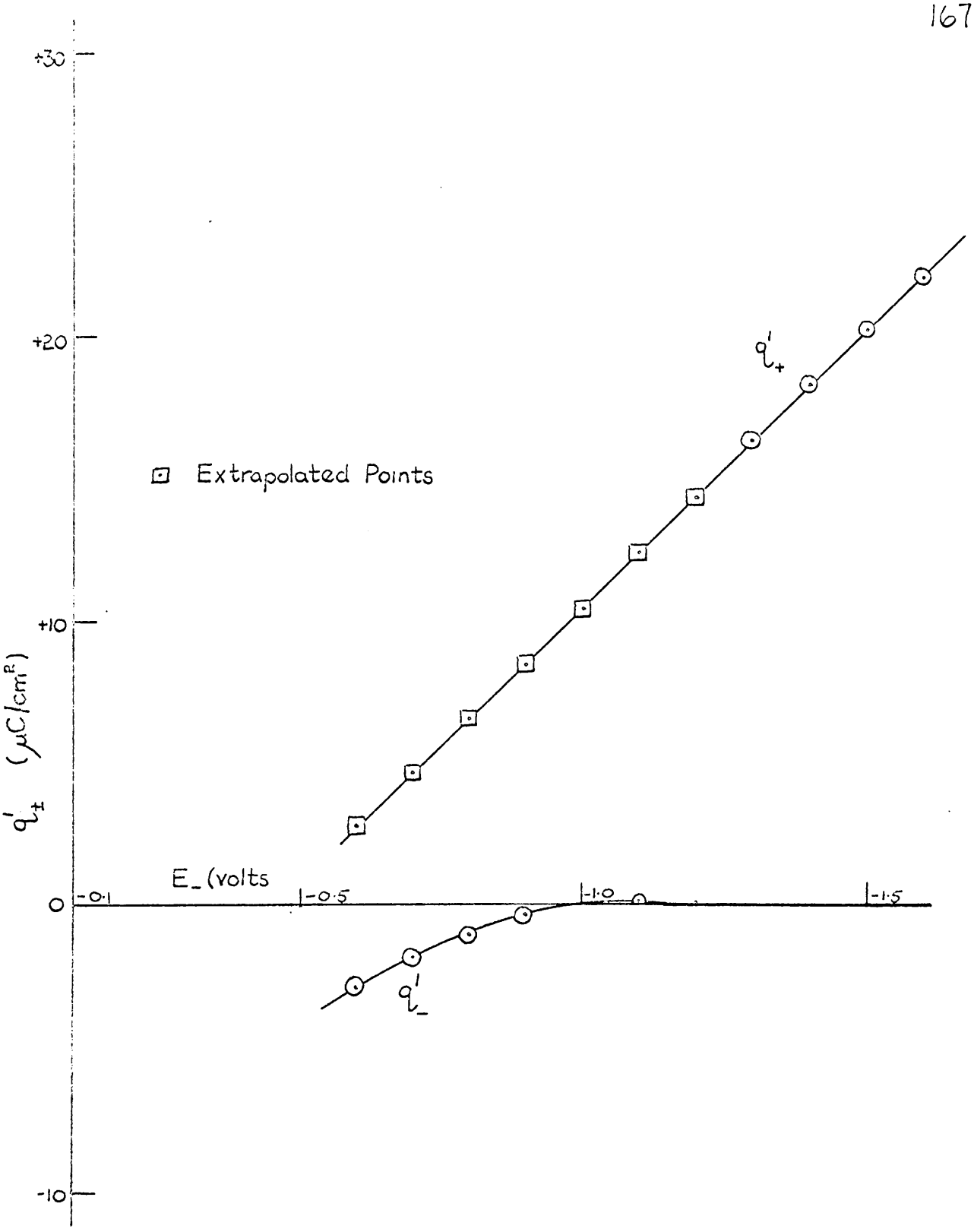

FIG. 26 SPECIFICALLY ADSORBED CHARGE IN KCl.

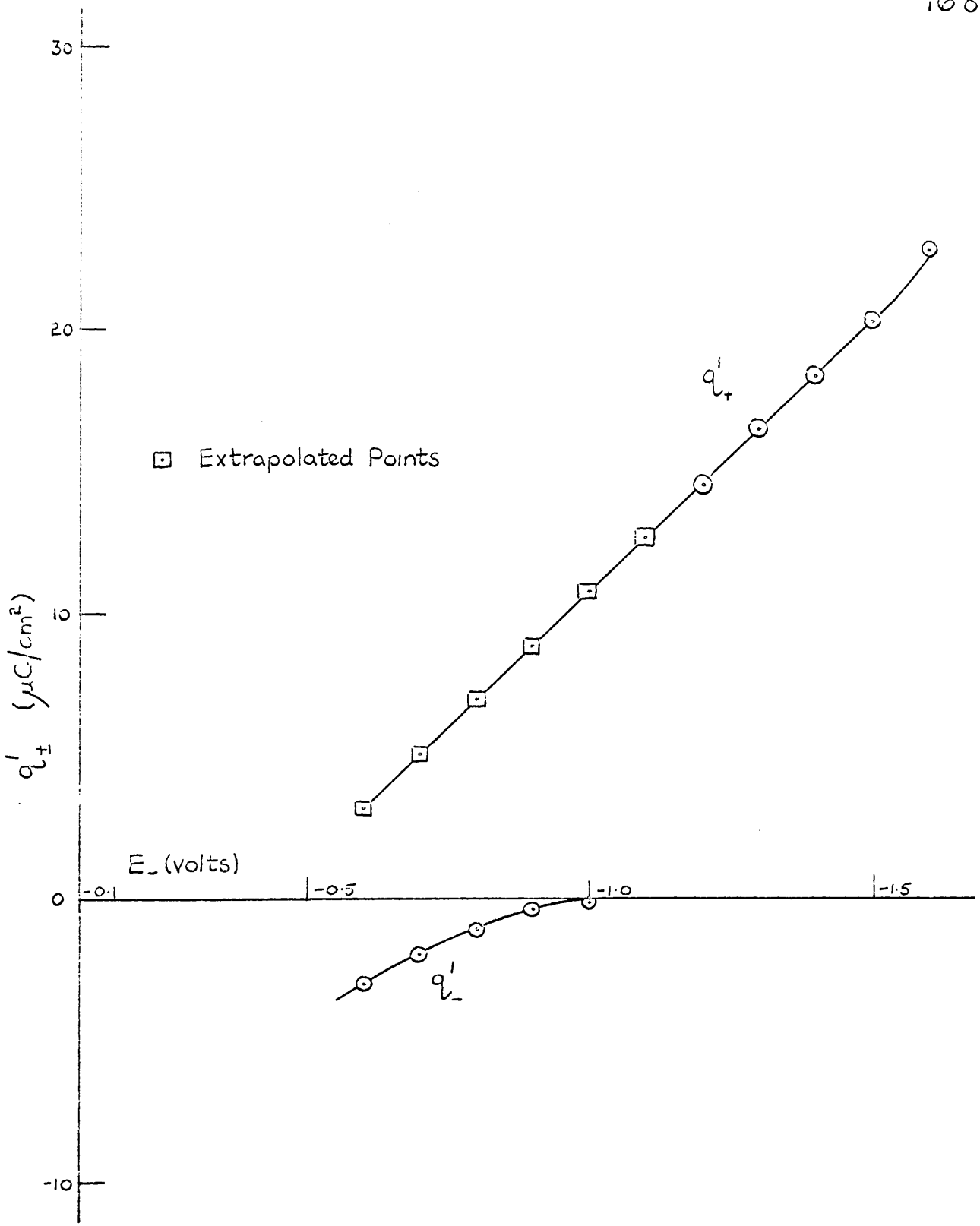

FIG. 27 SPECIFICALLY ADSORBED CHARGE IN CsCl.

q_+^1 vs q_M, in striking agreement with the basic assumption of a linear relationship made in the treatment described above.

From a study of the analysis, it can be seen that at a potential of -1.6v the amount of specific adsorption of cation is large. Damaskin (76) does not seem to have realised this when he compared his experimental values for $z_+F\Gamma_+$ with those calculated **from** diffuse layer theory on the assumption that no specific adsorption was occurring. Whilst the difference in these quantities at -1.6v is only of the order of $2\mu C/cm^2$, this does not necessarily indicate that specific adsorption is taking place only to the extent of about $2\mu C/cm^2$, with a diffuse layer charge of $18\mu C/cm^2$. What appears to be the case is that there is specific adsorption to the extent of about $22\mu C/cm^2$ with a deficiency of cations in the diffuse double layer ($q_+^{2-s} \approx -1\mu C/cm^2$). When $z_-F\Gamma_-$ remains negative at extreme cathodic potentials, i.e. anions are being attracted into, and not repelled from, the double layer, these negative values must reflect a large amount of cationic specific adsorption. This is to be expected, since at high negative electrode charges the forces tending to repel the anions will be large, and for anions to be attracted into the diffuse layer there must be an even larger positive charge present in the compact double layer due to

specifically adsorbed cations.

The small concentration difference, 0.071m and 0.100m, between the potassium chloride and caesium chloride will have a negligible effect on the results, which show that potassium and caesium ions are specifically adsorbed to essentially the same extent, and also that the anion is not specifically adsorbed beyond potentials of about -0.9v. Damaskin's values for $z_+F\Gamma_+$ in 0.1 N solutions of sodium and caesium chlorides in formamide (76), while consistently lower than those obtained in the present work, also appear to be independent of the cation, indicating a similar amount of cationic specific adsorption to occur in each case. The reason for the lower values obtained by Damaskin is not clear since no details of concentrations are given in his paper but it may be due to the use of too small a concentration range for the evaluation of $(\partial\gamma/\partial\mu)_E$. The above data suggest strongly that potassium, sodium, caesium and probably also rubidium ions are specifically adsorbed to essentially the same extent under the same conditions.

On the basis of the present results, the capacitance-charge curves can be examined in more detail than has hitherto been possible. The anodic rise can still be associated with specific adsorption of anions, whilst the cathodic rise is now seen to occur in a region of

high cationic specific adsorption. The capacitance of the region to the cathodic side of the hump can now be considered as reflecting the interplay between increasing dielectric saturation, tending to reduce the capacitance, and increasing specific adsorption, tending to increase the capacitance. In the region immediately beyond the hump, dielectric saturation must be the controlling factor, while in the vicinity of the final capacitance rise, dielectric saturation will be almost complete, and the increasing specific adsorption will take over as the controlling factor. A further effect which must be considered as contributing to the final rise is electrostriction of the solvent, which will have become important in this region due to the high electrical fields which must exist in the double layer at such high polarisations.

The maximum in the capacitance curve can still be attributed primarily to solvent orientation polarisation, and we now see that its virtual independence on the cation for the series K^+, Na^+, Rb^+, Cs^+ is due to their being specifically adsorbed to the same extent, so that any increase in capacitance along the series will be due to small differences in the sizes of the specifically adsorbed cations, or to differences in their polarisabilities. The capacitance hump for lithium chloride is probably lower due to a smaller amount of specific adsorption,

to be expected due to the difficulty in desolvation of the cation. The near independence on the nature of the cation of the capacitance of the minimum in the curves, slightly to the cathodic side of the e.c.m. can also be rationalised as resulting from the constancy of cationic specific adsorption.

Since the amount of specific adsorption of caesium, rubidium, potassium and sodium ions is the same, the dependence of the final capacitance rise on the nature of the cation must have its explanation in the relative sizes and polarisabilities of the specifically adsorbed cations. It is difficult to obtain a reliable estimate of the relative sizes, but consideration of the radii of the hydrated cations shows them to fall in the order $Cs^+ < Rb^+ < K^+ < Na^+$ and the radii of the solvated cations in formamide would be expected to be in the same order. If the cation is adsorbed by a mechanism involving partial desolvation, the distance from the mercury surface to the charge centre of the specifically adsorbed ion would also be expected to follow this general order, especially when polarisation of the ions, which have polarisabilities in the order $Cs^+ > Rb^+ > K^+ > Na^+$, is included in our model. The resulting capacitances would then decrease in magnitude along the series Cs^+, Rb^+, K^+, Na^+, which is in agreement with the experimentally observed order $Cs^+ > Rb^+ > K^+ \approx Na^+$ in the region

where cationic specific adsorption is thought to be the controlling factor in the measured capacitance.

The lithium ion does not fit easily into this picture, and unfortunately the extent of specific adsorption it experiences has not been determined. However, since its solvation sheath will be held much more strongly than those of the other alkali metal cations, we would expect it to be specifically adsorbed to a smaller extent. Also, its solvation sheath will have a different structure from that of the other ions, due to the small size of the lithium ion, and as we shall see later this would be expected to have a profound effect on the energetics of desolvation. If the lithium ion is adsorbed to a smaller extent, its effect on the capacitance in the far cathodic region, lying as it does between the rubidium chloride and potassium chloride, may be due to the smaller radius of the lithium ion as compared with the other specifically adsorbed ions more than compensating for the decrease in capacitance to be expected from the decrease in specific adsorption.

At first sight it is difficult to understand the constancy of specific adsorption along the series of the alkali metal cations. In order to investigate the problem further, we must consider the behaviour of the ions

in water and in formamide. Calorimetric determinations (85) of the enthalpies of solution of the alkali halides in formamide show that for a given halide ion the difference between the enthalpy of solution at infinite dilution (ΔH°_{sol}) of corresponding salts in water and formamide is a constant, independent of the cation. Since (86) the total enthalpy of solvation of an ion (ΔH_S) can be regarded as consisting of three terms:

(a) the enthalpy as a result of the charge of the ion (ΔH_c),

(b) the enthalpy which does not depend on the charge (ΔH_{nc}),

(c) the enthalpy required to make a hole in the solvent in order to accommodate the ion (ΔH_h),

$$\Delta H_S = \Delta H_c + \Delta H_{nc} + \Delta H_h \qquad \ldots\ldots(98)$$

Using quantum mechanical considerations Van Eck (86) showed that $-\Delta H_c$ for an "inert gas" cation could be set equal to the sum of the ionisation potential (I) and the electron affinity (E) of the corresponding metal atom. The enthalpy of solvation of a salt is built up additively from the individual values for the ions. Hence for the enthalpy of solvation of a salt MX in water

$$\Delta H_S^w(MX) = \Delta H_S^w(M^+) + \Delta H_S^w(X^-)$$

$$= -(I_M + E_M) + \Delta H_{nc}^w + \Delta H_h^w + \Delta H_S^w(X^-) \qquad \ldots\ldots(99)$$

and in formamide

$$\Delta H_S^f(MX) = \Delta H_S^f(M^+) + \Delta H_S^f(X^-)$$

$$= -(I_M + E_M) + \Delta H_{nc}^f + \Delta H_h^f + \Delta H_S^f(X^-) \qquad \ldots\ldots(100)$$

The enthalpy of solvation of a salt is related to the lattice enthalpy and the enthalpy of solution by

$$-\Delta H_s\,(MX) = \Delta H_{cryst}\,(MX) - \Delta H^{\circ}_{sol}\,(MX) \qquad \ldots\ldots(101)$$

Combination of equations (99), (100) and (101) leads to

$$\Delta H^{\circ}_{sol}\,(H_2O) - \Delta H^{\circ}_{sol}\,(HCONH_2) = \Delta H^{w}_{nc} + \Delta H^{w}_{h} - \Delta H^{f}_{nc} - \Delta H^{f}_{h} + \Delta H^{w}_{s}(X^-) - \Delta H^{f}_{s}(X^-) \qquad \ldots\ldots(102)$$

The constancy of the R.H.S. of this expression for salts with the same anion shows that $(\Delta H_{nc} + \Delta H_h)$ is a constant for the different cations in each solvent. Thus the enthalpies of solvation of the alkali metal ions in formamide must be in the same order as their aqueous solvation enthalpies. The lithium ion, because of its small size, may have quite different coordination in each solvent and thus (ΔH_c) will not have the same value for this ion in both water and formamide. This is readily seen in the tables of $\Delta H^{\circ}_{sol}(H_2O) - \Delta H^{\circ}_{sol}(HCONH_2)$ in reference 85, which show constant differences for the alkali salts of a given halide, except in the case of the lithium salt.

The reason for the constancy of the specific adsorption of the alkali metal cations is now apparent. In considering the role of the cation on the double layer, Grahame (72) pointed out that the free energy of hydration of a cation would be of the same order as the energy of "solvation" of the ion by mercury. If we accept this model of specific adsorption as solvation of the ion by mercury,

then the enthalpy of solvation of the cation can be written

$$\Delta H_s^m = -(I_M + E_M) + \Delta H_{nc}^m + \Delta H_h^m \qquad \ldots\ldots(103)$$

where the superscript m refers to mercury.

The entropy change accompanying specific adsorption is likely to be small, so that there will not be much error involved in considering the enthalpies as equivalent to the free energies of the processes. The enthalpy change on specific adsorption will be given by

$$-\Delta H = k(\Delta H_s^f - \Delta H_s^m) \qquad \ldots\ldots(104)$$

where we assume that the extent of desolvation on specific adsorption is k, with $k=1$ referring to complete desolvation. If the cations are desolvated to the same extent on specific adsorption, then

$$-\Delta H = k(\Delta H_{nc}^f + \Delta H_h^f - \Delta H_{nc}^m - \Delta H_h^m)$$

$$= \text{constant} \qquad \ldots\ldots(105)$$

for all cations considered, i.e. Cs^+, Rb^+, K^+, Na^+, since $\Delta H_{nc} + \Delta H_h$ would be expected to be constant for these ions in both solvents. Thus the free energy change in specific adsorption of these cations will be a constant, and consequently they would be expected to be specifically adsorbed to the same extent, as has been shown to be the case.

For salts of the halide ions with any given alkali metal cation, $[\Delta H^\circ_{sol}(H_2O) - \Delta H^\circ_{sol}(HCONH_2)]$ is found to increase along the series fluoride to iodide. If, as is reasonable for the relatively large anions, chloride,

bromide and iodide ions have the same solvation structure then $\Delta H_{nc} + \Delta H_{h}$ can be taken as constant for these ions in both solvents by analogy with the cationic situation. Thus $\Delta H^{\circ}_{sol}(H_2O) - \Delta H^{\circ}_{sol}(HCONH_2) = \Delta H_c^w - \Delta H_c^f + \text{constant}$..(106) The increase in the R.H.S. for the halide salts of a given cation therefore therefore reflects changes in the term $(\Delta H_c^w - \Delta H_c^f)$. If we now consider specific adsorption on the solvation model, similar changes in ΔH_c would be expected to occur, giving $(\Delta H_c^f - \Delta H_c^m)$ increasing from chloride to iodide. The enthalpy change in specific adsorption would be given by

$$-\Delta H = k(\Delta H_c^f - \Delta H_c^m + \text{constant}) \qquad \ldots\ldots(107)$$

Since the entropy changes in specific adsorption are probably small, this would indicate that the free energy $(-\Delta G)$ of specific adsorption would increase in the series,

$$Cl^- < Br^- < I^-$$

resulting in an increase of specific adsorption as we go along the series. This[15] the situation which is found to occur experimentally.

Similar arguments for aqueous systems would lead us to the same conclusions, viz. we would expect the specific adsorption to be the same for the four alkali metal cations, and also that specific adsorption of the halide ions would increase along the series chloride to iodide. If we examine the available data on the specifically adsorbed

charge of these ions, given by Bockris, Devanathan and Müller (32) we obtain the following figures (table 28)

TABLE 28

Anion	q'_{-} μC/cm at q_M = +10 μC/cm	Cation	q'_{+} μC/cm at q_M = −15 C/cm
Cl^-	14.6	K^+	0.2
Br^-	19.2	Cs^+	1.3
I^-	29.2		

These results agree with the predictions, as iodide is indeed specifically adsorbed to a greater extent than bromide or chloride, and in the case of potassium and caesium the results agree to within the experimental error, and thus would appear to be in accordance with the prediction of equality of adsorption.

Bockris et al (32) suggested that the degree and type of ionic solvation were the principal factors determining specific adsorption. The above analysis would tend to support this view, both for aqueous systems and also for the formamide system since it is clear that the relative amounts of specific adsorption are controlled by the energetics of ionic solvation, both by the solvent and the mercury. On this model specific adsorption is primarily an electrostatic interaction between the specifically adsorbed ion and the

metal surface which results in the ion attaining an energetically more favourable environment. It would be of interest to determine whether the correlation between ionic enthalpies of solvation and specific adsorption holds true in other solvent systems.

In an attempt to obtain a more quantitative explanation of the capacitance maximum in formamide, the Watts-Tobin theory (15) for a mercury-water interface was extended by taking into account the possibility of non-equivalent orientations of the solvent molecule at the mercury interface. The solvent contribution term was recomputed assuming that the solvent dipole had the possible orientations θ and η with respect to the surface of the mercury. The resulting expression for $C_{solvent}$

$$C_{solvent} = \frac{N\mu^2(\sin\theta+\sin\eta)^2}{x_2^2\, kT} \cdot \frac{\exp\{(V-\phi_{M\text{-}2})\mu(\sin\theta+\sin\eta)/x_2 kT\}}{[1+\exp\{(V-\phi_{M\text{-}2})\mu(\sin\theta+\sin\eta)/x_2 kT\}]} \quad \ldots\ldots(108)$$

reduces to the Watts-Tobin expression when $\sin\theta = \sin\eta = 1/\sqrt{3}$.

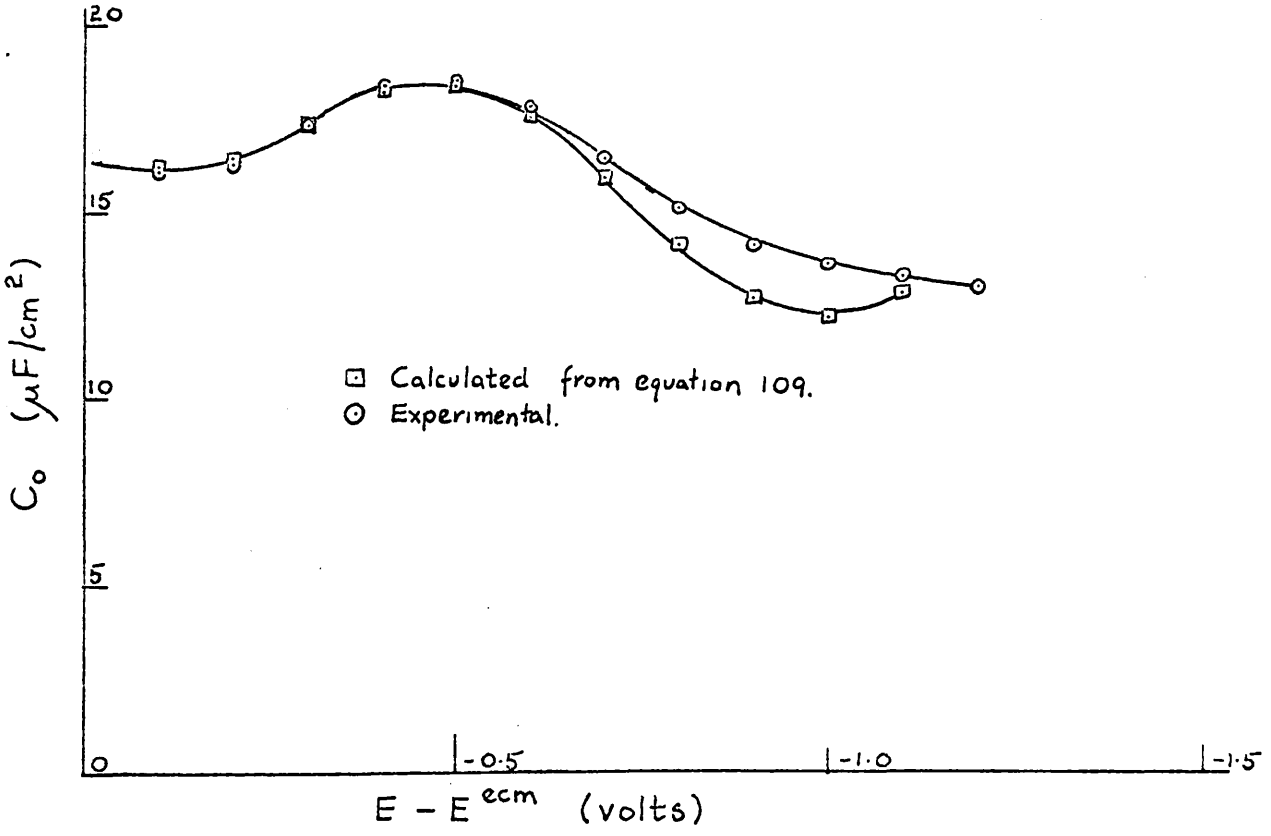

FIG. 28. CALCULATED CAPACITANCE.

Sustitution of this extended $C_{solvent}$ term into the Watts-Tobin expression was found to be insufficient to explain the results obtained for formamide. Accordingly, a fourth term was added to allow for the contribution of specifically adsorbed cation to the capacitance, resulting in the final expression.

$$C = \frac{\epsilon}{4\pi x_2} + \frac{N\mu_1^2}{x_2^2 kT}\left(\frac{c_1}{c_0}\right)^m \exp\left\{\frac{\mu_1(\phi_{m\cdot 2} - V_0)}{x_2 kT}\right\} + \frac{N\mu_2^2}{x_2^2 kT}\left(\frac{c_1}{c_0}\right)^m \exp\left\{-\frac{\mu_2(\phi_{m\cdot 2} + V_2)}{x_2 kT}\right\}$$
$$+ \frac{N\mu^2(\sin\theta + \sin\eta)^2 \exp\left\{(V - \phi_{m\cdot 2})\mu(\sin\theta + \sin\eta)/x_2 kT\right\}}{x_2^2 kT\left[1 + \exp\left\{(V - \phi_{m\cdot 2})\mu(\sin\theta + \sin\eta)/x_2 kT\right\}\right]} \quad \ldots\ldots\ldots (109)$$

Equation (109) was found to fit the capacitance-potential results quite closely in the region of the hump (figure 28) when the following values for the parameter were used:

$\epsilon = 3$; $N = 6\times10^{14}$ mol/cm^2 ; $\mu_1 = 4\times10^{-18}$ e.s.u. ; $\mu_2 = 4\times10^{-18}$ e.s.u. ; $\mu = 3.71\times10^{-18}$ e.s.u. ; $x_2 = 8.0$ Å ; $\theta = 40^\circ$; $\eta = 50^\circ$; $V_0 = 0.25$v ; $V_2 = 1.65$v ; $V = -0.5$v.

Thus the solvent orientation polarisation theory would seem to be a satisfactory explanation of the hump. It is not surprising that this expression is not in good agreement with the experimental results in the regions removed from the hump, since the double layer has a much more complex structure than the simple one adopted by Watts-Tobin.

In aqueous systems, the hump has been attributed to changes in the solvent structure at the interface, and also to effects associated with specific adsorption

of the anions. While solvent orientation polarisation would seem to be an adequate explanation of the capacitance hump, in the systems studied, we are unable, on the basis of the present data, to decide whether the explanation of Hills and Payne (55) is also compatible with the results. They considered the two opposing effects accompanying adsorption of excess solvent into the compact double layer,

(1) increase in the distortional component of the polarisabilty with increase in the surface density of dipoles, and,

(11) increase in the thickness of the compact double layer.

Information was obtained on these effects by measuring the surface excess entropy. At present there are insufficient reliable thermodynamic data available to enable a similar study to be carried out in formamide.

Explanations involving anionic specific adsorption have been proposed for aqueous systems by (a) Damaskin, Schwartz and Frumkin (74) who considered polarisation of solvent molecules by anions adsorbed into the IHP. and by (b) Bockris, Devanathan and Müller (32) suggesting lateral repulsion of anions as the main factor. These are clearly not applicable to formamide systems as they stand, since at the potential of the hump the anion is no longer specifically adsorbed. However, analogous

theories invoking effects due to cationic specific adsorption could be proposed.

Since the amount of cationic specific adsorption appears to be independent of the cation, at least in the alkali metal series, there would seem to be no way of choosing between these opposing theoretical approaches in formamide, since both would forecast a dependence of the magnitude of the hump on the specific adsorption of the cation. Any dependence of $q_{M,hump}$ on the extent of specific adsorption, expected on the second approach, will not be seen due to the constancy of specific adsorption. This is illustrated by figure 16, in which there is no appreciable change in $q_{M,hump}$ for the various cations.

APPENDICES

APPENDIX 1

Computer programme for the calculation of differential capacitance.

```
begin comment  A programme to calculate differential
capacitance;
integer NCA, NP, f, k, i, j, s, z, Nq, l;
real DT, dT, wg, K, gamma P, gamma g, h, tP, g, roe, wt,
M, alpha, S, Z, Co, As, int, grad, P, pi, tg, RMS, beta;
procedure LEAST SQ (x, y, n, a, b, rms);
value x, y, n;
integer n;
real a, b, rms;
begin integer i;
real A,B,C,D,E;
A:=B:=C:=D:=E:=0.0;
for i:=1 step 1 until n do
begin  sum x: A:=A + x[i];
       sum y: B:=B + y[i];
       sum xsq: C:=C + x[i]↑2;
       sum xy: D:=D + x[i]xy[i];
end;
a:=(AxD-BxC)/(A↑2-nxC);
b:=(AxB-nxD)/(A↑2-nxC);
for i:=1 step 1 until n do
```

```
E:=E + ((y[i]-a)/b-x[i] )↑2;
rms:=sqrt(E/n);
end  procedure LEAST SQ ;
comment  DATA
Nq  no of calculations
run identifiers ending with a semicolon
DT density of mercury
dT density of solution
f  frequency
K  area constant
h  mercury height
roe capillary orifice radius
wg  drop weight
tg drop time at same potential
NCA no of potentials investigated
P  potential
tP  drop time at this potential
NP  no of measurements at this potential
CP[i]  capacitance
GP[i]  conductance
tB[i]  balance time;
open (10);  open (20);
Nq:=read (20);
for i:=1 step 1 until Nq do
begin   copy text  (20,10,[ ;;]);
```

```
g:=981.605;
pi:=3.14159;
gamma P:=250.0;
DT:=read(20);
dT:=read(20);
f:=read(20);
K:=read (20);
h:=read (20);
roe:=read (20);
wg:=read (20);
tg:=read (20);
alpha:=(DT-dT)/DT;
beta:=gxDTx(3/(4xpixDT))↑(1/3)x10↑(-1)/2;
gamma g:=(alphaxgx10↑(-3)xwgx(0.159+5.706xroe/wg↑(1/3)))/roe;
M:=( wg+(3xgamma gxwg↑(2/3))/(betaxhx2)
  +(3xgamma g↑2xwg↑(1/3))/(betax h)↑2)/tg;
write text (10,[[cc]Results[c7s]M*=**]);
write (10, format ([s-nd.ddddd]),M);
write text (10,[[cc7s] Surface*Tension*=**] );
write(10,format([s-nddd.ddcc]), gamma g);
write text (10,[[7s]Pot1[8s]Its[6s]ST [6s] Co*approx[6s]
        Co*final[4s] Its[4s] RMS*dev[8s] Aw[cc]] );
NCA:=read (20);
for k:=1 sten 1 until NCA do
begin   P:=read (20);
```

```
tP:=read (20);
S:=gamma P;
for i:=1 step 1 until 10 do
begin
wt:=MxtP-(1.5xM↑(2/3)xtP↑(2/3)xgamma P)/(betaxh)
        -(1.5xM↑(1/3)xtP↑(1/3)xgamma p↑2)/(betaxh)↑2;
gamma P:=(alphaxgx10↑(-3)xwtx(0.159+5.706xroe/wt↑(1/3)))/roe;
s:=i;
if abs (S-gamma P)/S<0.001 then goto L1;
S:=gamma P;
end;
L1:  write (10, format([3s-ndd.ddddd]), P);
write (10, format([4s-ndd]), s);
write (10, format([4s-nddd.dd]), gamma P);
NP:=read (20);
begin  real array fnt, tB, GP, CP, Cs, Csc, Y[1:NP];
for i:=1 step 1 until NP do
begin   CP[i]:=read (20);
GP[i]:=read (20);
tB[i]:=read (20);
Cs[i]:=(1+1/(2xpixfxCP[i]/GP[i])↑2)xCP[i];
fnt[i]:=MxtB[i]-(1.5xM↑(2/3)xtB[i]↑(2/3)xgamma P)/(betaxh)
        -(1.5xM↑(1/3)xtB[i]↑(1/3)xgamma P↑2)/(betaxh)↑2;
Y[i]:=Cs[i]↑(3/2);
end;
```

```
LEAST SQ (fnt, Y, NP, int, grad, RMS);
Co:=grad↑(2/3)/K;
write (10, format ([3s-d.ddddd10+nd]), Co);
Z:=Co;
As:=pi×roe↑2;
for j:=1 step 1 until 10 do
begin    for i:=1 step 1 until NP do
begin    Csc[i]:=Cs[i]+Co×As;
Y[i]:= Csc[i]↑(3/2);
end;
LEAST SQ (fnt, Y, NP,int, grad, RMS);
Co:=grad↑(2/3)/K;
Aw:=(abs(int/grad))↑(2/3)×K;
if int<0 then Aw:=-Aw;
z:=j;
if abs (Z-Co)/Co<0.0001 then goto L2;
Z:=Co;
end;  end;
L2:  write (10, format ([3s-d.ddddd10+nd]), Co);
write, (10, format([3s-ndd]), z);
write (10, format ([3s-d.ddddd10+nd]), RMS);
write (10, format ([3s-d.ddddd10+ndcc]), Aw);
end;   end;
close (10);   close (20);
end →
```

APPENDIX 2

Curve-fitting and integration programme.

```
begin
procedure  CURVEFIT (n, p, mu, roe, s);
value  n, p, roe, mu;
integer  n, p;
real array  roe, mu, s;
begin  integer  i, j, k;
real array  Y, L, U [1:p+1, 1:p+1], x[1:p+1];
procedure  DECOMP (A, L, U, n);
value  A, n;
integer  n;
real array  A, L, U;
begin  integer  i, j, k;
for i:=1 step 1 until n do
for k:=1 step 1 until n do
begin   if k=1 then L[i,k]:=1;
if k<1 then
begin   L[i,k]:=A[i,k]/U[k,k];
for j:=1 step 1 until k-1 do
L[i,k]:=L[i,k]-L[i,j]xU[j,k]/U[k,k];
U[i,k]:=0;
end;
if k>1 then L[i,k]:=0;
```

```
if k > 1 then
begin   U[i,k]:=A[i,k];
for j:=1 step 1 until i-1 do
U[i,k]:=U[i,k] - L[i,j]x U[j,k];
end;  end;  end procedure DECOMP;
procedure INVERT (L, M, n);
value  L, n;
integer  n;
real array  L, M;
begin  integer  i, j, k;
for i:=1 step 1 until n do
for k:=1 step 1 until n do
begin   if i = k then  M[i,k]:=1/L[i,k];
if i< k then M[i,k]:=0;
if i> k then
begin   M[i,k]:=0;
for j:=1 step 1 until i-1 do
M[i,k]:=M[i,k] - (L[i,j]xM[j,k])/L[i,j];
end;  end;  end procedure INVERT;
procedure  TRANS (A,B,n);
value  A, n;
integer n;
real array  A, B;
begin integer i,j;
for i:=1 step 1 until n do
```

```
for j:=1 step 1 until n do
B[i,j]:=A[j,i];
end  procedure TRANS;
procedure  MM MULT (A, B, n, Y);
value  A,B, n;
integer n;
real array  A, B, Y;
begin  integer  i, j, k;
for i:=1 step 1 until n do
for k:=1 step 1 until n do
begin  Y[i,k]:=0;
for j:=1 step 1 until n do
Y[i,k]:=Y[i,k]+A[i,j]×B[j,k];
end;  end procedure  MM MULT;
procedure  MV MULT (A, x, n, b);
value  A, x, n;
integer  n;
real array  A, x, b;
begin  integer  i,j;
for i:=1 step 1 until n do
begin  b[i]:=0;
for j:=1 step 1 until n do
b[i]:=b[i]+A[i,j]×x[j];
end;  end  procedure  MV MULT;
for j:=1 step 1 until p+1 do
```

```
for k:=1 step 1 until p+1 do
begin  X[j,k]:=0;
for i:=1 step 1 until n do
begin  if roe[i] = 0 then goto L1;
X[j,k]:= X[j,k] +(roe[i] )↑(j+k-2);
L1 : end;  end;
for j:=1 step 1 until p+1 do
begin   x[j]:= 0;
for i:=1 step 1 until n do
begin   if roe[i] = 0 then goto L2;
x[j]:= x[j]+mu[i]xroe[i]↑(j-1);
L2 : end;  end;
DECOMP (X, L, U, p 1);
INVERT (L, X, p 1);
TRANS (U, L, p 1);
INVERT (L, U, p 1);
TRANS (U, L, p 1);
MM MULT (L, X, p 1, U);
MV MULT (U, x, p 1, s);
end;

real  X, Y, I;
integer  n, p, i, j, l, r, q;
open (10);  open (20);
comment  q is the no of sets of data;
```

```
q:= read (20);
for i:=1 step 1 until q do
begin
comment  n is the no of data points, p the highest power of
         x in the polynomial;
n:= read (20);  p:= read (20);
begin  real array  mu, roe[1:n], s[1:p+1], d, v[0:n];
for i:=1 step 1 until n do
begin  roe[i]:= read (20);
mu[i]:= read (20);
end;
CURVEFIT (n, p, mu, roe, s);
write text (10,[coefficients[c]] );
for i:=1 step 1 until p+1 do
output (10, s[i] );
v[0]:=0;
write text (10,[Sigma*delta*squared*=*] );
for i:=1 step 1 until n do
begin  d[i]:= s[i] ;
for j:=1 step 1 until p do
begin  if roe[i]=0 then goto L3;
d[i]:= d[i]+ s[j+1]x(roe[i])↑j;
L3 : end;
v[i]:= v[i-1] + (d[i] -mu[i] )↑2;
end;
```

```
output ( 10,v[n]);
comment  r is the no of pts at which integral is required;
r:=read (20);
comment  X is the pt up to which the fn is to be evaluated;
for i:=1 step 1 until r do
begin  X:=read (20);
I:= s[1]×X;
Y:= s[1] ;
for j:=2 step 1 until p+1 do
begin  if X=0 then goto L4;
Y:= Y+s[j]×X↑(j-1);
I:=I+s[j]×X↑j/j;
L4 : end;
write text (10,[X*=*]);
write (10, format([-d.ddddd10+nd; c]), X);
write text (10,[Y*=*]);
write (10, format([-d.ddddd10+nd; c]), Y);
write text (10,[Integral*=*]);
write (10, format([-d.ddddd10+nd; cc]), I);
end;  end;  end;
close (10);  close (20);
end →
```

BIBLIOGRAPHY

1. Parsons, R., Modern Aspects of Electrochemistry, Butterworths, London, (1954).
2. Lippmann, G., Ann. Chim. Phys., [5] 5, 494, (1875).
3. Gouy, G., Ann. Chim. Phys., [7] 29, 145, (1903).
4. Proskurnin, M. and Frumkin, A.N., Trans. Faraday Soc., 31, 110, (1935).
5. Grahame, D.C., J. Amer. Chem. Soc., 63, 1207, (1941).
6. von Helmholtz, H.L.F., Ann. Physik., 7, 337, (1879).
7. Gouy, G., Ann. de Phys., 7, 129, (1917).
8. Chapman, D.L., Phil. Mag., (6) 25, 475, (1913).
9. Stern, O., Z. Elektrochem., 30, 508, (1924).
10. Grahame, D.C. and Whitney, R.W., J. Chem. Phys., 9, 827, (1941).
11. Grahame, D.C., Chem. Rev., 41, 441, (1947).
12. Frumkin, A.N., Damaskin, B.B. and Nikolaeva-Fedorovich, N., Dokl. Akad. Nauk. S.S.S.R., 115, 751, (1957).
13. Grahame, D.C., J. Amer. Chem. Soc., 76, 4819, (1954); 79, 2093, (1957).
14. Joshi, K.M. and Parsons, R., Electrochim. Acta, 4, 129, (1961).
15. Watts-Tobin, R.J., Phil. Mag., 6, 133, (1961).
16. Macdonald, J.R., J. Chem. Phys., 22, 1857, (1954).
17. Macdonald, J.R. and Barlow, C.A. Jr., J. Chem. Phys., 36, 3062, (1962).

18. Devanathan, M.A.V., Trans. Faraday Soc., 50, 373, (1954).

19. Mott, N.F. and Watts-Tobin, R.J., Electrochim. Acta, 4, 79, (1961).

20. Macdonald, J.R. and Barlow, C.A. Jr., Proc. First Australian Conference on Electrochem. Pergammon, Oxford, (1964).

21. Grahame, D.C. and Soderberg, B.A., J. Chem. Phys., 22, 449, (1954).

22. Grahame, D.C., J. Chem. Phys., 21, 1054, (1953).

23. Parsons, R., J. Electroanal. Chem., 7, 136, (1964).

24. Balashova, N.A., Electrochim. Acta, 7, 559, (1962).

25. Kasarinov, V.E. and Balashova, N.A., Dokl. Akad. Nauk. S.S.S.R., 157, 1174, (1964).

26. Bockris, J.O'M., Müller, K., Wroblowa, H. and Kovac, Z., J. Electroanal. Chem., 10, 416, (1965).

27. Parsons, R., Proc. 2nd. Int. Congress Surface Activity, Butterworths, London, 3, 38, (1957).

28. Grahame, D.C., Ann. Rev. Phys. Chem., 6, 337, (1955).

29. Esin, O.A. and Markov, B.F., Acta Physicochim. U.R.S.S., 10, 353, (1939).

30. Grahame, D.C., Poth, M.A. and Cummings, J.I., J. Amer. Chem. Soc., 74, 4422, (1952).

31. Levine, S., Bell, G.M. and Calvert, D., Canad. J. Chem., 40, 518, (1962).

32. Bockris, J.O'M., Devanathan, M.A.V. and Müller, K., Proc. Roy. Soc., A274, 55, (1963).

32a. Bockris, J.O'M., Devanathan, M.A.V. and Müller, K., Proc. 1st. Australian Conf. on Electrochem., Pergammon, Oxford, (1964).

33. Grahame, D.C., J. Amer. Chem. Soc., 80, 4201, (1958).

34. Ershler, B.V., Zhur. Fiz. Khim., 20, 679, (1946).

35. Gouy, G., Ann. Chim. Phys., 8, 291, (1906).

36. Devanathan, M.A.V. and Parsons, R., Trans. Faraday Soc., 49, 673, (1953).

37. Craxford, S.R. and MacKay, H.A.C., J. Phys. Chem., 39, 545, (1935).

38. Corbusier, P. and Gierst, L., Anal. Chim. Acta, 15, 254, (1956).

39. Smith, G.S., Trans. Faraday Soc., 47, 63, (1951).

40. Smolders, C.A. and Duyvis, E.M., Rec. Trav. Chim., 80, 635, (1961).

41. Frumkin, A.N., Acta Scient. (Paris), 373, (1936).

42. Hickling, A. and Taylor, D., Disc. Faraday Soc., 1, 277, (1947).

43. Bowden, F.P. and Grew, K.E.W., Disc. Faraday Soc., 1, 91, (1947).

44. Brodd, R.J. and Hackerman, N., J. Electrochem. Soc., 104, 704, (1957).

45. McMullen, J.J. and Hackerman, N., J. Electrochem. Soc., 106, 341, (1959).

46. Philpot, L. St.J., Phil. Mag., 13, 775, (1932).

47. Frumkin, A.N., Z. Phys. Chem., 103, 55, (1923).

48. Loveland, J.W. and Elving, P.J., J. Phys. Chem., 56, 250, (1952).

49. Randles, J.E.B., Disc. Faraday Soc., 1, 11, (1947).

50. Watanabe, A., Tsuji, F., Yasuda, T. and Ueda, S., Bull. Inst. Chem. Res. Kyoto Univ., 34, 65, (1956).

51. Wien, M., Ann. Phys. (Leipzig), 58, 37, (1896).

52. Jones, G. and Christian, S.M., J. Amer. Chem. Soc., 57, 272, (1935).

53. Grahame, D.C., J. Amer. Chem. Soc., 71, 2975, (1949).

54. Randles, J.E.B., Trans. Faraday Soc., 50, 1246, (1954).

55. Hills, G.J. and Payne, R., Trans. Faraday Soc., 61, 316, (1965).

56. Nancollas, G.H. and Vincent, C.A., Chem. and Ind. 506, (1961).

57. Calvert, R., Cornelius, J.A., Griffiths, V.S. and Stock, D.I., J. Phys. Chem., 62, 47, (1958).

58. Grahame, D.C., J. Amer. Chem. Soc., 68, 301, (1946).

59. Nancollas, G.H. and Vincent, C.A., J. Sci. Inst. 40, 306, (1963).

60. Austin, M.J. and Parsons, R., Proc. Chem. Soc., 239, (1961).

61. Vincent, C.A., Ph.D. Thesis, Glasgow, 1963.

62. Conway, B.E. and Barradas, R.G., Electrochim. Acta, 5, 319, (1961).

63. Grahame, D.C., Coffin, E.M., Cummings, J.I. and Poth, M.A., J. Amer. Chem. Soc., 74, 1207, (1952).

64. Newcombe, R.J., Electrochim. Acta, 7, 685, (1962).

65. Harned, H.S., J. Amer. Chem. Soc., 51, 416, (1929).

66. McAuley, A., Ph.D. Thesis, Glasgow, 1961.

67. Devanathan, M.A.V. and Peries, P., Trans. Faraday Soc., 50, 1236, (1954).

68. Mancollas, G.H. and Vincent, C.A., Electrochim. Acta, 10, 97, (1965).

69. Harkins, W.D. and Brown, F.E., Int. Crit. Tables (N.Y.), 4, 435, (1928).

70. MacNevin, W.M. and Balis, E.W., J. Amer. Chem. Soc., 65, 660, (1943).

71. Payne, R., J. Chem. Phys., 42, 3371, (1965).

72. Grahame, D.C., J. Electrochem. Soc., 98, 343, (1951).

73. Ivanov, V.F., Damaskin, B.B., Frumkin, A.N., Ivaschenko, A.A. and Peshkova, N.I., Elektrokhimiya 1, 279, (1965).

74. Schwartz, E.P., Damaskin, B.B. and Frumkin, A.N., Zhur. Fiz. Khim., 36, 2419, (1962).

75. Dutkiewicz, E. and Parsons, R., J. Electroanal. Chem., 11, 196, (1966).

76. Damaskin, B.B., Ivanova, R.V. and Survila, A.I., Elektrokhimiya, 1, 767, (1965).

77. Minc, S. and Brzostowska, M., Roczniki Chem., 38, 301, (1964).

78. Kurland, R.J. and Wilson, E.B.Jr., J. Chem. Phys., 27, 585, (1957).

79. Costain, C.C. and Dowling, J.M., J. Chem. Phys., 32, 158, (1960).

80. Damaskin, B.B. and Ivanova, R.V., Zhur. Fiz. Khim., 38, 176, (1964).

81. Vincent, C.A., Private Communication.

82. Povarov, Yu.M., Kessler, Yu.M. and Gorbanev, A.I., Izv. Akad. Nauk. S.S.S.R. Ser. Khim., 1895, (1964).

83. Povarov, Yu.M., Kessler, Yu.M., Gorbanev, A.I. and Safonova, I.V., Dokl. Akad. Nauk. S.S.S.R. 155, 172, (1964).

84. Delahay, P., Symposium on Electrode Processes, Electrochem. Soc. Meeting, Cleveland, May, 1966.

85. Somsen, G. and Coops, J., Rec. Trav. Chim., 84, 985, (1965).

86. van Panthaleon van Eck, C.L., Thesis, Leiden, 1958.